Published for SISSA by Springer

Received: *July 18, 2024*
Revised: *October 10, 2024*
Accepted: *December 3, 2024*
Published: *January 8, 2025*

Amplitude analysis of $B^+ \to \psi(2S)K^+\pi^+\pi^-$ decays

The LHCb collaboration

E-mail: p.dargent@cern.ch

Abstract: The first full amplitude analysis of $B^+ \to \psi(2S)K^+\pi^+\pi^-$ decays is performed using proton-proton collision data corresponding to an integrated luminosity of $9\,\text{fb}^{-1}$ recorded with the LHCb detector. The rich $K^+\pi^+\pi^-$ spectrum is studied and the branching fractions of the resonant substructure associated with the prominent $K_1(1270)^+$ contribution are measured. The data cannot be described by conventional strange and charmonium resonances only. An amplitude model with 53 components is developed comprising 11 hidden-charm exotic hadrons. New production mechanisms for charged charmonium-like states are observed. Significant resonant activity with spin-parity $J^P = 1^+$ in the $\psi(2S)\pi^+$ system is confirmed and a multi-pole structure is demonstrated. The spectral decomposition of the $\psi(2S)\pi^+\pi^-$ invariant-mass structure, dominated by $X^0 \to \psi(2S)\rho(770)^0$ decays, broadly resembles the $J/\psi\phi$ spectrum observed in $B^+ \to J/\psi\phi K^+$ decays. Exotic $\psi(2S)K^+\pi^-$ resonances are observed for the first time.

Keywords: B Physics, Exotics, Hadron-Hadron Scattering, Spectroscopy

ArXiv ePrint: 2407.12475

https://doi.org/10.1007/JHEP01(2025)054

JHEP01(2025)054

Contents

1 Introduction

Multibody beauty to charmonium decays have played a pivotal role in hadron spectroscopy. Two decades ago, the Belle collaboration observed the narrow $\chi_{c1}(3872)$ state in $B^+ \to \chi_{c1}(3872)K^+ \to [J/\psi\pi^+\pi^-]K^+$ decays[1] [1]. This discovery challenged our understanding of the strong interaction and marked the beginning of spectroscopic studies of hadrons formed by more than three quarks, known as exotic hadrons. Since then, the $\chi_{c1}(3872)$ meson's quantum numbers, lineshape and decay modes have been extensively studied [2]. However, its true nature remains unclear, with interpretations ranging from conventional

[1]Inclusion of charge-conjugate modes is implied throughout this paper except where explicitly stated.

JHEP01(2025)054

charmonium ($c\bar{c}$) [3] to exotic states such as $D^{*0}\overline{D}^{0}$ molecules [4], tetraquarks ($c\bar{c}q\bar{q}$) [5] or quark-gluon hybrids ($c\bar{c}g$) [6]. The discovery of the charged charmonium-like $T_{c\bar{c}1}(4430)^{-}$ state in $B^{0} \to T_{c\bar{c}1}(4430)^{-}K^{+} \to [\psi(2S)\pi^{-}]K^{+}$ decays [7–9] represents another milestone for the study of exotic-hadron spectroscopy. The charged nature of the $T_{c\bar{c}1}(4430)^{-}$ state eliminates the possibility of a conventional charmonium interpretation, making it a potential tetraquark state with a minimal quark content of $c\bar{c}u\bar{d}$. Meanwhile, numerous states that do not conform to the traditional hadron picture have emerged, forming an exotic particle zoo whose structure largely remains a mystery [2].

To deepen our understanding of exotic states, it is crucial to confirm their existence in independent decay modes. The decay $B^{+} \to \psi(2S)K^{+}\pi^{+}\pi^{-}$ provides an excellent laboratory for this purpose as its topology enables a search for $T^{-}_{c\bar{c}}$ resonances, observed in $B^{0} \to T^{-}_{c\bar{c}}K^{+} \to [\psi(2S)\pi^{-}]K^{+}$ decays [7–9], and $T^{+}_{c\bar{c}\bar{s}}$ resonances, observed in $B^{+} \to T^{+}_{c\bar{c}\bar{s}}\phi \to [J/\psi K^{+}]\phi$ decays [10]. Unlike these three-body B-meson decay modes, the decay $B^{+} \to \psi(2S)K^{+}\pi^{+}\pi^{-}$ may also receive contributions from $X^{0} \to \psi(2S)\pi^{+}\pi^{-}$ or $T^{0}_{c\bar{c}\bar{s}} \to \psi(2S)K^{+}\pi^{-}$ states, including the possibility of exotic cascade decays, e.g. $X^{0} \to [T^{-}_{c\bar{c}} \to \psi(2S)\pi^{-}]\pi^{+}$, which have not yet been established. A better understanding of the rich $K^{+}\pi^{+}\pi^{-}$ resonance structure is also critical for analyses of $B^{+} \to K^{+}\pi^{+}\pi^{-}\gamma$ and $B^{+} \to K^{+}\pi^{+}\pi^{-}\mu^{+}\mu^{-}$ decays [11, 12], which are sensitive to phenomena beyond the Standard Model.

The Belle collaboration conducted the first and (to date) only study of the resonance structure in $B^{+} \to \psi(2S)K^{+}\pi^{+}\pi^{-}$ decays [13]. Due to the limited sample size, with fewer than 1000 signal events, a simplified amplitude fit in the three invariant-mass-squared combinations $m^{2}(K^{+}\pi^{+}\pi^{-})$, $m^{2}(K^{+}\pi^{-})$, and $m^{2}(\pi^{+}\pi^{-})$ was performed that could not account for contributions from exotic states. The LHCb collaboration studied the $\psi_{2}(3823)$ and $\chi_{c1}(3872)$ states in $B^{+} \to J/\psi K^{+}\pi^{+}\pi^{-}$ decays in one- [14] or two- [15] dimensional analyses that considered only narrow regions of the phase space. This paper presents the first four-body amplitude analysis with a vector particle in the final state exploiting the full seven-dimensional phase space of $B^{+} \to \psi(2S)K^{+}\pi^{+}\pi^{-}$ decays. The data sample was collected with the LHCb detector in proton-proton (pp) collisions at centre-of-mass energies[2] of 7, 8 and 13 TeV, corresponding to an integrated luminosity of $9\,\text{fb}^{-1}$.

The paper is structured as follows. After a description of the LHCb detector and the simulation in section 2, the event reconstruction and candidate selection are described in section 3. The amplitude analysis formalism is discussed in section 4, followed by the fit results presented in section 5. Experimental and model-dependent systematic uncertainties are evaluated in section 5.3 and our conclusions are given in section 6.

2 Detector and simulation

The LHCb detector [16, 17] is a single-arm forward spectrometer covering the pseudorapidity range $2 < \eta < 5$, designed for the study of particles containing b or c quarks. The detector includes a high-precision tracking system consisting of a silicon-strip vertex detector (VELO) surrounding the pp interaction region [18], a large-area silicon-strip detector located upstream

[2]Natural units with $\hbar = c = 1$ are used throughout the paper.

JHEP01(2025)054

of a dipole magnet with a bending power of about 4 T m, and three stations of silicon-strip detectors and straw drift tubes [19, 20] placed downstream of the magnet. The polarity of the dipole magnet is reversed periodically throughout the data-taking process to control systematic asymmetries. The tracking system provides a measurement of the momentum, p, of charged particles with a relative uncertainty that varies from 0.5% at low momentum to 1.0% at 200 GeV. The minimum distance of a track to a primary vertex (PV), the impact parameter (IP), is measured with a resolution of $(15 + 29/p_{\mathrm{T}})$ µm, where p_{T} is the component of the momentum transverse to the beam, in GeV. Different types of charged hadrons are distinguished using information from two ring-imaging Cherenkov detectors (RICH) [21].

The online event selection is performed by a trigger [22], which consists of a hardware stage, based on information from the calorimeter and muon systems, followed by a software stage, which applies a full event reconstruction. At the hardware trigger stage, events are required to have a muon with high p_{T} or a hadron, photon or electron with high transverse energy in the calorimeters. For hadrons, the transverse energy threshold is 3.5 GeV. The software trigger requires a two-, three- or four-track secondary vertex with a significant displacement from any primary pp interaction vertex. At least one charged particle must have a transverse momentum $p_{\mathrm{T}} > 1.6$ GeV and be inconsistent with originating from a PV. A multivariate algorithm [23] is used for the identification of secondary vertices consistent with the decay of a b hadron.

Simulated events are used to study the detector acceptance and specific background contributions. In the simulation, pp collisions are generated using Pythia [24, 25] with a specific LHCb configuration [26]. Decays of hadrons are described by EvtGen [27], in which final-state radiation is generated using Photos [28]. The simulated signal decays are generated according to a simplified amplitude model with an additional pure phase-space component. The interaction of the generated particles with the detector, and its response, are implemented using the Geant4 toolkit [29, 30] as described in ref. [31]. The simulation is corrected to match the distributions observed in data of the B^+ kinematics and the number of tracks in an event.

3 Event reconstruction

The selection of $B^+ \to \psi(2S)K^+\pi^+\pi^-$ candidates is performed by first reconstructing $\psi(2S) \to \mu^+\mu^-$ candidates from two oppositely charged particles, identified as muons, that originate from a common vertex displaced from the PV. Candidate $\psi(2S)$ mesons with a reconstructed invariant mass within ±50 MeV of the known $\psi(2S)$ mass [32] are combined with three additional charged tracks to form a B^+ vertex, which must be significantly displaced from any PV. Hadron candidates are required to be positively identified in the RICH detectors and the hadron candidate most likely to be a kaon is selected as the kaon candidate. The B^+ proper decay time is required to exceed 0.3 ps to suppress most of the prompt combinatorial background. The reconstructed invariant mass of the B^+ candidate is required to be between 5200 MeV and 5600 MeV. Its resolution is improved by performing a kinematic fit [33] in which the B^+ candidate is constrained to originate from the associated PV and the reconstructed $\psi(2S)$ invariant mass is constrained to its known value [32]. The four-momenta of the final-state particles for the amplitude analysis are taken from a kinematic

JHEP01(2025)054

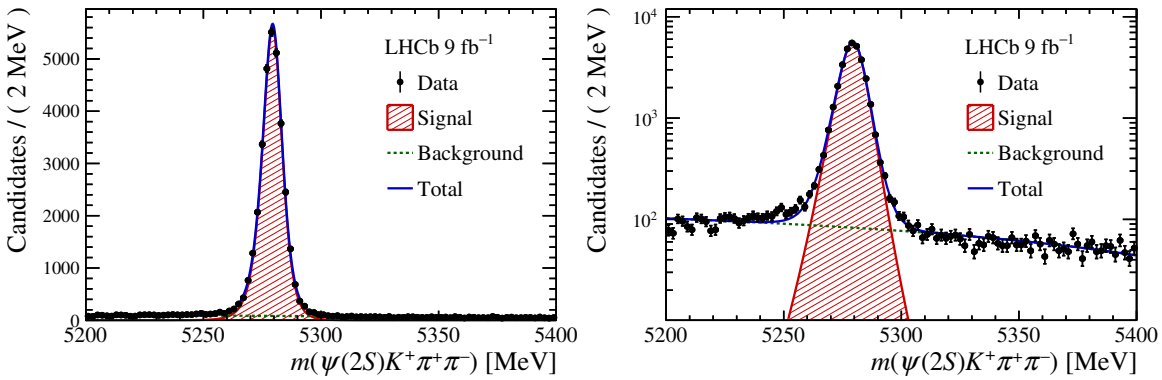

Figure 1. Invariant-mass distribution of selected $B^+ \to \psi(2S)K^+\pi^+\pi^-$ candidates with fit projection overlaid in (left) linear and (right) logarithmic scale.

fit that additionally constrains the reconstructed B^+ invariant mass to its known value [32]. Kinematic requirements are used to veto B^0 decays to $\psi(2S)K^+\pi^-$ or $\psi(2S)\phi(\to K^+K^-)$, where the K^- is misidentified as a pion, that are combined with a random pion. Candidates with an opening angle between any two tracks smaller than 0.5 mrad are removed to exclude clone tracks, i.e. tracks which share a large fraction of their hits.

A gradient boosted decision tree (BDT) [34, 35] is used to suppress background from random combinations of charged particles. The multivariate classifier is trained using as signal proxy a background-subtracted [36] data sample of $(732.7 \pm 1.3) \times 10^3$ $B^+ \to J/\psi K^+\pi^+\pi^-$ signal candidates selected in the same way as the $B^+ \to \psi(2S)K^+\pi^+\pi^-$ sample. Candidate $B^+ \to \psi(2S)K^+\pi^+\pi^-$ decays with invariant mass greater than 5400 MeV are used as background proxy. The features used in the BDT classifier are topological variables related to the vertex separation, the transverse momentum of the B^+ candidate and its flight distance with respect to the associated PV, as well as several variables quantifying the track quality, vertex reconstruction and particle identification. The selection on the output of the BDT classifier is chosen to optimise the significance of the $B^+ \to \psi(2S)K^+\pi^+\pi^-$ signal.

Figure 1 displays the $m(\psi(2S)K^+\pi^+\pi^-)$ distribution of the selected B^+ candidates. Only candidates within the signal region, defined as $m(\psi(2S)K^+\pi^+\pi^-) \in [5268, 5290]$ MeV, are retained for the amplitude analysis. This range corresponds to approximately twice the mass resolution around the known B^+ mass. An extended, unbinned maximum-likelihood fit is performed to the reconstructed $m(\psi(2S)K^+\pi^+\pi^-)$ distribution to determine the event yields. The signal component is modelled using a Johnson S_U function [37], while the combinatorial background is described by a second-order polynomial function. In the signal region, the signal yield is 30210 ± 180 with a background fraction of $f_{\rm B} = (2.93 \pm 0.05)\%$.

4 Phenomenology of the decay

The differential decay rate of a B^+ meson with mass m_{B^+}, decaying into three pseudoscalar particles and two muons with four-momenta $p_i = (E_i, \vec{p}_i)$ $(i \in \{1, 2, 3, 4, 5\})$, is given by

$$\mathrm{d}\Gamma = \frac{1}{2\, m_{B^+}} |\mathcal{A}_{B^+}(\mathbf{x})|^2 \, \mathrm{d}\Phi \,, \tag{4.1}$$

JHEP01(2025)054

where the transition amplitude $\mathcal{A}_{B^+}(\mathbf{x})$ describes the dynamics of the interaction as a function of the position in B^+ decay phase space, $\mathbf{x}$, and $\mathrm{d}\Phi$ is the phase-space element [38]. Each final-state particle contributes three observables, manifesting in its three-momentum, summing up to fifteen observables in total. Four of them are redundant due to four-momentum conservation and another three are removed due to angular momentum conservation. Moreover, the dimuon invariant mass is fixed to the known $\psi(2S)$ mass. The remaining seven independent degrees of freedom unambiguously determine the kinematics of the decay. Convenient choices for the kinematic observables include the invariant-mass combinations of the final-state particles $m^2_{ij} = (p_i + p_j)^2, m^2_{ijk} = (p_i + p_j + p_k)^2$, with $i, j, k \in \{\psi(2S), K^+, \pi^+, \pi^-\}$ as well as the $\psi(2S)$ helicity angle and the acoplanarity angle. These are defined as the angle between the μ^+ direction and the B^+ direction in the $\psi(2S)$ rest frame, θ; and the angle between the $\psi(2S)$ decay plane and the one formed by the K^+ and the $(\pi^+\pi^-)$ system, χ [39, 40]. No particular seven-dimensional basis is chosen in the amplitude fit, but the full four-vectors are used. The dimensionality is handled by the phase-space element which can be written in terms of any complete set of seven independent kinematic observables, $\mathbf{x} = (x_1, \ldots, x_7)$, as $\mathrm{d}\Phi = \phi(\mathbf{x})\,\mathrm{d}^7x$, where $\phi(\mathbf{x}) = |\partial\Phi/\partial(x_1, \ldots x_7)|$ is the phase-space density [41]. In contrast to three-body decays, the phase-space density function is not uniform in the usual kinematic variables.

The square of the total amplitude for the $B^+ \to \psi(2S)K^+\pi^+\pi^-$ decay is given by the spin-averaged coherent sum over all intermediate-state amplitudes $A_i(\mathbf{x}|\lambda_{\mu^+}, \lambda_{\mu^-})$,

$$|\mathcal{A}_{B^+}(\mathbf{x})|^2 = \sum_{\lambda_{\mu^+}, \lambda_{\mu^-}} \left| \sum_i a_i \, A_i(\mathbf{x}|\lambda_{\mu^+}, \lambda_{\mu^-}) \right|^2 , \tag{4.2}$$

where $\lambda_{\mu^+}(\lambda_{\mu^-})$ denotes the $\mu^+(\mu^-)$ spin projection. The complex coefficients $a_i = |a_i|\, e^{i\,\phi_i}$ are to be determined from data. To construct the intermediate-state amplitudes $A_i(\mathbf{x})$, the isobar approach is used, which assumes that the decay process can be factorised into subsequent two-body decay amplitudes [42–44]. This gives rise to two different decay topologies: quasi two-body decays such as $B^+ \to R_1\, R_2$ with $R_1 \to h_1\, h_2$ and $R_2 \to h_3\, \psi(2S)$ or cascade decays such as $B^+ \to \psi(2S)\, R_1$ with $R_1 \to h_1\, R_2$ and $R_2 \to h_2\, h_3$, where the $\psi(2S)$ meson further decays into a muon pair. In either case, the amplitude is parameterised as a product of orbital angular momentum, L, dependent form factors B_L, included for each vertex of the decay tree; Breit-Wigner propagators T_R, included for each resonance R; and an overall angular distribution represented by a spin factor S,

$$A_i(\mathbf{x}|\lambda_{\mu^+}, \lambda_{\mu^-}) = B_{L_{B_s}}(\mathbf{x})\,[B_{L_{R_1}}(\mathbf{x})\,T_{R_1}(\mathbf{x})]\,[B_{L_{R_2}}(\mathbf{x})\,T_{R_2}(\mathbf{x})]\,S_i(\mathbf{x}|\lambda_{\mu^+}, \lambda_{\mu^-})\,. \tag{4.3}$$

The lineshape of the $\psi(2S)$ resonance is set to a delta function and contributes a constant factor multiplying the final matrix element after integrating over the dimuon invariant mass.

4.1 Form factors and resonance lineshapes

To account for the finite size of the decaying resonances, the Blatt-Weisskopf penetration factors, derived in ref. [45] by assuming a square well interaction potential with radius r_{BW}, are used as form factors, B_L. They depend on the orbital angular momentum L between the resonance decay products, and the breakup momentum q defined as the magnitude of

JHEP01(2025)054

the three-momentum of one of the decay products in the rest frame of the resonance. Their explicit expressions for $L = \{0, 1, 2\}$ are

$$B_0(q) = 1, \quad B_1(q) = 1/\sqrt{1 + (q\, r_{\rm BW})^2} \quad \text{and} \quad B_2(q) = 1/\sqrt{9 + 3\,(q\, r_{\rm BW})^2 + (q\, r_{\rm BW})^4}. \tag{4.4}$$

Resonance lineshapes are described as functions of the energy-squared, s, by Breit-Wigner propagators

$$T_R(s) = (m_0^2 - s - i\, m_0\, \Gamma(s))^{-1}, \tag{4.5}$$

where the total width, $\Gamma(s)$, is normalised to give the nominal width, Γ_0, when evaluated at the nominal mass m_0. For a decay into two stable particles $R \to AB$, the energy dependence of the decay width can be described by

$$\Gamma_{R\to AB}(s) = \Gamma_0\, \frac{m_0}{\sqrt{s}} \left(\frac{q}{q_0}\right)^{2L+1} \frac{B_L(q)^2}{B_L(q_0)^2}\,, \tag{4.6}$$

where q_0 is the value of the breakup momentum evaluated at the nominal mass [46]. The energy-dependent width for a three-body decay $R \to ABC$ is computed numerically by integrating the transition amplitude-squared over the phase space,

$$\Gamma_{R\to ABC}(s) = \frac{1}{m_0} \int |A_{R\to ABC}|^2\, {\rm d}\Phi_3, \tag{4.7}$$

as described in ref. [47]. The three-body amplitude $A_{R\to ABC}$ is parameterised analogously to the amplitude in eq. 4.3. To calculate the energy-dependent width for decays of the type $R \to AB(\psi(2S) \to \mu^+\mu^-)$, we treat them as three-body $R \to AB\psi(2S)$ decays since the $\psi(2S)$ is sufficiently narrow to be considered stable. The running-width distributions for various three-body resonances, calculated from eq. 4.7, are shown in appendix A.

Equation 4.5, with the energy-dependent width from eq. 4.6, is used by default for resonances decaying into a two-body final state. For the $\rho(770)^0$ resonance, the Gounaris-Sakurai parameterisation is used instead [48], see appendix A. We use the parameterisation from ref. [49] to include $\rho - \omega$ mixing,

$$T(s) = T_{GS}(s) \left(1 + \delta \frac{s}{m_\omega^2} T_\omega(s)\right), \tag{4.8}$$

where T_ω is the relativistic Breit-Wigner propagator (eq. 4.5) of the ω meson and δ is the $\rho - \omega$ mixing parameter. A fit to the data of the pion vector form factor determines the electromagnetic mixing parameter to be $|\delta_{em}| = (1.57 \pm 0.15 \pm 0.05) \times 10^{-3}$ [49]. By relating the electromagnetic current to the clean $d\bar{d}$ source in $B^0 \to J/\psi\pi^+\pi^-$ decays, it is argued in ref. [50] that the mixing effect can be described by $\delta_{B^0\to J/\psi\pi\pi} = -3|\delta_{em}|$ in $B^0 \to J/\psi\pi^+\pi^-$ decays. Following a similar argument and assuming a clean $u\bar{u}$ source for the ρ production in $B^+ \to \psi(2S)K^+\pi^+\pi^-$ decays, we initially fix the mixing parameter to $\delta = +3|\delta_{em}|$. The parameter δ is argued to be real in ref. [51] as confirmed experimentally in refs. [49, 52]. We therefore fix the phase of δ to zero. These assumptions are tested after the amplitude model is built.

The $K^+\pi^-$ and $\pi^+\pi^-$ S-wave contributions, referred to as $[K^+\pi^-]_{\rm S}$ and $[\pi^+\pi^-]_{\rm S}$ in the following, are described with the K-matrix formalism [53] to preserve coupled-channel unitarity.

JHEP01(2025)054

The $\pi^+\pi^-$ S-wave K-matrix parameterisation is taken from ref. [54], with parameters taken from ref. [55], and considers the effects of five coupled channels $(\pi\pi, KK, \pi\pi\pi\pi, \eta\eta, \eta\eta')$, five poles and a nonresonant contribution. The $K^+\pi^-$ S-wave couples to two channels $K\pi$ and $K\eta'$, and contains only one pole, the $K_0^*(1430)$ resonance. The isospin state $I = \frac{1}{2}$ contributes to both channels, while $I = \frac{3}{2}$ couples to $K\pi$ only. The parameterisation is taken from ref. [56]. The couplings to $K^+\pi^-$ and $\pi^+\pi^-$ K-matrix poles and channels depend on the production mode, which is modelled using the P-vector approach [57]. More details about the S-wave models are provided in appendix A.

Nonresonant contributions in a state of well-defined relative orbital angular momentum are denoted by surrounding the particle system with brackets and indicating the partial-wave state with a subscript; for example $[\pi^+\pi^-]_{\mathrm{P}}$ refers to a nonresonant dipion P-wave. The lineshape for nonresonant contributions is set to a constant.

4.2 Spin densities

The spin amplitudes are phenomenological descriptions of decay processes which are required to be Lorentz invariant and compatible with angular momentum conservation and, where appropriate, parity conservation. They are constructed in the covariant Zemach (Rarita-Schwinger) tensor formalism [58–60] and resemble spin-orbit couplings near threshold. In the following, we briefly introduce the fundamental objects of the covariant tensor formalism which connect the particle's four-momenta to the spin dynamics of the reaction and give a general recipe to calculate the spin factors for arbitrary decay trees. Further details can be found in refs. [61, 62].

An integer spin-S particle with four-momentum p, and spin projection λ, is represented by the polarisation tensor $\epsilon_{(S)}(p, \lambda)$, which is symmetric, traceless and orthogonal to p. These so-called Rarita-Schwinger conditions reduce the 4^S elements of the rank-S tensor to $2S + 1$ independent elements in accordance with the number of degrees of freedom of a spin-S state [59, 63]. The spin projection operator $P_{(S)}^{\mu_1\ldots\mu_S\nu_1\ldots\nu_S}(p_R)$, for a resonance R, with spin $S = \{0, 1, 2\}$, and four-momentum p_R, is given by [62]

$$
\begin{aligned}
P_{(0)}^{\mu\nu}(p_R) &= 1, \\
P_{(1)}^{\mu\nu}(p_R) &= \sum_{\lambda_R} \varepsilon^{\mu}(p_R, \lambda_R)\, \varepsilon^{*\nu}(p_R, \lambda_R) = -\,g^{\mu\nu} + \frac{p_R^{\mu}\, p_R^{\nu}}{p_R^2}, \\
P_{(2)}^{\mu\nu\alpha\beta}(p_R) &= \frac{1}{2}\left[P_{(1)}^{\mu\alpha}(p_R)\, P_{(1)}^{\nu\beta}(p_R) + P_{(1)}^{\mu\beta}(p_R)\, P_{(1)}^{\nu\alpha}(p_R)\right] - \frac{1}{3}\, P_{(1)}^{\mu\nu}(p_R)\, P_{(1)}^{\alpha\beta}(p_R)\,,
\end{aligned}
\tag{4.9}
$$

where $g^{\mu\nu}$ is the Minkowski metric. Contracted with an arbitrary tensor, the projection operator selects the part of the tensor which satisfies the Rarita-Schwinger conditions. For a decay process $R \to AB$, with relative orbital angular momentum L between particles A and B, the angular momentum tensor is obtained by projecting the rank-L tensor $q_R^{\nu_1}\, q_R^{\nu_2} \ldots q_R^{\nu_L}$, constructed from the relative momenta $q_R = p_A - p_B$, onto the spin-L subspace,

$$
L_{(L)\mu_1\ldots\mu_L}(p_R, q_R) = (-1)^L\, P_{(L)\mu_1\ldots\mu_L\nu_1\ldots\nu_L}(p_R)\, q_R^{\nu_1} \ldots q_R^{\nu_L}. \tag{4.10}
$$

Its $|\vec{q}_R|^L$ dependence accounts for the influence of the centrifugal barrier on the transition amplitudes.

JHEP01(2025)054

Following the isobar approach, the full decay amplitude is described as a product of two-body decay amplitudes. Initially, one considers the $\psi(2S)$ meson as a final-state vector particle in the decay $B^+ \to \psi(2S)K^+\pi^+\pi^-$. Then, each sequential two-body decay $R \to A\,B$, with relative orbital angular momentum L_{AB}, and total intrinsic spin S_{AB}, contributes a term to the overall spin factor given by

$$S_{R\to AB}(\mathbf{x}|L_{AB}, S_{AB}; \lambda_R, \lambda_A, \lambda_B) = \varepsilon_{(S_R)}(p_R, \lambda_R)\, \tilde{E}(S_R, L_{AB}, S_{AB})\, L_{(L_{AB})}(p_{AB}, q_{AB}) \times \Omega(\mathbf{x}|S_{AB}; \lambda_A, \lambda_B), \tag{4.11}$$

where

$$\Omega(\mathbf{x}|S_{AB}; \lambda_A, \lambda_B) = P_{(S_{AB})}(p_R)\, \tilde{E}(S_{AB}, S_A, S_B)\, \varepsilon^*_{(S_A)}(p_A, \lambda_A)\, \varepsilon^*_{(S_B)}(p_B, \lambda_B)\,. \tag{4.12}$$

Here, a polarisation vector is assigned to the decaying particle and the complex conjugate vectors for each decay product. The spin and orbital angular momentum couplings are described by the tensors $P_{(S_{AB})}(p_R)$ and $L_{(L_{AB})}(p_{AB}, q_{AB})$, respectively. Firstly, the two spins S_A and S_B are coupled to a total spin-S_{AB} state, $\Omega(\mathbf{x}|S_{AB})$, by projecting the corresponding polarisation vectors onto the spin-S_{AB} subspace transverse to the momentum of the decaying particle. Afterwards, the spin and orbital angular momentum tensors are properly contracted with the polarisation vector of the decaying particle to give a Lorentz scalar. This requires in some cases to include the tensor $\varepsilon_{\alpha\beta\gamma\delta}\, p_R^\delta$ via

$$\tilde{E}(j_a, j_b, j_c) = \begin{cases} 1 & \text{if } j_a + j_b + j_c \text{ even} \\ \varepsilon_{\alpha\beta\gamma\delta}\, p_R^\delta & \text{if } j_a + j_b + j_c \text{ odd} \end{cases}, \tag{4.13}$$

where $\varepsilon_{\alpha\beta\gamma\delta}$ is the Levi-Civita symbol and j refers to the arguments of $\tilde{E}$ defined in eqs. 4.11 and 4.12. Its antisymmetric nature ensures the correct parity transformation behaviour of the amplitude.

The spin factor for a given decay chain, for example $B^+ \to \psi(2S)\, R_1$ with $R_1 \to A\, R_2$ and $R_2 \to BC$, is obtained by combining the two-body terms and performing a sum over all unobservable, intermediate spin projections

$$S'_i(\mathbf{x}|\lambda_\psi) = \sum_{\lambda_{R_1}, \lambda_{R_2}} S_{B^+\to\psi R_1}(\mathbf{x}|L_{\psi R_1}; \lambda_\psi, \lambda_{R_1})\, S_{R_1\to AR_2}(\mathbf{x}|L_{AR_2}; \lambda_{R_1}\lambda_{R_2})\, S_{R_2\to BC}(\mathbf{x}|L_{BC}; \lambda_{R_2}), \tag{4.14}$$

where $\lambda_{B^+} = \lambda_A = \lambda_B = \lambda_C = 0$, $S_{\psi R_1} = L_{\psi R_1}$, $S_{BC} = 0$ and $S_{AR_2} = L_{AR_2}$, as B^+, A, B and C are pseudoscalar particles. The $\psi(2S) \to \mu^+\mu^-$ decay is incorporated by the modification

$$S_i(\mathbf{x}|\lambda_{\mu^+}, \lambda_{\mu^-}) = \sum_{\lambda_\psi} S'_i(\mathbf{x}|\lambda_\psi)\, \epsilon^\alpha_{(1)}(p_\psi, \lambda_\psi)\, \bar{u}(\lambda_{\mu^-})\gamma_\alpha \nu(\lambda_{\mu^+}), \tag{4.15}$$

where $\bar{u}(\lambda_{\mu^-})$ and $\nu(\lambda_{\mu^+})$ are the Dirac spinors for the fermions μ^- and μ^+ and the gamma matrix, γ_α, describes a vector current. As a last step, the completeness relations of the polarisation tensors in eq. 4.9 are used to simplify the spin-factor expressions.

JHEP01(2025)054

4.3 Decay fractions

The hadronic amplitudes are normalised prior to the amplitude fit such that

$$\int \sum_{\lambda_{\mu^+},\lambda_{\mu^-}} \left|A_i(\mathbf{x}|\lambda_{\mu^+},\lambda_{\mu^-})\right|^2 \mathrm{d}\Phi = 1. \tag{4.16}$$

This ensures that all amplitude coefficients, a_i, are of comparable scale, and makes the fit robust against the choice of starting values for these parameters. To provide implementation-independent measurements, in addition to the complex coefficients a_i, the fit fractions are defined as

$$F_i \equiv \frac{\int \sum_{\lambda_{\mu^+},\lambda_{\mu^-}} \left|a_i\, A_i(\mathbf{x}|\lambda_{\mu^+},\lambda_{\mu^-})\right|^2 \mathrm{d}\Phi}{\int |\mathcal{A}_{B^+}(\mathbf{x})|^2 \,\mathrm{d}\Phi}, \tag{4.17}$$

and are a measure of the relative strength between the different transitions. For cascade decays, such as $B^+ \to \psi(2S)K_1(1270)^+$ with $K_1(1270)^+ \to \{K^+\rho(770)^0, K^*(892)^0\pi^+, \ldots\}$, we also define the combined subchannel fit fractions by

$$F_{R_i} \equiv \frac{\int \sum_{\lambda_{\mu^+},\lambda_{\mu^-}} \left|\sum_{j\in R_i} a_j\, A_j(\mathbf{x}|\lambda_{\mu^+},\lambda_{\mu^-})\right|^2 \mathrm{d}\Phi}{\int |\mathcal{A}_{B^+}(\mathbf{x})|^2 \,\mathrm{d}\Phi}, \tag{4.18}$$

where R_i labels the three-body resonance (e.g. $R_i = K_1(1270)^+$) and j labels the subdecay mode (e.g. $j = \{K^+\rho(770)^0, K^*(892)^0\pi^+, \ldots\}$). Then the relative contribution of the subdecay j to the three-body resonance R_i is given by the partial fit fractions

$$f_j^{R_i} \equiv \frac{\int \sum_{\lambda_{\mu^+},\lambda_{\mu^-}} \left|a_j\, A_j(\mathbf{x}|\lambda_{\mu^+},\lambda_{\mu^-})\right|^2 \mathrm{d}\Phi}{\int \sum_{\lambda_{\mu^+},\lambda_{\mu^-}} \left|\sum_{k\in R_i} a_k\, A_k(\mathbf{x}|\lambda_{\mu^+},\lambda_{\mu^-})\right|^2 \mathrm{d}\Phi}. \tag{4.19}$$

The interference between amplitude pairs are quantified by the fractions

$$I_{ij} \equiv \frac{\int \sum_{\lambda_{\mu^+},\lambda_{\mu^-}} 2\,\Re[a_i a_j^*\, A_i(\mathbf{x}|\lambda_{\mu^+},\lambda_{\mu^-}) A_j^*(\mathbf{x}|\lambda_{\mu^+},\lambda_{\mu^-})]\,\mathrm{d}\Phi}{\int |\mathcal{A}_{B^+}(\mathbf{x})|^2 \,\mathrm{d}\Phi}. \tag{4.20}$$

Constructive interference leads to $I_{ij} > 0$, while destructive interference leads to $I_{ij} < 0$. Note that $\sum_i F_i + \sum_{j<k} I_{j,k} = 1$.

We ensure that strong decays in the cascade topology have the same pattern regardless of the production mechanism by sharing couplings between related subdecays. For example, given the two a_i parameters required for the S-wave decay $B^+[S] \to \psi(2S)\, K_1(1270)^+$ with $K_1(1270)^+ \to \rho(770)^0\, \pi^+$ and $K_1(1270)^+ \to K^*(892)^0\, \pi^+$, the amplitude for the P-wave decay $B^+[P] \to \psi(2S)\, K_1(1270)^+$ with $K_1(1270)^+ \to \rho(770)^0\, \pi^+$ and $K_1(1270)^+ \to K^*(892)^0\, \pi^+$ only requires one additional global complex parameter to represent the different production processes of $B^+[S] \to \psi(2S)\, K_1(1270)^+$ and $B^+[P] \to \psi(2S)\, K_1(1270)^+$, while the relative magnitude and phase between $K_1(1270)^+ \to \rho(770)^0\, \pi^+$ and $K_1(1270)^+ \to K^*(892)^0\, \pi^+$ are the same regardless of the production mechanism. In the following, if no angular momentum is specified, the lowest angular momentum state compatible with angular momentum conservation and, where appropriate, parity conservation, is implied.

JHEP01(2025)054

5 Amplitude fit

The total probability density function (PDF) describing the phase-space distribution of $B^+ \to \psi(2S)K^+\pi^+\pi^-$ candidates in the signal region is composed of the signal, $\mathcal{P}_{\rm S}(\mathbf{x}|\theta_{\rm S})$, and the background, $\mathcal{P}_{\rm B}(\mathbf{x}|\theta_{\rm B})$, PDFs,

$$\mathcal{P}(\mathbf{x}|\theta) = (1 - f_{\rm B})\,\mathcal{P}_{\rm S}(\mathbf{x}|\theta_{\rm S}) + f_{\rm B}\,\mathcal{P}_{\rm B}(\mathbf{x}|\theta_{\rm B}), \tag{5.1}$$

where $f_{\rm B}$ is the background fraction determined in section 3 and $\theta = (\theta_{\rm S}, \theta_{\rm B})$ is the total set of fit parameters. The likelihood function is defined as $\mathcal{L}(\theta) = \prod_i \mathcal{P}(\mathbf{x}_i|\theta)$. Assuming *CP* invariance, B^- decays are *CP* conjugated and treated as $B^+ \to \psi(2S)K^+\pi^+\pi^-$ decays.

The signal PDF is built from the total amplitude-squared as

$$\mathcal{P}_S(\mathbf{x}) = \frac{|\mathcal{A}_{B^+}(\mathbf{x})|^2\,\epsilon(\mathbf{x})\,\phi(\mathbf{x})}{\int |\mathcal{A}_{B^+}(\mathbf{x})|^2\,\epsilon(\mathbf{x})\,{\rm d}\Phi}, \tag{5.2}$$

where $\epsilon(\mathbf{x})$ describes the efficiency variation across the phase space. As the efficiency in the numerator leads to an additive constant in the $\log\mathcal{L}(\theta)$ function that does not depend on any fit parameters, it can be neglected in the minimisation procedure. The efficiency function still enters via the normalisation integral, which is evaluated with the Monte Carlo (MC) integration technique [47, 64–66] using simulated events that have been propagated through the full LHCb detector simulation and selection. The size of the fully selected MC integration sample is more than 20 times larger than the data sample. Since the invariant-mass resolution is much smaller than the decay widths of all considered resonances, resolution effects are neglected in the amplitude fit.

Candidates in the $m(\psi(2S)K^+\pi^-\pi^+)$ sideband regions, which are defined as $[5200, 5240]\,{\rm MeV} \cup [5320, 5400]\,{\rm MeV}$, are used to model the background PDF,

$$\mathcal{P}_{\rm B}(\mathbf{x}|\theta_{\rm B}) = \frac{B(\mathbf{x}|\theta_{\rm B})\,\epsilon(\mathbf{x})\,\phi(\mathbf{x})}{\int B(\mathbf{x}|\theta_{\rm B})\,\epsilon(\mathbf{x})\,{\rm d}\Phi}. \tag{5.3}$$

The background function $B(\mathbf{x}|\theta_{\rm B})$ describes the distribution in phase space relative to the signal efficiency times phase-space density term, which is ommitted in the numerator as in the signal PDF. Candidates from the low- and high-mass sidebands are added together such that they have the same relative contribution. The background function is constructed by training a BDTG algorithm [67] to match the phase-space distribution of the MC integration sample to the data sidebands. The value of $B(\mathbf{x}_i|\theta_{\rm B})$ for a given data point $\mathbf{x}_i$ is then obtained by applying a pseudo seven-dimensional interpolation method to the weighted MC integration sample [68].

5.1 Signal model selection

The strange-meson spectrum comprises an abundance of resonances potentially contributing to $B^+ \to \psi(2S)K^+\pi^+\pi^-$ decays in various topologies and angular-momentum configurations. Several conventional charmonium states with masses within the phase-space limit also need to be considered. A multitude of hidden-charm exotic states might contribute as well. The full list of considered intermediate-state amplitudes can be found in appendix B.

JHEP01(2025)054

With the number of possible amplitudes of the order of 100, it is not feasible to fit them all at once and a reasonably sized subset is chosen to avoid overfitting. An algorithmic model-building procedure is employed that starts with a small set of amplitudes (*start* model), which are expected to contribute, and successively adds amplitudes until a reasonable agreement between the data and fit is achieved. The quality of the fit in the seven-dimensional phase space is quantified by binning the data and calculating the metric

$$\chi^2 = \sum_{i=1}^{N_{\text{bins}}} \frac{(N_i - \hat{N}_i)^2}{\sigma_i^2 + \hat{\sigma}_i^2}, \tag{5.4}$$

where N_i is the number of selected candidates in a given bin, $\hat{N}_i$ is the event count predicted by the fitted amplitude model and N_{bins} is the number of bins. The uncertainties are given by $\sigma_i^2 = N_i$ and $\hat{\sigma}_i^2 = \sum_{j \in \text{bin}\, i} w_j^2$, where the weights w_j match the MC integration sample to the fitted PDF. A robust χ^2 calculation is ensured by employing an adaptive binning algorithm [69]. The phase space is divided such that each bin is populated by at least 25 candidates (N_{bins}=1091) leading to smaller hyper-volumes in regions of high event density. The χ^2 value divided by the number of degrees of freedom, $\nu = N_{\text{bins}} - 1 - N_{\text{par}}$ where N_{par} is the number of free fit parameters, should be close to unity. Individual amplitudes are added one-by-one to the *start* model and the set of new models is fitted to the data. The amplitude that improves the χ^2/ν value the most is kept and added to the *start* model. The remaining amplitudes are tested again in the subsequent loop until the incremental improvement in fit quality falls below the threshold $\Delta\chi^2/\nu = 0.02$ [68, 70].

Initially, only conventional hadron states are considered. The model-building algorithm improves the χ^2/ν value from 2.54 to 2.05. While this is a significant improvement with respect to the *start* model, the fit quality is still poor. The amplitudes included in this *no-exotics* model are detailed in appendix C along with fit projections. The largest discrepancy in the data description is observed for the $\psi(2S)\pi^+\pi^-$ invariant-mass distribution. The masses and widths of all resonances are fixed to their external values (cf. appendix B); determining them from the fit marginally improves the fit quality by $\Delta\chi^2/\nu = 0.08$ but does not change the conclusion that nonconventional hadron contributions are needed to describe the data.

As a next step, the model-building procedure is repeated from scratch with the inclusion of the previously observed exotic resonances listed in appendix B, which could potentially contribute to the $\psi(2S)\pi^+\pi^-$, $\psi(2S)\pi^\pm$ or $\psi(2S)K^+$ subsystems. The χ^2/ν value is improved to 1.31 and the description of the $\psi(2S)\pi^+\pi^-$ invariant-mass distribution is notably better. Fit projections and amplitude model details are given in appendix C. This *known-exotics* model includes four $X^0 \to \psi(2S)\pi^+\pi^-$ states and the $T_{c\bar{c}s1}(4000)^+ \to \psi(2S)K^+$ state observed in $B^+ \to J/\psi\phi K^+$ decays [10]. The $\psi(2S)\pi^+$ system is described primarily by two axial vector contributions, $T_{c\bar{c}1}(4200)^+$ and $T_{c\bar{c}1}(4430)^+$, with smaller contributions from two vector states, $T^*_{c\bar{c}1}(4055)^+$ and $T^*_{c\bar{c}}(4100)^+$. This fit also determines the mass and width of the four X^0 states and the two axial vector $\psi(2S)\pi^+$ states. Fitting any other resonance's mass and width does not improve the fit result, thus they remain fixed to the external values given in appendix B.

As some disagreements between fit and data remain, especially in the $m(\psi(2S)K^+\pi^-)$ projection, we explored adding additional $T^0_{c\bar{c}s} \to \psi(2S)K^+\pi^-$ exotic contributions of various quantum numbers. For a given new $T^0_{c\bar{c}s}$ resonance hypothesis, likelihood scans over the

JHEP01(2025)054

allowed m_0 mass range are performed with the width fixed to $\Gamma_0 = \{50, 100, 200\}$ MeV. Local minima in the likelihood profiles are identified and used to create a pool of potential new states and quantum number assignments. Subsequent iterations of the model-building algorithm add one of these states until the convergence criterion is reached. The initial values for the mass and width of new states are set based on the likelihood scans but are floating in the fits. This procedure adds three new $T^0_{c\bar{c}s} \to \psi(2S)K^+\pi^-$ states. Additional new $X^0 \to \psi(2S)\pi^+\pi^-$, $T^{++}_{c\bar{c}s} \to \psi(2S)K^+\pi^+$, $T^{\pm}_{c\bar{c}} \to \psi(2S)\pi^\pm$ or $T^{+}_{c\bar{c}s} \to \psi(2S)K^+$ contributions do not lead to significant improvements in the description of the data, but are considered in alternative models for studies of systematic uncertainties. Lastly, we prune the model by removing four insignificant amplitudes. The resulting model is henceforth referred to as the *baseline* model.

5.2 Baseline model results

The *baseline* model consists of 53 amplitudes, has 98 free parameters and achieves a χ^2/ν (χ^2/N_{bins}) value of 1.21 (1.10). From pseudoexperiments, we estimate that this corresponds to a p-value of 0.002 (3.1σ) before accounting for systematic uncertainties. Figure 2 displays the fit projections. The fit fractions are given in tables 1 and 2. Fit results for the amplitude coefficients and interference fractions can be found in appendix D. Six $K'^+ \to K^+\pi^+\pi^-$ resonances are included that decay via $K^*(892)^0\pi^+$, $K^+\rho(770)^0$ or S-wave intermediate states. The largest conventional hadron contribution comes from the $K_1(1270)^+$ resonance produced in S-, P- and D-wave B^+ decays. The extracted branching fractions of the $K_1(1270)^+$ resonant substructure agrees well with other measurements as detailed in appendix E. The first subleading component arises from $K^*(1680)^+$ decays. The $K_1(1270)^+$ and $K^*(1680)^+$ are the only two resonances included in the $B^+ \to \psi(2S)K^+\pi^+\pi^-$ analysis by Belle [13]. In addition, we observe $K_1(1400)^+, K^*(1410)^+, K^*_2(1430)^+$ and $K(1460)^+$ decays. No other established strange resonances exist within the kinematic limit of the decay.

The *baseline* model includes only one conventional charmonium resonance, $\psi(4360)$, with a subpercent fit fraction. Two other charmonium resonances included in the *no-exotics* model, $\psi(4415)$ and $\psi(4660)$, are no longer significant after considering exotic contributions. The masses and widths of the conventional hadrons are fixed to external measurements. Floating these parameters does not significantly improve the fit quality for any resonance ($\Delta\chi^2/\nu < 0.01$). In total, four $X^0 \to \psi(2S)\pi^+\pi^-$, three $T^{\pm}_{c\bar{c}} \to \psi(2S)\pi^\pm$, one $T^{+}_{c\bar{c}s} \to \psi(2S)K^+$ and three $T^0_{c\bar{c}s} \to \psi(2S)K^+\pi^-$ components are part of the *baseline* model. Exotic resonance parameters are floated in the fit except for those of the $T^*_{c\bar{c}1}(4055)^+$ and $T_{c\bar{c}s1}(4000)^+$ states. The $T^*_{c\bar{c}1}(4055)^+$ state has a small fit fraction with mass and width well-constrained from external measurements [32]. Since the pole mass of the $T_{c\bar{c}s1}(4000)^+$ state lies outside of the phase-space boundaries, the fit is not sensitive to its mass and width values. Exotic cascade decays of the type $X^0 \to T^{\pm}_{c\bar{c}}\pi^\mp$ are assumed to be charge symmetric, i.e. the magnitudes of the amplitude coefficients are equal for $X^0 \to T^{+}_{c\bar{c}}\pi^-$ and $X^0 \to T^{-}_{c\bar{c}}\pi^+$ decays. For the relative phase, we test 0 and π for each X^0 resonance separately and select the one that gives the larger likelihood value. Table 3 lists the measured masses and widths, quantum numbers and significance of all exotic states.

The significance is determined from a likelihood-ratio test. A given resonance is removed from the model (this might correspond to several amplitudes) and a new fit is performed. From the change of the likelihood value, $\Delta(-2\ln\mathcal{L})$, we compute the signif-

JHEP01(2025)054

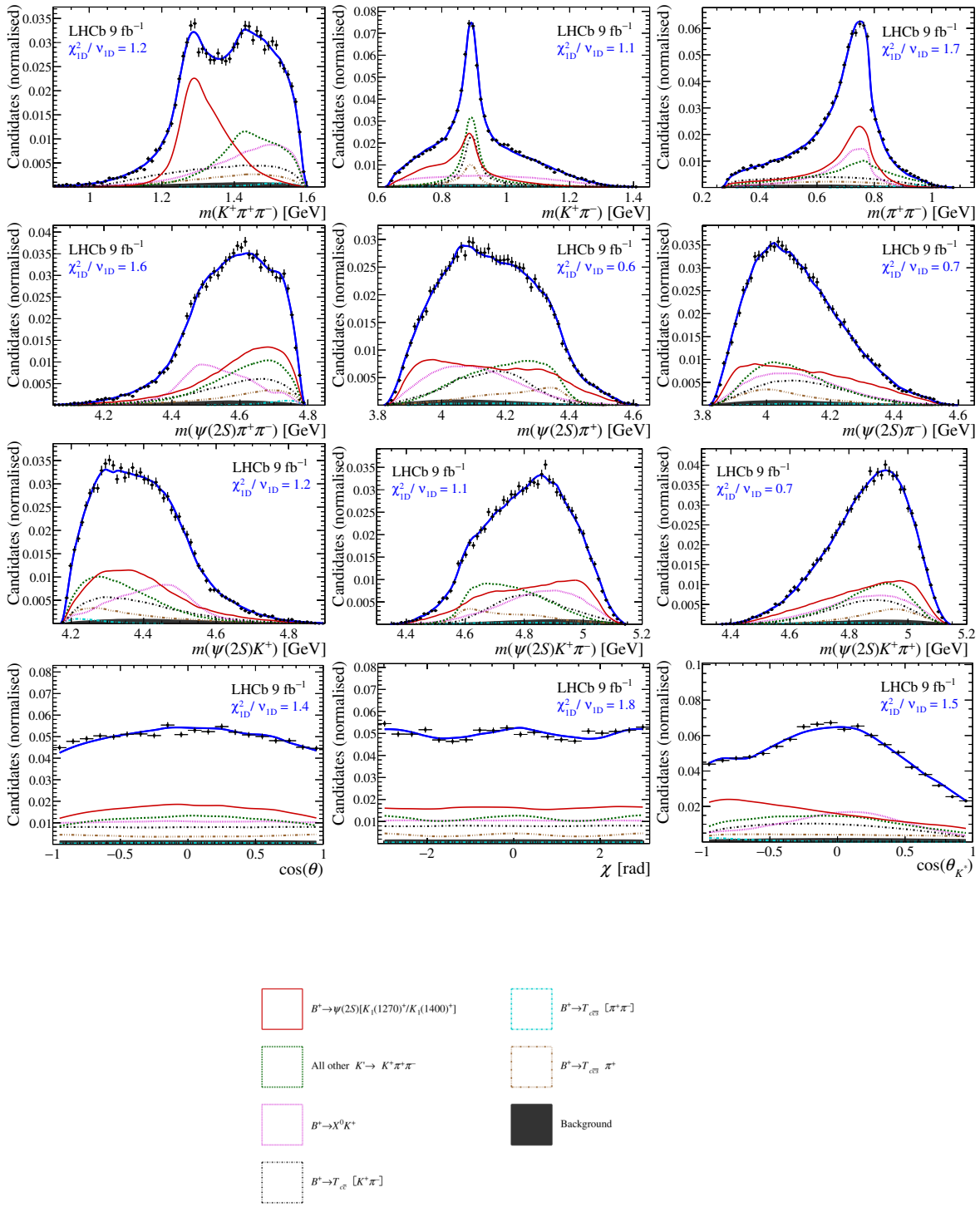

Figure 2. Phase-space projections of $B^+ \to \psi(2S)K^+\pi^+\pi^-$ candidates in the signal region (points with error bars) and fit projections (solid, blue line) for the *baseline* model. The displayed χ^2_{1D}/ν_{1D} value on each projection gives the sum of squared normalised residuals divided by the number of bins minus one. The multidimensional χ^2 value is $\chi^2/\nu = 1.20$ with $\nu = 992$.

JHEP01(2025)054

icance as $n_\sigma = \sqrt{2}\,\mathrm{erfc}^{-1}(\mathrm{Prob}_{\chi^2}(\Delta(-2\ln\mathcal{L}),\mathrm{ndf}))$, where $\mathrm{Prob}_{\chi^2}(\Delta(-2\ln\mathcal{L}),\mathrm{ndf}))$ is the chi-squared distribution and erfc^{-1} is the inverse error function converting the p-value into Gaussian standard deviations. This assumes that $\Delta(-2\ln\mathcal{L})$ follows a chi-squared distribution under the null hypothesis (i.e. the resonance is not present in the data). If the mass and width are fixed, the effective number of degrees of freedom, ndf, is set to the number of additional fit parameters under the hypothesis that the resonance exists, ΔN_{par}. Otherwise, we set it to $\mathrm{ndf} = 2\Delta N_{\mathrm{par}}$ [8, 10]. This method is verified to be conservative through the use of pseudoexperiments. The statistical significance of all exotic states is above 8 standard deviations (σ) and stays above 7σ when considering systematic uncertainties (see section 5.3).

To verify the nominal quantum-number assignment of the exotic states, fits are performed under alternative spin-parity hypotheses with spin up to 2. The likelihood-ratio test is used to quantify the rejection of these hypotheses. For all exotic states that are part of the *baseline* model, every alternative spin-parity hypothesis is excluded by more than 8σ.

The largest exotic contribution comes from the scalar resonance $T^*_{c\bar{c}0}(4475)^0$, which predominantly decays as $T^*_{c\bar{c}0}(4475)^0 \to \psi(2S)\rho(770)^0$. Its mass agrees well with the $\chi_{c0}(4500)$ state observed in the decay $\chi_{c0}(4500) \to J/\psi\phi$ [10], however it is significantly broader. Note that the Breit-Wigner parameters are known to be highly model-dependent and the two measurements take different partial decay widths as the total decay width ($T^*_{c\bar{c}0}(4475)^0 \to \psi(2S)\pi^+\pi^-$ versus $\chi_{c0}(4500) \to J/\psi\phi$). This is compounded by the fact that the $T^*_{c\bar{c}0}(4475)^0$ or $\chi_{c0}(4500)$ masses are close to the $\psi(2S)\rho(770)^0$ threshold, which can significantly distort the lineshapes. A possible explanation of the disagreeing decay widths might thus be that coupled-channel effects are not accounted for in either measurement. The $B^+ \to J/\psi\phi K^+$ analysis also includes a huge nonresonant $J/\psi\phi$ 0^+ component that makes the comparison less straightforward. Adding an equivalent nonresonant $\psi(2S)\rho(770)^0$ 0^+ component to the *baseline* model results in a small fit fraction, $(0.48 \pm 0.36)\%$, and decreases the $T^*_{c\bar{c}0}(4475)^0$ decay width by 16 MeV. Assuming isospin conservation in strong decays, we interpret these as genuinely different states in the following, with the $T^*_{c\bar{c}0}(4475)^0$ state having isospin $I = 1$ and the $\chi_{c0}(4500)$ state having $I = 0$, as indicated by their decay modes $\psi(2S)\rho(770)^0$ and $J/\psi\phi$. However, if the $T^*_{c\bar{c}0}(4475)^0$ state were the $c\bar{c}(d\bar{d} - u\bar{u})$ isospin partner of the $\chi_{c0}(4500)$ interpreted as $c\bar{c}s\bar{s}$, one would generally expect a larger mass difference of $m_{\chi_{c0}(4500)} - m_{T^*_{c\bar{c}0}(4475)^0} \approx +200$ MeV.

The $T_{c\bar{c}1}(4650)^0$ and $T^*_{c\bar{c}0}(4710)^0$ states agree within uncertainties with the $\chi_{c1}(4685)$ and $\chi_{c0}(4700)$ resonances observed in $B^+ \to J/\psi\phi K^+$ decays [10]. Nevertheless, for them to be identical would require a significant isospin violating effect, which seems implausible. The mass and the width of the $T^*_{c\bar{c}1}(4800)^0$ vector state are not well constrained due to its proximity to the phase-space limit. Within the large uncertainties, the $T^*_{c\bar{c}1}(4800)^0$ resonance parameters are loosely compatible with the $X(4630)^0$ resonance observed in $B^+ \to J/\psi\phi K^+$ decays [10]. However, the quantum numbers of the $X(4630)^0$ resonance are not yet unambiguously determined. The $J^P = 1^-$ assignment for $X(4630)^0$ is favoured over $J^P = 2^-$ with a significance of 3σ and other assignments are disfavoured by more than 5σ [10].

A large axial vector component in the $\psi(2S)\pi^+$ system is described by two resonances, $T_{c\bar{c}1}(4200)^+$ and $T_{c\bar{c}1}(4430)^+$. They are predominantly produced in the quasi-two-body topology, $B^+ \to T^+_{c\bar{c}}K^*(892)^0$ and $B^+ \to T^+_{c\bar{c}}[K^+\pi^-]_S$, but are also seen in $X^0 \to T^\pm_{c\bar{c}}\pi^\mp$ and $T^0_{c\bar{c}\bar{s}} \to T^-_{c\bar{c}}K^+$ cascade decays. This is the first observation of production modes other than

JHEP01(2025)054

$B^0 \to T^-_{c\bar{c}} K^+$. The mass and width of the $T_{c\bar{c}1}(4430)^+$ agree well with those measured in $\overline{B}^0 \to \psi(2S)K^-\pi^+$ decays [8, 9]. The second, lighter, axial vector state is compatible with the one reported in the Belle analysis of $\overline{B}^0 \to J/\psi K^-\pi^+$ decays [71], where $J^P = 1^+$ is preferred over $J^P = 2^-$ by 4.4σ and other assignments are excluded. The LHCb analysis of the $\overline{B}^0 \to \psi(2S)K^-\pi^+$ decay indicated a similar structure in the 0^- or 1^+ $\psi(2S)\pi^+$ wave [8]. The $T_{c\bar{c}1}(4200)^+$ state also has similar mass and width to the $T_{c\bar{c}}(4250)^+$ state reported in a Belle analysis of $\overline{B}^0 \to \chi_{c1}(1P)K^-\pi^+$ decays [72], where $J = 0$ is the default assumption, though $J = 1$ cannot be excluded. This is the first time that the $J^P = 1^+$ assignment for the $T_{c\bar{c}1}(4200)^+$ has been unambiguously demonstrated.

A subpercent level contribution from a vector state, $T^*_{c\bar{c}1}(4055)^+$, is also observed. The mass and width of this state are fixed to the parameters of the $T_{c\bar{c}}(4055)^+$ state seen in the reaction $e^+e^- \to \gamma\psi(2S)\pi^+\pi^-$ [73]. A similar structure has been reported in $\overline{B}^0 \to \chi_{c1}(1P)K^-\pi^+$ ($T_{c\bar{c}}(4050)^+$ [72]) and $\overline{B}^0 \to \eta_{c1}(1S)K^-\pi^+$ ($T_{c\bar{c}}(4100)^+$ [74]) decays. None of those measurements determined the quantum numbers. No stable fit results are obtained when floating the $T^*_{c\bar{c}1}(4055)^+$ resonance parameters. This might be due to the existence of several small 1^- $\psi(2S)\pi^+$ wave contributions that cannot be resolved with the current statistical precision or by residual model deficiencies of the other partial waves being absorbed into the $T^*_{c\bar{c}1}(4055)^+$ description. Thus the high significance of the $T^*_{c\bar{c}1}(4055)^+$ component should not be considered as a confirmation of a specific state but rather an effective description of a generic 1^- $\psi(2S)\pi^+$ wave contribution.

The baseline model includes the high-mass tail of the $T_{c\bar{c}\bar{s}1}(4000)^+$ resonance observed in $B^+ \to J/\psi\phi K^+$ decays [10]. As alternative models, we replaced the $T_{c\bar{c}\bar{s}1}(4000)^+$ by the $T_{c\bar{c}\bar{s}1}(4220)^+$ assuming it to be an axial vector or vector state. Both hypotheses are disfavoured by more than 5σ. Replacing the $T_{c\bar{c}\bar{s}1}(4000)^+$ state by a nonresonant component with an exponential lineshape, $\exp\left(-\alpha\, m^2(\psi(2S)K^+)\right)$, is also disfavoured by more than 5σ. Nonetheless, the results of this analysis should not be considered as an independent confirmation of the $T_{c\bar{c}\bar{s}1}(4000)^+$ state as no sufficient sensitivity to the mass and width values is achieved. All $T^0_{c\bar{c}\bar{s}} \to \psi(2S)K^+\pi^-$ states are previously unobserved states. If interpreted as tetraquark states, their minimal quark content would be $c\bar{c}\bar{s}d$. The $T_{c\bar{c}\bar{s}1}(4600)^0$ and $T_{c\bar{c}\bar{s}1}(4900)^0$ could be radial excitations of the 1^+ $T_{c\bar{c}\bar{s}1}(4000)^0 \to J/\psi K^0_S$ resonance, for which evidence was found in $B^0 \to J/\psi\phi K^0_S$ decays [75].

The *baseline* model features two broad vector resonances that lie at the edges of the phase space, $T^*_{c\bar{c}1}(4800)^0$ and $T^*_{c\bar{c}\bar{s}1}(5200)^0$. For these states, we perform an additional significance test comparing the Breit-Wigner lineshape hypothesis against a nonresonant hypothesis with exponential lineshape. The Breit-Wigner hypothesis is favoured by 5.4σ for the $T^*_{c\bar{c}1}(4800)^0$ and 2.6σ for the $T^*_{c\bar{c}\bar{s}1}(5200)^0$. The proximity to the phase-space boundaries and large uncertainties make the interpretation of these components as genuine resonances challenging. Without independent confirmation of these states from other measurements, they should be considered an effective description of several $J^P = 1^-$ contributions (within or outside the $B^+ \to \psi(2S)K^+\pi^+\pi^-$ phase space) that cannot be disentangled with the existing data.

The resonant nature of the exotic states is probed using a quasi-model-independent partial-wave analysis (QMIPWA) [8, 76]. The nominal Breit-Wigner lineshape of a given resonance is replaced by a parameterisation that treats the magnitude and phase of the

JHEP01(2025)054

Decay channel	Fit fraction [%]
$B^+ \to T^*_{c\bar{c}0}(4475)^0 K^+$	$18.45 \pm 1.31 \pm 2.92$
$B^+ \to \psi(2S)\, K^*(1680)^+$	$8.15 \pm 1.31 \pm 3.51$
$B^+ \to \psi(2S)\, K_1(1270)^+$	$7.60 \pm 0.85 \pm 1.35$
$B^+[P] \to \psi(2S)\, K_1(1270)^+$	$7.52 \pm 0.60 \pm 1.08$
$B^+[D] \to \psi(2S)\, K_1(1270)^+$	$6.81 \pm 0.45 \pm 1.18$
$B^+ \to \psi(2S)\, K_1(1400)^+$	$5.78 \pm 0.62 \pm 0.92$
$B^+ \to \psi(2S)\, K(1460)^+$	$5.26 \pm 0.48 \pm 0.87$
$B^+[P] \to T_{c\bar{c}1}(4200)^+\, K^*(892)^0$	$4.60 \pm 0.54 \pm 2.17$
$B^+ \to T_{c\bar{c}s1}(4600)^0 \pi^+$	$4.42 \pm 0.98 \pm 2.17$
$B^+ \to K^*_2(1430)^+ \psi(2S)$	$4.35 \pm 0.29 \pm 0.26$
$B^+ \to T_{c\bar{c}1}(4200)^+\, K^*(892)^0$	$4.02 \pm 0.88 \pm 1.01$
$B^+ \to T_{c\bar{c}1}(4430)^+\, [K^+\pi^-]_S$	$3.41 \pm 0.54 \pm 0.78$
$B^+ \to T^*_{c\bar{c}1}(4800)^0 K^+$	$3.24 \pm 0.50 \pm 0.79$
$B^+ \to T_{c\bar{c}1}(4650)^0 K^+$	$2.89 \pm 0.45 \pm 0.45$
$B^+[D] \to T_{c\bar{c}1}(4200)^+\, K^*(892)^0$	$2.78 \pm 0.33 \pm 0.61$
$B^+ \to T_{c\bar{c}s1}(4900)^0 \pi^+$	$2.60 \pm 0.66 \pm 1.94$
$B^+[D] \to \rho(770)^0\, T_{c\bar{c}s1}(4000)^+$	$2.06 \pm 0.22 \pm 0.84$
$B^+ \to \psi(2S)\, K^*(1410)^+$	$1.79 \pm 0.35 \pm 0.74$
$B^+ \to T^*_{c\bar{c}0}(4710)^0 K^+$	$1.73 \pm 0.28 \pm 0.40$
$B^+ \to T^*_{c\bar{c}s1}(5200)^0 \pi^+$	$1.59 \pm 0.46 \pm 0.61$
$B^+ \to T_{c\bar{c}s1}(4000)^+\, [\pi^+\pi^-]_S$	$1.24 \pm 0.23 \pm 0.34$
$B^+ \to T_{c\bar{c}1}(4430)\, K^*(892)^0$	$0.75 \pm 0.43 \pm 2.24$
$B^+ \to \psi(4360) K^+$	$0.64 \pm 0.14 \pm 0.12$
$B^+ \to T^*_{c\bar{c}1}(4055)\, K^*(892)^0$	$0.52 \pm 0.10 \pm 0.11$
$B^+[P] \to \psi(2S)\, K_1(1400)^+$	$0.48 \pm 0.18 \pm 0.40$
Sum B^+	$102.69 \pm 4.40 \pm 7.41$

Table 1. Fit fractions of the intermediate-state amplitudes contributing to $B^+ \to \psi(2S)K^+\pi^+\pi^-$ decays for the *baseline* model. The uncertainties are statistical and systematic. The systematic uncertainties are dominated by the choice of amplitude components. The states $T^*_{c\bar{c}1}(4800)^0, T^*_{c\bar{c}s1}(5200)^0$, $T_{c\bar{c}s1}(4000)^+$ and $T^*_{c\bar{c}1}(4055)^+$ should be considered as effective descriptions of generic partial wave contributions due to insufficient sensitivity of the amplitude fit.

lineshape at eight discrete positions in the invariant-mass region around the nominal mass as independent pairs of free parameters to be determined by the fit. The lineshape is then modelled elsewhere by interpolating between these values using cubic splines [77]. The Argand diagrams for the largest $X^0 \to \psi(2S)\pi^+\pi^-$, $T^0_{c\bar{c}s} \to \psi(2S)K^+\pi^-$ and $T^\pm_{c\bar{c}} \to \psi(2S)\pi^\pm$ components are shown in figure 3 and demonstrate a counter-clockwise circular phase motion as expected from a resonance. More details and QMIPWA studies of the other exotic states are given in appendix F.

JHEP01(2025)054

Decay channel	Partial fit fraction $f_j^{R_j}$ [%]
$K_1(1270)^+ \to \rho(770)^0 K^+$	50.71± 2.18± 3.19
$K_1(1270)^+ \to K^*(892)^0 \pi^+$	19.86± 1.44± 2.05
$K_1(1270)^+ \to [K^+\pi^-]_S \, \pi^+$	11.35± 1.45± 2.11
$K_1(1270)^+[D] \to K^*(892)^0 \pi^+$	8.32± 0.85± 1.54
Sum $K_1(1270)^+$	90.24± 1.83± 3.67
$K_1(1400)^+ \to K^*(892)^0 \pi^+$	86.80± 3.78± 5.34
$K_1(1400)^+ \to \rho(770)^0 K^+$	22.08± 4.40± 6.25
Sum $K_1(1400)^+$	108.88± 0.82± 1.84
$K(1460)^+ \to [\pi^+\pi^-]_S \, K^+$	45.13± 4.22±10.91
$K(1460)^+ \to K^*(892)^0 \pi^+$	35.41± 4.08± 9.72
Sum $K(1460)^+$	80.54± 0.67± 3.66
$K_2^*(1430)^+ \to K^*(892)^0 \pi^+$	76.70± 3.04± 2.43
$K_2^*(1430)^+ \to \rho(770)^0 K^+$	12.71± 2.30± 1.80
Sum $K_2^*(1430)^+$	89.41± 0.75± 0.66
$K^*(1410)^+ \to K^*(892)^0 \pi^+$	88.50± 8.39±12.65
$K^*(1410)^+ \to \rho(770)^0 K^+$	38.36±10.46±19.07
Sum $K^*(1410)^+$	126.86± 4.83±13.38
$K^*(1680)^+ \to K^*(892)^0 \pi^+$	49.69± 6.72±13.32
$K^*(1680)^+ \to \rho(770)^0 K^+$	31.16± 6.11±11.27
Sum $K^*(1680)^+$	80.85± 0.64± 3.89
$T^*_{c\bar{c}0}(4475)^0 \to \rho(770)^0 \psi(2S)$	99.04± 0.49± 1.66
$T^*_{c\bar{c}0}(4475)^0 \to T_{c\bar{c}1}(4200)^- \pi^+$	0.50± 0.25± 0.39
$T^*_{c\bar{c}0}(4475)^0 \to T_{c\bar{c}1}(4200)^+ \pi^-$	0.50± 0.25± 0.39
Sum $T^*_{c\bar{c}0}(4475)^0$	100.03± 0.02± 1.42
$T_{c\bar{c}1}(4650)^0 \to \rho(770)^0 \psi(2S)$	86.66± 7.85± 8.49
$T_{c\bar{c}1}(4650)^0 \to T_{c\bar{c}1}(4200)^- \pi^+$	6.62± 2.03± 2.46
$T_{c\bar{c}1}(4650)^0 \to T_{c\bar{c}1}(4200)^+ \pi^-$	6.61± 2.03± 2.47
Sum $T_{c\bar{c}1}(4650)^0$	99.89± 7.37± 7.56
$T^*_{c\bar{c}0}(4710)^0 \to \rho(770)^0 \psi(2S)$	92.35±10.83±15.11
$T^*_{c\bar{c}0}(4710)^0 \to T_{c\bar{c}1}(4430)^+ \pi^-$	17.00± 3.82± 3.38
$T^*_{c\bar{c}0}(4710)^0 \to T_{c\bar{c}1}(4430)^- \pi^+$	17.00± 3.82± 3.37
Sum $T^*_{c\bar{c}0}(4710)^0$	126.35±10.56±14.40
$T^*_{c\bar{c}1}(4800)^0 \to \rho(770)^0 \psi(2S)$	41.52± 5.19±10.44
$T^*_{c\bar{c}1}(4800)^0 \to T_{c\bar{c}1}(4200)^- \pi^+$	18.03± 5.14± 6.59
$T^*_{c\bar{c}1}(4800)^0 \to T_{c\bar{c}1}(4200)^+ \pi^-$	18.03± 5.14± 6.58
$T^*_{c\bar{c}1}(4800)^0 \to T_{c\bar{c}1}(4430)^+ \pi^-$	5.44± 2.45± 2.29
$T^*_{c\bar{c}1}(4800)^0 \to T_{c\bar{c}1}(4430)^- \pi^+$	5.44± 2.45± 2.29
Sum $T^*_{c\bar{c}1}(4800)^0$	88.47±11.26±13.07
$T_{c\bar{c}\bar{s}1}(4600)^0 \to \psi(2S) \, K^*(892)^0$	50.87± 7.79±11.55
$T_{c\bar{c}\bar{s}1}(4600)^0 \to T_{c\bar{c}1}(4200)^- K^+$	16.53± 3.79±12.75
$T_{c\bar{c}\bar{s}1}(4600)^0 \to T_{c\bar{c}\bar{s}1}(4000)^+ \pi^-$	9.84± 3.28± 5.34
Sum $T_{c\bar{c}\bar{s}1}(4600)^0$	77.23± 5.22±17.80
$T^*_{c\bar{c}\bar{s}1}(5200)^0 \to \psi(2S) \; [K^+\pi^-]_S$	66.28±15.03±17.35
$T^*_{c\bar{c}\bar{s}1}(5200)^0 \to T_{c\bar{c}\bar{s}1}(4000)^+ \pi^-$	9.37±14.12±13.23
Sum $T^*_{c\bar{c}\bar{s}1}(5200)^0$	75.65± 9.18±13.39
$T_{c\bar{c}\bar{s}1}(4900)^0 \to \psi(2S) \, K^*(892)^0$	100
$\psi(4430) \to \psi(2S) \; [\pi^+\pi^-]_S$	100

Table 2. Partial fit fractions of the cascade decays contributing to $B^+ \to \psi(2S)K^+\pi^+\pi^-$ decays for the *baseline* model. The uncertainties are statistical and systematic. The systematic uncertainties are dominated by the choice of amplitude components. The states $T^*_{c\bar{c}1}(4800)^0, T^*_{c\bar{c}\bar{s}1}(5200)^0$, $T_{c\bar{c}\bar{s}1}(4000)^+$ and $T^*_{c\bar{c}1}(4055)^+$ should be considered as effective descriptions of generic partial wave contributions due to insufficient sensitivity of the amplitude fit.

JHEP01(2025)054

Resonance	J^P	m_0 [MeV]	Γ_0 [MeV]	$\Delta(-2\ln\mathcal{L})$	$\Delta N_{\rm par}$	Sign. [σ]	Res. PDG	m_0 [MeV]	Γ_0 [MeV]
$T^*_{c\bar{c}0}(4475)^0$	0^+	4475± 7 ±12	231±19±32	675	6	> 20 (19)	$\chi_{c0}(4500)$	4474±4	77^{+12}_{-10}
$T_{c\bar{c}1}(4650)^0$	1^+	4653±14±27	227±26±22	286	6	15 (13)	$\chi_{c1}(4685)$	4684^{+15}_{-17}	126±40
$T^*_{c\bar{c}0}(4710)^0$	0^+	4710± 4 ±5	64± 9 ±10	255	6	14 (10)	$\chi_{c0}(4700)$	4694^{+16}_{-5}	87^{+18}_{-10}
$T^*_{c\bar{c}1}(4800)^0$	1^-	4785±37±119	457±93±157	382	8	17 (12)	$X(4630)$	4626^{+24}_{-110}	174^{+140}_{-80}
$T^*_{c\bar{c}1}(4055)^+$	1^-	4054 (fixed)	45 (fixed)	81	2	8 (7)	$T_{c\bar{c}}(4055)^+$	4054±3.2	45±13
$T_{c\bar{c}1}(4200)^+$	1^+	4257±11±17	308±20±32	842	16	> 20 (> 20)	$T_{c\bar{c}1}(4200)^+$	4196^{+35}_{-32}	370^{+100}_{-150}
$T_{c\bar{c}1}(4430)^+$	1^+	4468±21±80	251±42±82	305	10	15 (8)	$T_{c\bar{c}1}(4430)^+$	4478^{+15}_{-18}	181±31
$T_{c\bar{c}\bar{s}1}(4600)^0$	1^+	4578±10±18	133±28±69	287	8	15 (12)			
$T_{c\bar{c}\bar{s}1}(4900)^0$	1^+	4925±22±47	255±55±127	177	4	12 (8)			
$T^*_{c\bar{c}\bar{s}1}(5200)^0$	1^-	5225±86±181	226±76±374	149	6	10 (8)			
$T_{c\bar{c}\bar{s}1}(4000)^+$	1^+	4003 (fixed)	131 (fixed)	597	4	> 20 (14)	$T_{c\bar{c}\bar{s}1}(4000)^+$	4003^{+7}_{-15}	131±30

Table 3. Left: resonance parameters determined from the fit and the significance of the resonance, where the uncertainties are statistical and systematic. The significances are evaluated accounting for statistical (total) uncertainties. Right: if available, the states listed in the Particle Data Group (PDG) [32] with the same J^P quantum numbers and closest mass are listed for comparison. The states $T^*_{c\bar{c}1}(4800)^0, T^*_{c\bar{c}\bar{s}1}(5200)^0$, $T_{c\bar{c}\bar{s}1}(4000)^+$ and $T^*_{c\bar{c}1}(4055)^+$ should be considered as effective descriptions of generic partial wave contributions due to insufficient sensitivity of the amplitude fit.

JHEP01(2025)054

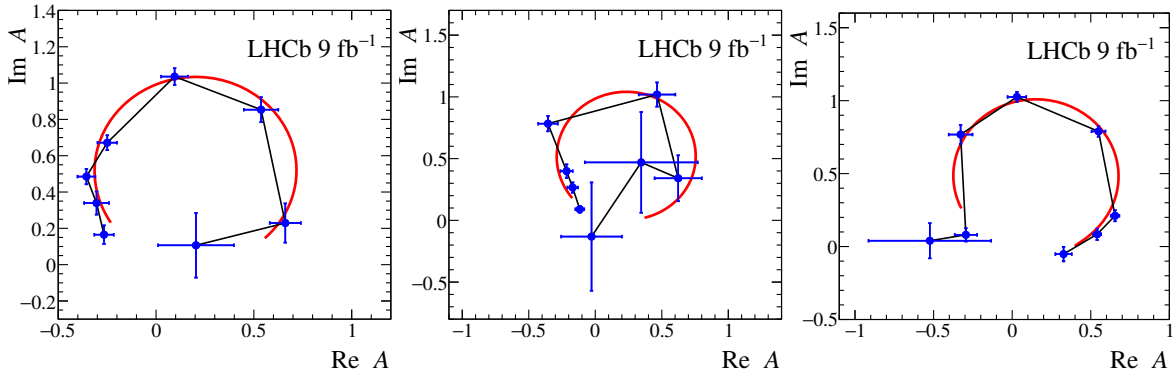

Figure 3. Argand diagram for the quasi-model-independent partial-wave analysis for the (left) $T^{*}_{c\bar{c}0}(4475)^0$, (middle) $T_{c\bar{c}\bar{s}1}(4600)^0$, and (right) $T_{c\bar{c}1}(4200)^{\pm}$ resonances. The fitted lineshape knots are displayed as connected points with error bars and the invariant mass increases counterclockwise. The Breit-Wigner lineshape with the mass and width from the nominal fit is superimposed (red line).

5.3 Systematic uncertainties

Several sources of systematic uncertainty are considered. Experimental issues are discussed first, followed by uncertainties related to the amplitude model and formalism. The overall fit procedure is tested by generating pseudoexperiments from the *baseline* fit model using the measured values and subsequently fitting them with the same model. For each pseudoexperiment and fit parameter, a pull is calculated by dividing the difference between the fitted and generated values by the statistical uncertainty. The means of the pull distributions are assigned as systematic uncertainties due to an intrinsic fit bias.

The treatment of the phase-space acceptance relies on simulated data. The integration error due to the limited size of the simulated sample used to normalise the signal PDF is estimated by bootstrapping the simulated sample. The standard deviation of the fit results is assigned as systematic uncertainty. To assess the uncertainty due to possible data-simulation differences, alternative phase-space acceptances are derived by varying the selection requirements, for the simulated sample only, on quantities that are expected not to be well described by the simulation. This includes the trigger [78] and tracking efficiencies [79], as well as the particle identification [80, 81] and multivariate selection classifier performances.

The uncertainty of the background fraction is propagated to the amplitude fit by varying this parameter within its uncertainty, which also accounts for alternative signal and background invariant-mass models. Alternative background phase-space distributions are derived by using additional kinematic observables to train the BDTG algorithm or by using only candidates from the low- or high-mass sideband. The amplitude fit is repeated with these alternative background PDFs and the largest deviation to the nominal result is used as systematic uncertainty.

The uncertainties due to fixed masses and widths of resonances are evaluated by varying them one-by-one within their quoted errors. The radii of the normalised Blatt-Weisskopf barrier factors are set to $r_{\rm BW} = 4\,{\rm GeV}^{-1}$ for the B^+, $r_{\rm BW} = 1.2\,{\rm GeV}^{-1}$ for all three-body resonances and $r_{\rm BW} = 2.2\,{\rm GeV}^{-1}$ for all two-body resonances. Each of these three values is obtained by maximising the likelihood of amplitude fits while fixing the values of the

JHEP01(2025)054

other two. To evaluate the associated systematic uncertainties, the radial parameters are varied by $\pm 1\,\mathrm{GeV}^{-1}$.

As argued in section 4.1, the $\rho - \omega$ mixing parameter δ is initially fixed to $|\delta| = +3|\delta_{em}| = (4.71 \pm 0.47) \times 10^{-3}$ [49] and $\arg(\delta) = 0$ during the model selection. When floating these parameters using the *baseline* model, we obtain $|\delta| = (3.9 \pm 0.5) \times 10^{-3}$ and $\arg(\delta) = (-11 \pm 7)^\circ$, in good agreement with the assumption. There are multiple topologies with potentially different quark sources for the ρ production to be considered in $B^+ \to \psi(2S)K^+\pi^+\pi^-$ decays. Thus we allow for different $|\delta|$ values for certain channels and obtain:

$$\begin{aligned} K_1(1270)^+ &: |\delta| = (3.6 \pm 0.9) \times 10^{-3}, \\ \text{all other } K'^+ \to K^+\,\rho(770)^0 &: |\delta| = (3.8 \pm 1.3) \times 10^{-3}, \\ T^*_{c\bar{c}0}(4475)^0 &: |\delta| = (6.0 \pm 0.8) \times 10^{-3}, \\ \text{all other } X^0 \to \psi(2S)\,\rho(770)^0 &: |\delta| = (6.1 \pm 1.2) \times 10^{-3}, \\ B^+ \to T^+_{c\bar{c}\bar{s}}\,\rho(770)^0 &: |\delta| = (3.9 \pm 2.0) \times 10^{-3}, \end{aligned} \tag{5.5}$$

where the uncertainties are statistical only. With $|\delta| \approx 2.3|\delta_{em}|$ and $|\delta| \approx 2.4|\delta_{em}|$, the parameter values for the $K_1(1270)^+$ and the other K'^+ resonances are slightly lower but within uncertainties consistent with a pure $u\bar{u}$ source. Somewhat larger isospin-breaking effects are observed for the exotic $X^0 \to \psi(2S)\rho(770)^0$ topologies $|\delta| \approx 3.8|\delta_{em}|$. A large value of $|\delta| \approx 11|\delta_{em}|$ was also found for $\chi_{c1}(3872) \to J/\psi\rho(770)^0$ decays in ref. [15]. In the nominal fit, we fix the parameters to the ones obtained from the dedicated fit displayed in eq. 5.5. A systematic uncertainty is assigned by using $|\delta| = +3|\delta_{em}|$ for all topologies and varying it within the uncertainties of $|\delta_{em}|$.

The P-vectors for the nominal dipion S-wave model consider the direct coupling to the $\pi\pi$ and KK channels and up to four poles depending on the production mode, see appendix A. Additional channels and poles are added to assign a systematic uncertainty. A similar procedure is performed for the $K\pi$ S-wave description.

Several alternative lineshape parameterisations are considered as part of the systematic studies. The Gounaris-Sakurai description for the $\rho(770)^0$ resonance is replaced by a relativistic Breit-Wigner function. As an alternative to the $\pi\pi$ S-wave K-matrix parameterisation, the Omnès function based on dispersion integrals is used [82, 83]. Alternative energy-dependent widths for three-body resonances are derived from eq. 4.7 taking only the dominant three-body decay mode into account. For the $T^*_{c\bar{c}0}(4475)^0$ state, a coupled-channel decay width is used which includes the $\psi(2S)\rho(770)^0$ and $J/\psi\phi$ channels,

$$\Gamma(s) = \Gamma_0 \frac{g_{\psi(2S)\rho}\,\rho_{\psi(2S)\rho}(s) + g_{J/\psi\phi}\,\rho_{J/\psi\phi}(s)}{g_{\psi(2S)\rho}\,\rho_{\psi(2S)\rho}(m_0^2) + g_{J/\psi\phi}\,\rho_{J/\psi\phi}(m_0^2)}. \tag{5.6}$$

We find $g_{J/\psi\phi}/g_{\psi(2S)\rho} = 0.26 \pm 0.18$ and similar mass and width as in the nominal fit. The fit is not able to discriminate between the $J/\psi\phi$ and $J/\psi\rho(770)^0$ coupled channels. For each alteration, an amplitude fit is performed and the standard deviation of the obtained fit results is assigned as a systematic uncertainty. The impact of nearby open-charm thresholds is also studied by using coupled-channel decay widths for the various exotic resonances. In

JHEP01(2025)054

all cases no sensitivity to the $D_{(s)}^{(*)}D_{(s)}^{(*)}$ open-charm coupling is observed and no systematic uncertainty is attributed.

A range of modifications to the *baseline* model are examined to assign an additional uncertainty due to the choice of amplitude components. Fit results for the eleven alternative models can be found in appendix D, tables 16 to 21. The set of alternative models encompasses an "extended K'^+" model (Model 1), where we include additional decay modes and angular momentum configurations of the selected $K'^+ \to K^+\pi^+\pi^-$ resonances as well as an "additional K'^+" model (Model 2) that includes additional K'^+ resonances. In a similar fashion, the "extended exotic" model (Model 3) includes additional decay modes and angular momentum configurations of the selected exotic states. We searched for new exotic states with the highest significance in each mass dimension to create "additional exotic" models. Model 4 includes additional $1^+\,\psi(2S)\pi^+\pi^-, 2^-\,\psi(2S)\pi^+$ and $0^-\,\psi(2S)\pi^+$ states, while Model 5 includes additional $0^+\,\psi(2S)K^+\pi^-, 0^+\,\psi(2S)K^+\pi^+$ and $0^-\,\psi(2S)K^+$ states. The statistical significance of each of those additional states is below 4σ. An "additional nonresonant" model (Model 6) that adds several nonresonant amplitudes is also considered. Another alternative model is derived by repeating the iterative model building with modified binning for the χ^2 calculation (Model 7). Further models are constructed by adding 25 additional amplitudes to the *baseline* model and applying a regularisation method [47, 84, 85]. Either a Cauchy [86] (Model 8) or a LASSO [87, 88] regularisation term (Model 9) is used. Lastly, fits are performed using the canonical helicity formalism instead of the covariant tensor formalism. The definition of S- and D-wave amplitudes differs between the formalisms [62, 89, 90]. There are also differences in the energy-dependent form factors [91]. The results are thus not expected to be strictly identical when switching from one formalism to the other, even if a complete set of partial waves would be used. The nominal set of partial-wave amplitudes is used for the canonical helicity fit in Model 10, while Model 11 adds additional partial waves. From this set of alternative models, we compute the sample variance for each observable and take it as the model uncertainty.

The total systematic uncertainty is obtained by summing the components in quadrature. A full breakdown of the different sources of systematic uncertainty for all fit parameters and observables is given in appendix D. The total systematic uncertainty is significantly larger than the statistical uncertainty, with the largest contributions coming from the alternative amplitude models. The smallest significance value found when performing the dominant systematic variations is taken as the significance accounting for systematic uncertainty in table 3.

6 Summary

The first full amplitude analysis of $B^+ \to \psi(2S)K^+\pi^+\pi^-$ decays is performed using proton-proton collision data corresponding to $9\,\text{fb}^{-1}$ recorded with the LHCb detector. The $K^+\pi^+\pi^-$ spectrum is described by six K'^+ resonances that decay via $K^*(892)^0\pi^+$, $K^+\rho(770)^0$ or S-wave intermediate states. Branching fractions measurements of the $K_1(1270)^+$ resonant substructure are found to be in good agreement with previous analyses.

A good description of the data in the full seven-dimensional phase space could only be obtained by adding a multitude of exotic hidden-charm components to the model. Four

JHEP01(2025)054

$X^0 \to \psi(2S)\pi^+\pi^-$ states are identified and the spectrum shows similarities to previously observed $J/\psi\phi$ resonances. A simultaneous coupled-channel fit of $B^+ \to \psi(2S)K^+\pi^+\pi^-$ and $B^+ \to J/\psi\phi K^+$ could provide more insights into the quark-level interpretation of these states. Further understanding might be gained by examining the structures of $X^0 \to J/\psi\omega$ or $X^0 \to \psi(2S)\omega$ exotic states.

New production modes of charged charmonium-like states are observed. The $T_{c\bar{c}1}(4430)^\pm$ resonance is confirmed with a high significance. The quantum numbers of the $T_{c\bar{c}1}(4200)^\pm$ resonance are determined to be 1^+, for the first time with a significance exceeding 5σ. Further studies with more abundant $B^0 \to \psi(2S)K^+\pi^-$ and $B^0 \to J/\psi K^+\pi^-$ samples are required to improve our knowledge of the charged charmonium-like spectrum. Hidden-charm exotic states that decay to the $\psi(2S)K^+\pi^-$ final state are observed for the first time. If interpreted as tetraquark states, their minimal quark content would be $c\bar{c}\bar{s}d$. The $T_{c\bar{c}\bar{s}1}(4600)^0$ and $T_{c\bar{c}\bar{s}1}(4900)^0$ might be radial excitations of the $T_{c\bar{c}\bar{s}1}(4000)^0$ resonance seen in $B^0 \to T_{c\bar{c}\bar{s}1}(4000)^0\phi \to [J/\psi K^0_S]\phi$ decays. Despite the high significance of all exotic states, their broad nature and the extremely complex amplitude model with 53 components make the interpretation challenging. In particular, the broad vector states at the edges of the phase space, $T^*_{c\bar{c}1}(4800)^0$ and $T^*_{c\bar{c}\bar{s}1}(5200)^0$, should be considered as effective descriptions rather than genuine resonances at this point. The same applies to the $T_{c\bar{c}\bar{s}1}(4000)^+$ and $T^*_{c\bar{c}1}(4055)^+$ contributions, for which the amplitude fit does not provide sufficient sensitivity to measure their masses and widths.

The $K^+\pi^+\pi^-$ component of the amplitude model provides valuable input for studies of new physics effects in $B^+ \to K^+\pi^+\pi^-\gamma$ or $B^+ \to K^+\pi^+\pi^-\mu^+\mu^-$ decays. As the first full four-body amplitude analysis featuring a vector particle in the final state, the research outlined in this paper establishes a groundwork for subsequent investigations into similar decay modes, such as $B^+ \to J/\psi K^+\pi^+\pi^-$, $B^+ \to \chi_{c1}(1P)K^+\pi^+\pi^-$ or $B^+ \to \chi_{c1}(3872)K^+\pi^+\pi^-$, that could shed further light on the intricate spectrum of exotic hadrons.

Acknowledgments

We express our gratitude to our colleagues in the CERN accelerator departments for the excellent performance of the LHC. We thank the technical and administrative staff at the LHCb institutes. We acknowledge support from CERN and from the national agencies: CAPES, CNPq, FAPERJ and FINEP (Brazil); MOST and NSFC (China); CNRS/IN2P3 (France); BMBF, DFG and MPG (Germany); INFN (Italy); NWO (Netherlands); MNiSW and NCN (Poland); MCID/IFA (Romania); MICIU and AEI (Spain); SNSF and SER (Switzerland); NASU (Ukraine); STFC (United Kingdom); DOE NP and NSF (U.S.A.). We acknowledge the computing resources that are provided by CERN, IN2P3 (France), KIT and DESY (Germany), INFN (Italy), SURF (Netherlands), PIC (Spain), GridPP (United Kingdom), CSCS (Switzerland), IFIN-HH (Romania), CBPF (Brazil), and Polish WLCG (Poland). We are indebted to the communities behind the multiple open-source software packages on which we depend. Individual groups or members have received support from ARC and ARDC (Australia); Key Research Program of Frontier Sciences of CAS, CAS PIFI, CAS CCEPP, Fundamental Research Funds for the Central Universities, and Sci. & Tech. Program of Guangzhou (China); Minciencias (Colombia); EPLANET, Marie Skłodowska-

JHEP01(2025)054

Curie Actions, ERC and NextGenerationEU (European Union); A*MIDEX, ANR, IPhU and Labex P2IO, and Région Auvergne-Rhône-Alpes (France); AvH Foundation (Germany); ICSC (Italy); Severo Ochoa and María de Maeztu Units of Excellence, GVA, XuntaGal, GENCAT, InTalent-Inditex and Prog. Atracción Talento CM (Spain); SRC (Sweden); the Leverhulme Trust, the Royal Society and UKRI (United Kingdom).

A Lineshape parameterisations

Model for $\rho(770)^0$ resonance. We use the Gounaris-Sakurai parameterisation for the $\rho(770)^0 \to \pi^+\pi^-$ propagator [48]:

$$T_{GS}(s) = \frac{1 + f(m_0^2)/m_0^2}{m_0^2 + f(s) - s - i\, m_0\, \Gamma(s)}\,, \tag{A.1}$$

where $\Gamma(s)$ takes on the same form as in eq. 4.6 with $r_{\text{BW}} = 0\,\text{GeV}^{-1}$ and the function $f(s)$ is defined as

$$f(s) = \Gamma_0\, \frac{m_0^2}{q_0^3} \left[q^2 \left(h(s) - h(m_0^2) \right) + \left(s - m_0^2 \right) q_0^2 \left. \frac{dh}{d\sqrt{s}} \right|_{m_0} \right], \tag{A.2}$$

$$h(s) = \frac{2}{\pi}\, \frac{q}{\sqrt{s}} \ln\left(\frac{\sqrt{s} + 2\,q}{2\,m_\pi} \right). \tag{A.3}$$

S-wave models. In the K-matrix formalism, the lineshape is written as

$$T(s) = \left(I - i\hat{K}\hat{\rho} \right)^{-1} \hat{P}, \tag{A.4}$$

where $\hat{P}$ is the process specific production vector, $\hat{\rho}$ is the phase space matrix and $\hat{K}$ is the K matrix. For the $\pi\pi$ S-wave, the K-matrix parameterisation is taken from ref. [55],

$$\hat{K}_{ij} = f(s) \left(\sum_\alpha \frac{g_i^\alpha\, g_j^\alpha}{m_\alpha^2 - s} + f_{ij}^{\text{scatt}}\, \frac{1\,\text{GeV}^2 - s_0^{\text{scatt}}}{s - s_0^{\text{scatt}}} \right), \tag{A.5}$$

where the index $i \in \{\pi\pi, KK, \pi\pi\pi\pi, \eta\eta, \eta\eta'\}$ indicates the channel and α indicates the pole. Slowly varying scattering contributions are described by f_{ij}^{scatt}, while the function $f(s)$ suppresses the kinematic singularity and introduces the Adler zero near the $\pi\pi$ threshold: $f(s) = \frac{1\,\text{GeV}^2 - s_{A_0}}{s - s_{A_0}}(s - m_\pi^2/2)$. The production vector, $\hat{P}$ has the same pole structure as the K matrix,

$$\hat{P}_i = \left(\sum_\alpha \frac{\beta^\alpha\, g_i^\alpha}{m_\alpha^2 - s} + f_i^{\text{prod}}\, \frac{1\,\text{GeV}^2 - s_0^{\text{prod}}}{s - s_0^{\text{prod}}} \right), \tag{A.6}$$

where the complex parameter β^α describes the production strength of pole α, the complex parameter f_i^{prod} describes the direct coupling to channel i and s_0^{prod} is a single real parameter. As these parameters are process specific, they need to be determined from data. The $K\pi$ S-wave couples to two channels $K\pi$ and $K\eta'$, and contains only one pole, the $K_0^*(1430)$

JHEP01(2025)054

resonance. The isospin state $I = \frac{1}{2}$ contributes to both channels, while $I = \frac{3}{2}$ couples to $K\pi$ only. Their parameterisations are

$$\hat{K}_{ij}^{\frac{1}{2}} = \frac{s - s_0^{\frac{1}{2}}}{m_K^2 + m_\pi^2} \left(\frac{g_i^1 g_j^1}{m_1^2 - s} + C_{ij0} + C_{ij1}\tilde{s} + C_{ij2}\tilde{s}^2 \right), \tag{A.7}$$

$$\hat{K}^{\frac{3}{2}} = \frac{s - s_0^{\frac{3}{2}}}{m_K^2 + m_\pi^2} \left(D_{110} + D_{111}\tilde{s} + D_{112}\tilde{s}^2 \right), \tag{A.8}$$

where all parameters and definitions are taken from ref. [56]. The Q-vector approximation is used, which simplifies eq. A.4 to

$$T(s) = \left(I - i\hat{K}\hat{\rho} \right)^{-1} \hat{K}\hat{\alpha}, \tag{A.9}$$

where $\hat{\alpha}$ is a diagonal matrix containing a complex parameter for each channel to be determined from data.

Running-width functions for three-body resonances. For the $K(1460)^+$ resonance, the energy-dependent width is reproduced from ref. [70]. We further use the energy-dependent widths for the $K_1(1270)^+$, $K_1(1400)^+$, $K^*(1410)^+$ and $K^*(1680)^+$ mesons from ref. [47]. For all other resonances decaying into a three-body final state, an energy-dependent width functions is derived from eq. 4.7 assuming a uniform phase-space population. This is straightforward to implement for resonances with limited available information and has been found to provide reasonable approximations in other studies [47, 85] The running width functions of the three-body resonances included in the *baseline* model are shown in figure 4.

B Considered decay chains

Tables 4 to 7 list all previously observed resonances that might contribute to $B^+ \to \psi(2S)K^+\pi^+\pi^-$ decays. If quantum numbers are unknown, all possible spin-parity combinations with $J \leq 2$ are tested. We consider the following decay channels for all $K'^+ \to K^+\pi^+\pi^-$, $X^0 \to \psi(2S)\pi^+\pi^-$, $T^0_{c\bar{c}s} \to \psi(2S)K^+\pi^-$, $T^{++}_{c\bar{c}s} \to \psi(2S)K^+\pi^+$, $T^{\pm}_{c\bar{c}} \to \psi(2S)\pi^\pm$ and $T^{+}_{c\bar{c}s} \to \psi(2S)K^+$ resonances (unless forbidden by conservation laws):

- $K'^+ \to K^+\rho(770)^0, K^+\rho(1450)^0, K^*(892)^0\pi^+, K^*(1410)^0\pi^+, K^+[\pi\pi]_S, [K\pi]_S\pi^+$;
- $X^0 \to \psi(2S)\rho(770)^0, \psi(2S)[\pi\pi]_S, T^{\pm}_{c\bar{c}}\pi^\mp$;
- $T^0_{c\bar{c}s} \to \psi(2S)K^*(892)^0, \psi(2S)[K\pi]_S, T^-_{c\bar{c}}K^+, Z_s^+\pi^-$;
- $T^{++}_{c\bar{c}s} \to T^+_{c\bar{c}}K^+, T^+_{c\bar{c}s}\pi^+$;
- $B^+ \to T^+_{c\bar{c}}\, K^*(892^0), T^+_{c\bar{c}}\, [K\pi]_S$;
- $B^+ \to T^+_{c\bar{c}s}\, \rho(770)^0, T^+_{c\bar{c}s}\, [\pi\pi]_S$.

Nonresonant and single resonance amplitudes are obtained from the same topologies by setting e.g. the K'^+ lineshape to unity.

JHEP01(2025)054

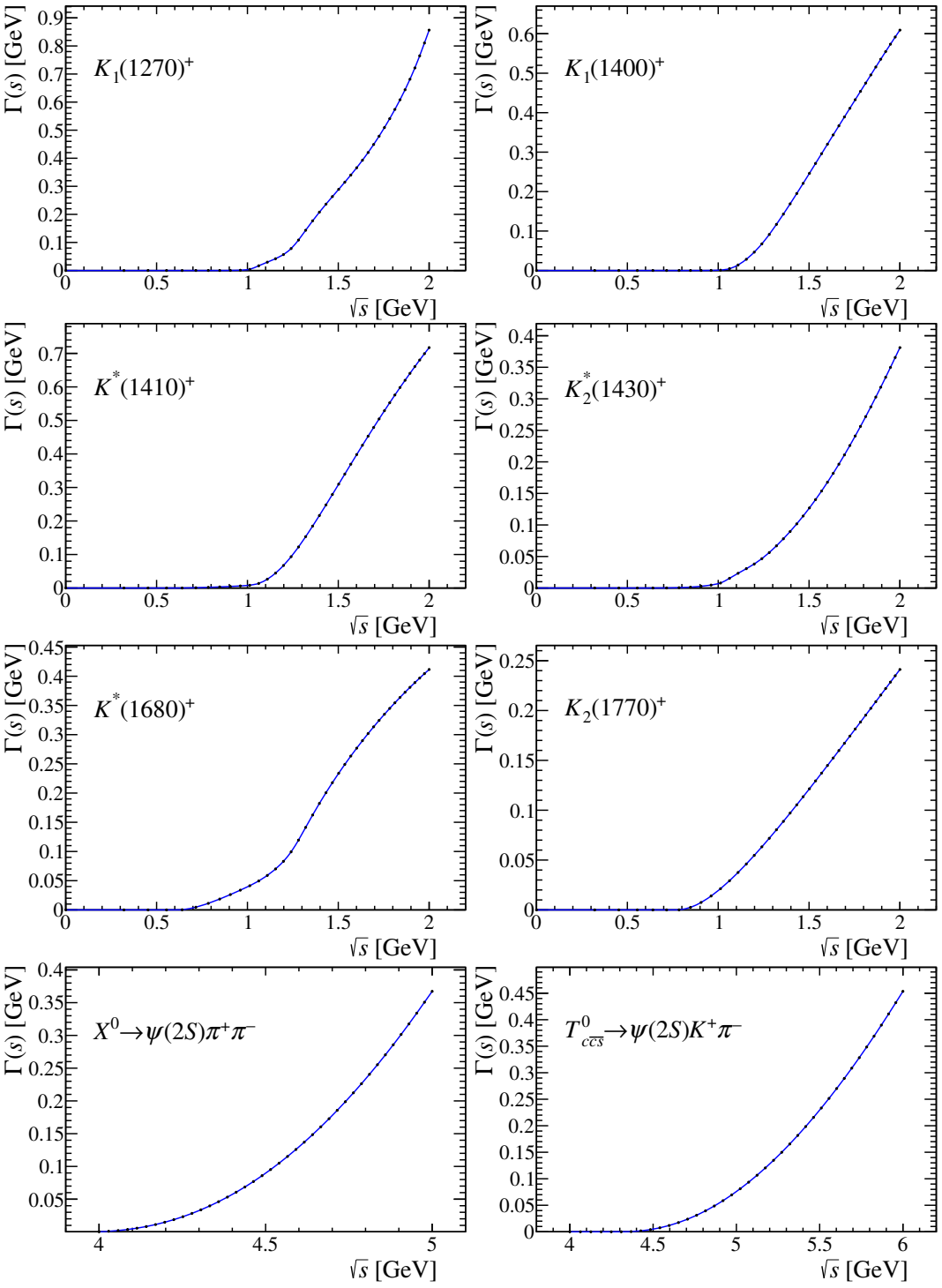

Figure 4. Running-width functions of the three-body resonances.

JHEP01(2025)054

Name	J^P	m[MeV]	Γ[MeV]	Source
$K_1(1270)^+$	1^+	1290±2	116±3	[70]
$K_1(1400)^+$	1^+	1403±7	174±13	[32]
$K^*(1410)^+$	1^-	1414±15	232±21	[32]
$K_2^*(1430)^+$	2^+	1427.3±1.5	100±2.1	[32]
$K(1460)^+$	0^-	1482.4±15	335.6±11	[70]
$K_2^*(1580)^+$	2^-	1580	110	[32]
$K(1630)^+$	$?^?$	1629±7	16^{+19}_{-16}	[32]
$K_1(1650)^+$	1^+	1650±50	150±50	[32]
$K^*(1680)^+$	1^-	1718±18	322±110	[32]
$K_2(1770)^+$	2^-	1773±8	186±14	[32]

Table 4. Resonances potentially contributing to the $K^+\pi^+\pi^-$ subsystem.

Name	J^P	m[MeV]	Γ[MeV]	Decay Channel
$\psi(4040)$	1^-	4039±1	80±10	DD
$\chi_{c1}(4140)$	1^+	4146.5±3.0	19^{+7}_{-5}	$J/\psi\phi$
$\psi(4160)$	1^-	4191±5	70±10	DD
$X(4160)$	$?^?$	4153^{+23}_{-21}	136^{+60}_{-35}	$J/\psi\phi, D^*D^*$
$\psi(4230)$	1^-	4222.7±2.6	49±8	$J/\psi\pi\pi, \psi(2S)\pi\pi$
$\chi_{c1}(4274)$	1^+	4286^{+8}_{-9}	51±7	$J/\psi\phi$
$X(4350)$	$?^?$	4351±5	13^{+18}_{-10}	$J/\psi\phi$
$\psi(4360)$	1^-	4372±9	115±13	$J/\psi\pi\pi, \psi(2S)\pi\pi, h_c\pi\pi$
$\psi(4415)$	1^-	4421±4	62±20	DD
$\chi_{c0}(4500)$	0^+	4474±4	77^{+12}_{-10}	$J/\psi\phi$
$X(4630)$	$1^-(2^-)$	4626^{+24}_{-110}	174^{+140}_{-80}	$J/\psi\phi$
$\psi(4660)$	1^-	4630±6	72^{+14}_{-12}	$\psi(2S)\pi\pi$
$\chi_{c1}(4685)$	1^+	4684^{+15}_{-17}	126±40	$J/\psi\phi$
$\chi_{c0}(4700)$	0^+	4694^{+16}_{-5}	87^{+18}_{-10}	$J/\psi\phi$

Table 5. Resonances potentially contributing to the $\psi(2S)\pi^+\pi^-$ subsystem and decay channels in which they were seen. All values taken from the PDG [32].

Name	J^P	m[MeV]	Γ[MeV]	Decay Channel
$T_{c\bar{c}1}(3900)^\pm$	1^+	3887.1±2.6	28.4±2.6	$J/\psi\pi$
$T^*_{c\bar{c}1}(4020)^\pm$	1^-	4024.1±1.9	13±5	$h_c(1P)\pi, D^*D^*$
$T_{c\bar{c}}(4050)^\pm$	$?^?$	4051^{+24}_{-40}	82^{+50}_{-28}	$\chi_{c1}(1P)\pi$
$T_{c\bar{c}}(4055)^\pm$	$?^?$	4054±3.2	45±13	$\psi(2S)\pi$
$T_{c\bar{c}}(4100)^\pm$	$0^+/1^-$	4096±28	152±75	$\eta_c(1S)\pi$
$T_{c\bar{c}1}(4200)^\pm$	$1^+(2^-)$	4196^{+35}_{-32}	370^{+100}_{-150}	$J/\psi\pi$
$T_{c\bar{c}}(4240)^\pm$	$0^-(1^+)$	4239^{+50}_{-21}	220^{+120}_{-90}	$\psi(2S)\pi$
$T_{c\bar{c}}(4250)^\pm$	$?^?$	4248^{+190}_{-50}	177^{+320}_{-70}	$\chi_{c1}(1P)\pi$
$T_{c\bar{c}1}(4430)^\pm$	1^+	4478^{+15}_{-18}	181±31	$J/\psi\pi, \psi(2S)\pi$

Table 6. Resonances potentially contributing to the $\psi(2S)\pi^\pm$ subsystem and decay channels in which they were seen. All values taken from the PDG [32].

Name	J^P	m[MeV]	Γ[MeV]	Decay Channel
$T_{c\bar{c}\bar{s}1}(4000)^+$	1^+	4003^{+7}_{-15}	131±30	$J/\psi K$
$T_{c\bar{c}\bar{s}1}(4220)^+$	$1^+(1^-)$	4216^{+49}_{-38}	233^{+110}_{-90}	$J/\psi K$

Table 7. Resonances potentially contributing to the $\psi(2S)K^+$ subsystem and decay channels in which they were seen. All values taken from the PDG [32].

JHEP01(2025)054

C Model selection

Figure 5 and figure 6 display the fit projections of the *no-exotics* and *known-exotics* models, respectively. Fit results of the *start*, *no-exotics*, *known-exotics* and *baseline* models are compared in tables 8 and 9.

Decay channel F_i[%]	*Start*	*No-exotics*	*Known-exotics*	*Baseline*
$B^+ \to \psi(2S)\, K_1(1270)^+$	52.98±1.13	26.56±0.80	7.50±0.86	7.60±0.85
$B^+ \to \psi(2S)\, K^*(1680)^+$	30.48±0.72	22.26±0.77	5.23±0.73	8.15±1.31
$B^+ \to \psi(2S)\, K(1460)^+$	10.69±0.32	6.04±0.52	5.74±0.45	5.26±0.48
$B^+ \to K_2^*(1430)^+\psi(2S)$	6.89±0.47	6.91±0.33	4.25±0.25	4.35±0.29
$B^+ \to \psi(2S)\, K_1(1400)^+$	6.43±0.94	2.27±0.32	5.38±0.69	5.78±0.62
$B^+ \to \psi(2S)\, K^*(1410)^+$	2.88±0.31	2.61±0.37	2.36±0.43	1.79±0.35
$B^+[P] \to \psi(2S)\, K_1(1270)^+$	–	8.50±0.43	4.83±0.46	7.52±0.60
$B^+[D] \to \psi(2S)\, K_1(1270)^+$	–	8.46±0.47	7.17±0.50	6.81±0.45
$B^+ \to \psi(2S)\, [[\pi^+\pi^-]_S\, K^+]_A$	–	6.68±0.56	–	–
$B^+[P] \to \psi(2S)\, K^*(1410)^+$	–	4.88±0.42	–	–
$B^+[P] \to \psi(2S)\, K^*(1680)^+$	–	3.96±0.56	–	–
$B^+ \to K_2(1770)^+\psi(2S)$	–	3.81±0.30	–	–
$B^+ \to \psi(4415)K^+$	–	1.82±0.41	–	–
$B^+[P] \to \psi(2S)\, K_1(1400)^+$	–	1.18±0.17	0.68±0.18	0.48±0.18
$B^+ \to \psi(4360)K^+$	–	1.10±0.40	1.11±0.19	0.64±0.14
$B^+ \to \psi(2S)\, K_1(1650)^+$	–	0.76±0.16	–	–
$B^+ \to \psi(2S)\, [\rho(770)^0 K^+]_P$	–	0.36±0.21	–	–
$B^+ \to \psi(4660)K^+$	–	0.32±0.10	–	–
$B^+ \to \psi(2S)\, [K^*(892)^0\pi^+]_P$	–	0.06±0.07	–	–
$B^+ \to T^*_{c\bar{c}0}(4475)^0 K^+$	–	–	16.96±1.22	18.45±1.31
$B^+[P] \to T_{c\bar{c}1}(4200)^+ K^*(892)^0$	–	–	7.35±0.53	4.60±0.54
$B^+ \to T^*_{c\bar{c}1}(4800)^0 K^+$	–	–	4.32±0.52	3.24±0.50
$B^+ \to T_{c\bar{c}1}(4430)^+\, [K^+\pi^-]_S$	–	–	3.85±0.52	3.41±0.54
$B^+ \to T^*_{c\bar{c}0}(4710)^0 K^+$	–	–	3.03±0.42	1.73±0.28
$B^+ \to T_{c\bar{c}1}(4650)^0 K^+$	–	–	2.31±0.40	2.89±0.45
$B^+[D] \to T_{c\bar{c}1}(4200)^+ K^*(892)^0$	–	–	2.05±0.31	2.78±0.33
$B^+ \to T_{c\bar{c}1}(4430)^+ K^*(892)^0$	–	–	1.92±1.30	0.75±0.43
$B^+[D] \to \rho(770)^0 T_{c\bar{c}\bar{s}1}(4000)^+$	–	–	1.84±0.20	2.06±0.22
$B^+ \to T_{c\bar{c}1}(4200)^+ K^*(892)^0$	–	–	1.36±0.85	4.02±0.88
$B^+ \to T_{c\bar{c}\bar{s}1}(4000)^+\, [\pi^+\pi^-]_S$	–	–	1.12±0.21	1.24±0.23
$B^+ \to T^*_{c\bar{c}1}(4055) K^*(892)^0$	–	–	1.04±0.15	0.52±0.10
$B^+ \to [\psi(2S)\, K^*(892)^0]_S \pi^+$	–	–	0.41±0.51	–
$B^+ \to [\psi(2S)\, K^+]_A\, [\pi^+\pi^-]_S$	–	–	0.32±0.13	–
$B^+[P] \to T_{c\bar{c}}(4100)^+ K^*(892)^0$	–	–	0.31±0.13	–
$B^+[P] \to [\psi(2S)\, K^+]_V \rho(770)^0$	–	–	0.07±0.05	–
$B^+ \to T_{c\bar{c}\bar{s}1}(4600)^0 \pi^+$	–	–	–	4.42±0.98
$B^+ \to T_{c\bar{c}\bar{s}1}(4900)^0 \pi^+$	–	–	–	2.60±0.66
$B^+ \to T^*_{c\bar{c}\bar{s}1}(5200)^0 \pi^+$	–	–	–	1.59±0.46
Sum B^+	110.34±1.99	108.56±1.21	92.50±2.15	102.69±4.40
$T^*_{c\bar{c}0}(4475)^0$ mass [MeV]	–	–	4467.1±7.6	4474.5±6.9
$T^*_{c\bar{c}0}(4475)^0$ width [MeV]	–	–	259.2±22.6	230.8±19.5
$T_{c\bar{c}1}(4650)^0$ mass [MeV]	–	–	4506.1±15.4	4652.5±14.4
$T_{c\bar{c}1}(4650)^0$ width [MeV]	–	–	250.0±25.2	227.0±26.3
$T^*_{c\bar{c}0}(4710)^0$ mass [MeV]	–	–	4696.4±5.6	4710.2±4.4
$T^*_{c\bar{c}0}(4710)^0$ width [MeV]	–	–	98.8±10.5	63.6±8.7
$T^*_{c\bar{c}1}(4800)^0$ mass [MeV]	–	–	4748.0±33.1	4784.6±37.4
$T^*_{c\bar{c}1}(4800)^0$ width [MeV]	–	–	444.2±78.9	457.1±93.4
$T_{c\bar{c}1}(4200)^+$ mass [MeV]	–	–	4311.0±14.5	4257.3±10.8
$T_{c\bar{c}1}(4200)^+$ width [MeV]	–	–	343.3±18.8	308.2±20.4
$T_{c\bar{c}1}(4430)^+$ mass [MeV]	–	–	4481.7±13.1	4468.2±21.0
$T_{c\bar{c}1}(4430)^+$ width [MeV]	–	–	180.5±23.5	250.9±41.6
$T_{c\bar{c}\bar{s}1}(4600)^0$ mass [MeV]	–	–	–	4577.8±9.5
$T_{c\bar{c}\bar{s}1}(4600)^0$ width [MeV]	–	–	–	133.0±28.4
$T_{c\bar{c}\bar{s}1}(4900)^0$ mass [MeV]	–	–	–	4924.9±22.0
$T_{c\bar{c}\bar{s}1}(4900)^0$ width [MeV]	–	–	–	255.0±54.6
$T^*_{c\bar{c}\bar{s}1}(5200)^0$ mass [MeV]	–	–	–	5225.1±85.7
$T^*_{c\bar{c}\bar{s}1}(5200)^0$ width [MeV]	–	–	–	226.2±75.5
$\Delta(-2\ln\mathcal{L})$	0.0	−6214.2	−11038.0	−12021.3
N_{par}	18	74	88	98
χ^2/ν	2.54	2.05	1.31	1.21
χ^2/N_{bins}	2.50	1.91	1.20	1.10

Table 8. Fit results of the *start*, *no-exotics*, *known-exotics* and *baseline* models, part 1. Uncertainties are statistical only.

JHEP01(2025)054

Decay channel F_i[%]	*Start*	*No-exotics*	*Known-exotics*	*Baseline*
$K_1(1270)^+ \to \rho(770)^0 K^+$	71.49±1.50	45.70±1.87	46.52±2.33	50.71±2.18
$K_1(1270)^+ \to K^*(892)^0 \pi^+$	33.40±1.24	26.16±1.06	21.63±1.77	19.86±1.44
$K_1(1270)^+ \to [K^+\pi^-]_S \pi^+$	0.00±0.00	6.25±0.98	9.85±1.28	11.35±1.45
$K_1(1270)^+[D] \to K^*(892)^0 \pi^+$	–	6.75±0.58	9.35±1.09	8.32±0.85
$K_1(1270)^+ \to \rho(1450)^0 K^+$	–	7.12±1.60	–	–
$K_1(1270)^+ \to K^*(1410)^0 \pi^+$	–	6.45±1.05	–	–
Sum $K_1(1270)^+$	104.89±0.77	98.42±3.03	87.35±1.59	90.24±1.83
$K_1(1400)^+ \to K^*(892)^0 \pi^+$	100	100	80.56±4.15	86.80±3.78
$K_1(1400)^+ \to \rho(770)^0 K^+$	–	–	29.32±4.62	22.08±4.40
Sum $K_1(1400)^+$	100	100	109.88±0.70	108.88±0.82
$K^*(1410)^+ \to K^*(892)^0 \pi^+$	100	86.92±5.04	71.42±8.38	88.50±8.39
$K^*(1410)^+ \to \rho(770)^0 K^+$	–	50.09±6.23	57.57±9.24	38.36±10.46
Sum $K^*(1410)^+$	100	137.01±1.27	128.99±3.96	126.86±4.83
$K_2^*(1430)^+ \to K^*(892)^0 \pi^+$	80.70±0.38	77.88±2.48	78.90±2.92	76.70±3.04
$K_2^*(1430)^+ \to \rho(770)^0 K^+$	36.15±0.17	11.74±1.83	11.31±2.16	12.71±2.30
Sum $K_2^*(1430)^+$	116.86±0.54	89.62±0.65	90.22±0.80	89.41±0.75
$K(1460)^+ \to [\pi^+\pi^-]_S K^+$	47.43±2.14	27.78±3.04	41.60±3.72	45.13±4.22
$K(1460)^+ \to K^*(892)^0 \pi^+$	36.40±2.05	31.89±3.72	38.26±3.61	35.41±4.08
$K(1460)^+ \to \rho(770)^0 K^+$	–	24.56±3.12	–	–
Sum $K(1460)^+$	83.83±0.09	84.22±1.07	79.86±0.42	80.54±0.67
$K_1(1650)^+[D] \to K^*(892)^0 \pi^+$	–	100	–	–
$K^*(1680)^+ \to \rho(770)^0 K^+$	77.92±2.00	80.86±1.63	81.58±5.43	31.16±6.11
$K^*(1680)^+ \to K^*(892)^0 \pi^+$	11.32±1.47	8.03±1.01	16.62±5.05	49.69±6.72
Sum $K^*(1680)^+$	89.24±0.67	88.89±0.72	98.20±3.14	80.85±0.64
$K_2(1770)^+ \to \rho(770)^0 K^+$	–	68.79±3.59	–	–
$K_2(1770)^+ \to K^*(892)^0 \pi^+$	–	23.21±3.18	–	–
Sum $K_2(1770)^+$	–	92.00±0.81	–	–
$T^*_{c\bar{c}0}(4475)^0 \to \rho(770)^0 \psi(2S)$	–	–	97.56±0.71	99.04±0.49
$T^*_{c\bar{c}0}(4475)^0 \to T_{c\bar{c}1}(4200)^- \pi^+$	–	–	1.28±0.38	0.50±0.25
$T^*_{c\bar{c}0}(4475)^0 \to T_{c\bar{c}1}(4200)^+ \pi^-$	–	–	1.28±0.38	0.50±0.25
Sum $T^*_{c\bar{c}0}(4475)^0$	–	–	100.13±0.04	100.03±0.02
$T_{c\bar{c}1}(4650)^0 \to \rho(770)^0 \psi(2S)$	–	–	73.56±10.54	86.66±7.85
$T_{c\bar{c}1}(4650)^0 \to T_{c\bar{c}1}(4200)^- \pi^+$	–	–	3.78±1.94	6.62±2.03
$T_{c\bar{c}1}(4650)^0 \to T_{c\bar{c}1}(4200)^+ \pi^-$	–	–	3.77±1.94	6.61±2.03
Sum $T_{c\bar{c}1}(4650)^0$	–	–	81.11±8.55	99.89±7.37
$T^*_{c\bar{c}0}(4710)^0 \to \rho(770)^0 \psi(2S)$	–	–	67.06±8.29	92.35±10.83
$T^*_{c\bar{c}0}(4710)^0 \to T_{c\bar{c}1}(4430)^+ \pi^-$	–	–	22.61±2.97	17.00±3.82
$T^*_{c\bar{c}0}(4710)^0 \to T_{c\bar{c}1}(4430)^- \pi^+$	–	–	22.53±2.96	17.00±3.82
Sum $T^*_{c\bar{c}0}(4710)^0$	–	–	112.20±7.48	126.35±10.56
$T^*_{c\bar{c}1}(4800)^0 \to \rho(770)^0 \psi(2S)$	–	–	42.65±4.41	41.52±5.19
$T^*_{c\bar{c}1}(4800)^0 \to T_{c\bar{c}1}(4200)^+ \pi^-$	–	–	21.09±4.17	18.03±5.14
$T^*_{c\bar{c}1}(4800)^0 \to T_{c\bar{c}1}(4200)^- \pi^+$	–	–	21.07±4.17	18.03±5.14
$T^*_{c\bar{c}1}(4800)^0 \to T_{c\bar{c}1}(4430)^+ \pi^-$	–	–	4.46±2.01	5.44±2.45
$T^*_{c\bar{c}1}(4800)^0 \to T_{c\bar{c}1}(4430)^- \pi^+$	–	–	4.44±2.00	5.44±2.45
Sum $T^*_{c\bar{c}1}(4800)^0$	–	–	93.71±9.74	88.47±11.26
$T_{c\bar{c}\bar{s}1}(4600)^0 \to \psi(2S)\, K^*(892)^0$	–	–	–	50.87±7.79
$T_{c\bar{c}\bar{s}1}(4600)^0 \to T_{c\bar{c}1}(4200)^- K^+$	–	–	–	16.53±3.79
$T_{c\bar{c}\bar{s}1}(4600)^0 \to T_{c\bar{c}\bar{s}1}(4000)^+ \pi^-$	–	–	–	9.84±3.28
Sum $T_{c\bar{c}\bar{s}1}(4600)^0$	–	–	–	77.23±5.22
$T^*_{c\bar{c}\bar{s}1}(5200)^0 \to \psi(2S)\ [K^+\pi^-]_S$	–	–	–	66.28±15.03
$T^*_{c\bar{c}\bar{s}1}(5200)^0 \to T_{c\bar{c}\bar{s}1}(4000)^+ \pi^-$	–	–	–	9.37±14.12
Sum $T^*_{c\bar{c}\bar{s}1}(5200)^0$	–	–	–	75.65±9.18
$\psi(4430) \to \psi(2S)\ [\pi^+\pi^-]_S$	–	100	100	100
$\psi(4415) \to \psi(2S)\ [\pi^+\pi^-]_S$	–	100	–	–
$\psi(4660) \to \psi(2S)\ [\pi^+\pi^-]_S$	–	100	–	–
$T_{c\bar{c}\bar{s}1}(4900)^0 \to \psi(2S)\, K^*(892)^0$	–	–	–	100

Table 9. Fit results of the *start*, *no-exotics*, *known-exotics* and *baseline* models, part 2. Uncertainties are statistical only.

JHEP01(2025)054

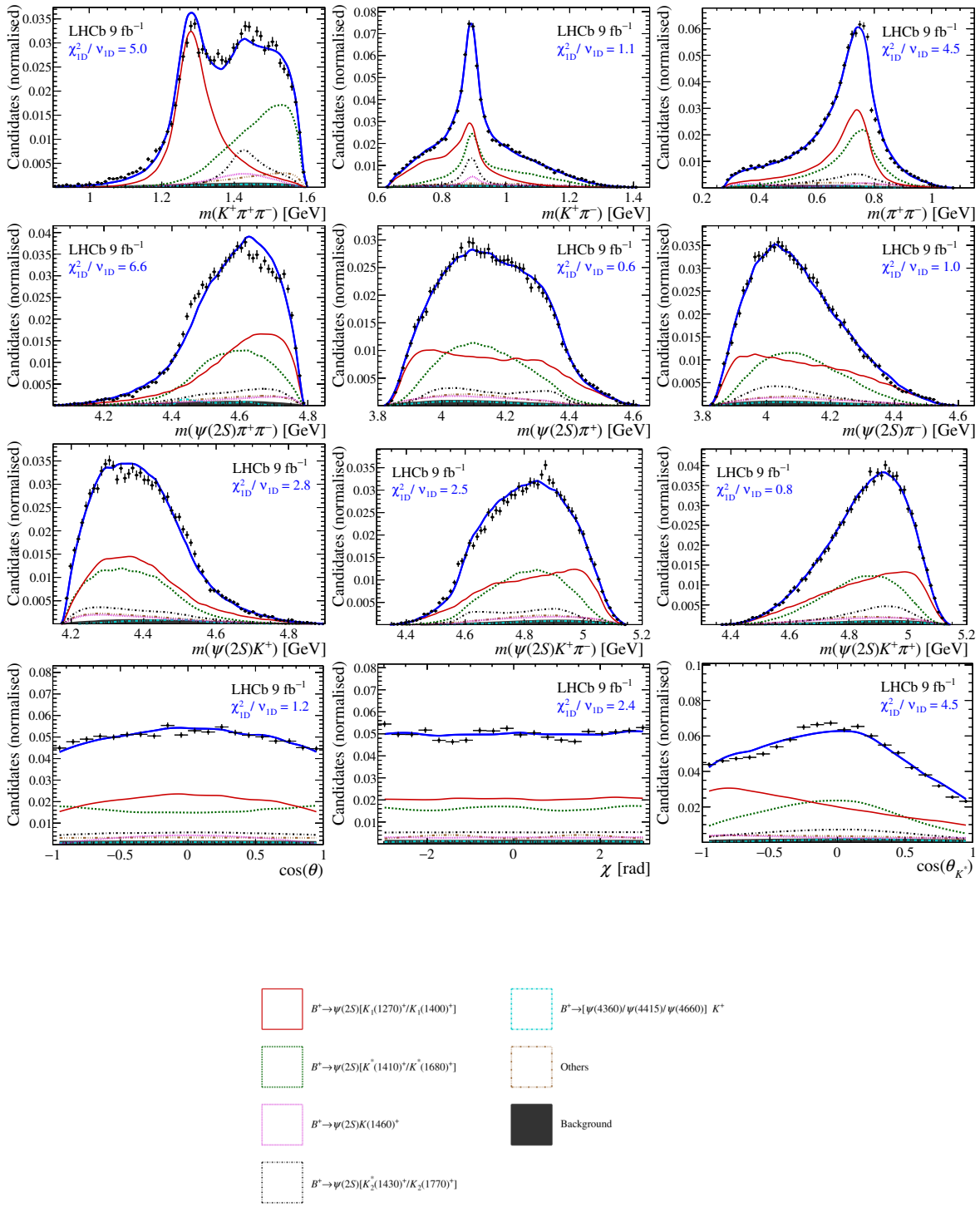

Figure 5. Phase-space projections of $B^+ \to \psi(2S)K^+\pi^+\pi^-$ candidates in the signal region (points with error bars) and fit projections (solid, blue line) for the *no-exotics* model. The displayed χ^2_{1D}/ν_{1D} value on each projection gives the sum of squared normalised residuals divided by the number of bins minus one. The multi-dimensional χ^2 value is $\chi^2/\nu = 2.05$ with $\nu = 1016$.

JHEP01(2025)054

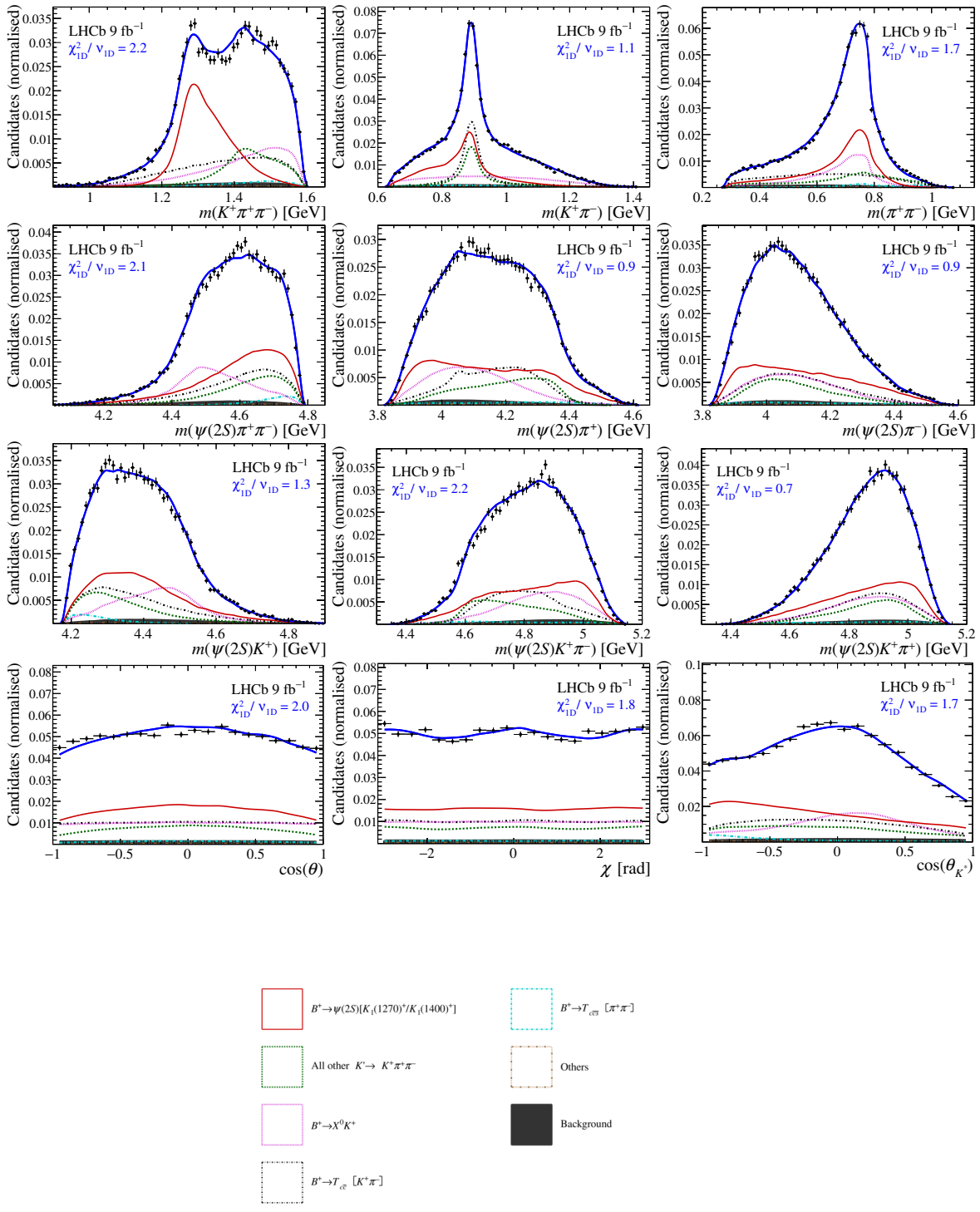

Figure 6. Phase-space projections of $B^+ \to \psi(2S)K^+\pi^+\pi^-$ candidates in the signal region (points with error bars) and fit projections (solid, blue line) for the *known-exotics* model. The displayed χ^2_{1D}/ν_{1D} value on each projection gives the sum of squared normalised residuals divided by the number of bins minus one. The multi-dimensional χ^2 value is $\chi^2/\nu = 1.31$ with $\nu = 1002$.

JHEP01(2025)054

D Amplitude models

Table 10 list the moduli and phases of the complex amplitude coefficients obtained by fitting the *baseline* model to the $B^+ \to \psi(2S)K^+\pi^+\pi^-$ candidates. The systematic uncertainties are summarised in tables 11 and 12 for all fit parameters and in tables 13 and 14 for the fit fractions. Table 15 lists the interference fractions ordered by magnitude for the *baseline* model. Figures 7 to 10 show additional fit projections of the *baseline* model in slices of the phase space.

Tables 16 to 21 summarise the fit results of the alternative models used for systematic studies. The code implementation of the *baseline* model and all alternative models, as well as instructions to generate pseudodata from them, can be found in ref. [92].

JHEP01(2025)054

Amplitude coupling	Magnitude	Phase [°]
$B^+[D] \to T_{c\bar{c}1}(4200)^+ K^*(892)^0$	0.85±0.07±0.14	−52.6± 5.4±4.2
$B^+[D] \to \psi(2S)\, K_1(1270)^+$	0.95±0.07±0.11	−210.8± 3.9±3.7
$B^+[D] \to \rho(770)^0 T_{c\bar{c}\bar{s}1}(4000)^+$	0.73±0.06±0.16	5.1± 5.1±5.6
$B^+[P] \to T_{c\bar{c}1}(4200)^+ K^*(892)^0$	1.09±0.09±0.26	−124.6± 6.0±5.8
$B^+[P] \to \psi(2S)\, K_1(1270)^+$	0.99±0.07±0.11	−120.5± 3.8±3.5
$B^+[P] \to \psi(2S)\, K_1(1400)^+$	0.33±0.06±0.11	110.6±10.2±7.0
$B^+ \to K_2^*(1430)^+ \psi(2S)$	0.93±0.07±0.08	125.9± 4.5±5.0
$B^+ \to T^*_{c\bar{c}1}(4055) K^*(892)^0$	0.37±0.04±0.05	141.7± 7.7±4.1
$B^+ \to T_{c\bar{c}1}(4200)^+ K^*(892)^0$	1.02±0.13±0.16	20.9± 8.8±6.0
$B^+ \to T_{c\bar{c}1}(4430)^+ K^*(892)^0$	0.44±0.13±0.29	−10.5±15.9±7.8
$B^+ \to T_{c\bar{c}1}(4430)^+ \left[K^+\pi^-\right]_S$	1.40±0.15±0.51	174.1± 6.5±4.9
$B^+ \to T_{c\bar{c}\bar{s}1}(4000)^+ \left[\pi^+\pi^-\right]_S$	0.71±0.08±0.20	−378.8± 7.6±6.1
$B^+ \to \psi(2S)\, K_1(1400)^+$	1.14±0.10±0.15	−144.6± 6.0±5.7
$B^+ \to \psi(2S)\, K(1460)^+$	0.69±0.06±0.13	226.4± 5.0±4.7
$B^+ \to \psi(2S)\, K^*(1410)^+$	0.64±0.08±0.17	134.7± 7.3±5.4
$B^+ \to \psi(2S)\, K^*(1680)^+$	1.02±0.14±0.31	162.7± 7.7±6.5
$K_1(1270)^+[D] \to K^*(892)^0 \pi^+$	0.41±0.03±0.04	−172.1± 3.3±3.4
$K_1(1270)^+ \to K^*(892)^0 \pi^+$	0.62±0.03±0.04	83.3± 3.2±3.4
$K_1(1270)^+ \to \left[K^+\pi^-\right]_S \pi^+$	0.51±0.04±0.08	−59.9± 4.5±5.3
$K_1(1400)^+ \to \rho(770)^0 K^+$	0.50±0.06±0.09	234.0± 7.7±5.7
$K(1460)^+ \to \left[\pi^+\pi^-\right]_S K^+$	0.95±0.10±0.49	1.0± 5.8±4.9
$K_2^*(1430)^+ \to \rho(770)^0 K^+$	0.41±0.04±0.04	−330.9± 6.3±4.8
$K^*(1410)^+ \to \rho(770)^0 K^+$	0.66±0.12±0.22	75.1±10.4±5.5
$K^*(1680)^+ \to \rho(770)^0 K^+$	0.79±0.13±0.25	−147.2±10.0±5.9
$T^*_{c\bar{c}0}(4475)^0 \to T_{c\bar{c}1}(4200)^+ \pi^-$	0.15±0.04±0.06	−58.8±13.4±7.4
$T^*_{c\bar{c}0}(4475)^0 \to \rho(770)^0 \psi(2S)$	2.17±0.17±0.29	52.3± 6.2±5.5
$T_{c\bar{c}1}(4650)^0 \to T_{c\bar{c}1}(4200)^+ \pi^-$	0.22±0.04±0.06	−30.6±11.2±5.4
$T_{c\bar{c}1}(4650)^0 \to \rho(770)^0 \psi(2S)$	0.80±0.09±0.10	−143.1±10.4±5.1
$T^*_{c\bar{c}0}(4710)^0 \to T_{c\bar{c}1}(4430)^+ \pi^-$	0.27±0.05±0.26	−94.6±10.2±5.6
$T^*_{c\bar{c}0}(4710)^0 \to \rho(770)^0 \psi(2S)$	0.64±0.08±0.10	−36.4±10.3±6.5
$T^*_{c\bar{c}1}(4800)^0 \to T_{c\bar{c}1}(4200)^+ \pi^-$	0.39±0.07±0.14	11.8±10.8±5.2
$T^*_{c\bar{c}1}(4800)^0 \to T_{c\bar{c}1}(4430)^+ \pi^-$	0.22±0.06±0.10	308.0±16.4±5.6
$T^*_{c\bar{c}1}(4800)^0 \to \rho(770)^0 \psi(2S)$	0.60±0.07±0.22	−63.3±10.2±6.3
$T_{c\bar{c}\bar{s}1}(4600)^0 \to T_{c\bar{c}1}(4200)^- K^+$	0.43±0.06±0.16	117.6± 8.9±5.6
$T_{c\bar{c}\bar{s}1}(4600)^0 \to T_{c\bar{c}\bar{s}1}(4000)^+ \pi^-$	0.34±0.06±0.08	101.5± 8.8±5.0
$T_{c\bar{c}\bar{s}1}(4600)^0 \to \psi(2S)\, K^*(892)^0$	0.76±0.14±0.30	185.7±14.1±6.0
$T_{c\bar{c}\bar{s}1}(4900)^0 \to \psi(2S)\, K^*(892)^0$	0.82±0.12±0.35	19.8±10.8±7.2
$T^*_{c\bar{c}\bar{s}1}(5200)^0 \to T_{c\bar{c}\bar{s}1}(4000)^+ \pi^-$	0.30±0.30±0.78	37.4±35.8±7.5
$T^*_{c\bar{c}\bar{s}1}(5200)^0 \to \psi(2S)\ \left[K^+\pi^-\right]_S$	0.73±0.55±1.41	−186.8±16.2±7.6
$\psi(4360) \to \psi(2S)\ \left[\pi^+\pi^-\right]_S$	0.81±0.09±0.15	−126.1± 8.0±6.0

Table 10. Fit result of the amplitude couplings for the *baseline model*. Uncertainties are statistical and systematic.

JHEP01(2025)054

Fit Parameter	1	2	3	4	5	6	7	8	9	10	Total
$B^+[D] \to T_{c\bar{c}1}(4200)^+ K^*(892)^0$ Amp	0.06	0.26	0.30	0.03	0.49	0.49	0.15	0.16	0.87	1.53	1.94
$B^+[D] \to T_{c\bar{c}1}(4200)^+ K^*(892)^0$ Phase	0.13	0.25	0.26	0.04	0.43	0.23	0.15	0.16	0.19	0.35	0.77
$B^+[D] \to \psi(2S) K_1(1270)^+$ Amp	0.29	0.34	0.29	0.04	0.36	0.38	0.21	0.30	0.62	1.22	1.60
$B^+[D] \to \psi(2S) K_1(1270)^+$ Phase	0.17	0.35	0.26	0.17	0.47	0.26	0.01	0.34	0.30	0.42	0.95
$B^+[D] \to \rho(770)^0 T_{c\bar{c}\bar{s}1}(4000)^+$ Amp	0.30	0.32	0.27	0.06	0.33	0.50	0.03	0.17	0.53	2.53	2.71
$B^+[D] \to \rho(770)^0 T_{c\bar{c}\bar{s}1}(4000)^+$ Phase	0.73	0.38	0.17	0.16	0.37	0.20	0.27	0.24	0.15	0.35	1.09
$B^+[P] \to T_{c\bar{c}1}(4200)^+ K^*(892)^0$ Amp	0.03	0.31	0.18	0.09	0.56	0.43	0.17	0.23	0.69	2.58	2.81
$B^+[P] \to T_{c\bar{c}1}(4200)^+ K^*(892)^0$ Phase	0.63	0.31	0.19	0.10	0.46	0.19	0.06	0.21	0.10	0.29	0.97
$B^+[P] \to \psi(2S) K_1(1270)^+$ Amp	0.41	0.29	0.20	0.03	0.25	0.27	0.16	0.26	0.35	1.45	1.65
$B^+[P] \to \psi(2S) K_1(1270)^+$ Phase	0.03	0.54	0.18	0.12	0.43	0.20	0.07	0.31	0.17	0.42	0.94
$B^+[P] \to \psi(2S) K_1(1400)^+$ Amp	0.01	0.32	0.19	0.32	0.78	0.22	0.04	0.14	0.61	1.38	1.78
$B^+[P] \to \psi(2S) K_1(1400)^+$ Phase	0.46	0.19	0.14	0.03	0.32	0.13	0.00	0.18	0.13	0.19	0.68
$B^+ \to K_2^*(1430)^+ \psi(2S)$ Amp	0.02	0.32	0.34	0.02	0.43	0.38	0.14	0.24	0.77	0.64	1.27
$B^+ \to K_2^*(1430)^+ \psi(2S)$ Phase	0.47	0.49	0.14	0.16	0.61	0.34	0.08	0.23	0.17	0.38	1.11
$B^+ \to T^*_{c\bar{c}1}(4055) K^*(892)^0$ Amp	0.20	0.28	0.19	0.03	0.30	0.26	0.04	0.09	0.55	0.98	1.26
$B^+ \to T^*_{c\bar{c}1}(4055) K^*(892)^0$ Phase	0.11	0.24	0.13	0.05	0.25	0.12	0.13	0.12	0.14	0.25	0.53
$B^+ \to T_{c\bar{c}1}(4200)^+ K^*(892)^0$ Amp	0.30	0.38	0.19	0.22	0.60	0.30	0.09	0.20	0.53	0.73	1.27
$B^+ \to T_{c\bar{c}1}(4200)^+ K^*(892)^0$ Phase	0.35	0.19	0.12	0.05	0.37	0.20	0.06	0.26	0.11	0.18	0.69
$B^+ \to T_{c\bar{c}1}(4430)^+ K^*(892)^0$ Amp	0.39	0.68	0.16	0.05	0.44	0.33	0.10	0.16	0.27	2.01	2.25
$B^+ \to T_{c\bar{c}1}(4430)^+ K^*(892)^0$ Phase	0.27	0.11	0.14	0.20	0.21	0.13	0.02	0.11	0.08	0.13	0.49
$B^+ \to T_{c\bar{c}1}(4430)^+ \left[K^+\pi^-\right]_S$ Amp	0.33	0.42	0.30	0.14	0.32	0.30	0.13	0.56	0.64	3.14	3.35
$B^+ \to T_{c\bar{c}1}(4430)^+ \left[K^+\pi^-\right]_S$ Phase	0.14	0.27	0.21	0.07	0.45	0.25	0.08	0.23	0.15	0.28	0.75
$B^+ \to T_{c\bar{c}\bar{s}1}(4000)^+ \left[\pi^+\pi^-\right]_S$ Amp	0.32	0.12	0.47	0.21	0.55	0.53	0.14	2.15	0.43	0.73	2.52
$B^+ \to T_{c\bar{c}\bar{s}1}(4000)^+ \left[\pi^+\pi^-\right]_S$ Phase	0.20	0.25	0.15	0.19	0.50	0.24	0.17	0.24	0.18	0.26	0.81
$B^+ \to \psi(2S) K_1(1400)^+$ Amp	0.09	0.34	0.29	0.03	0.61	0.38	0.10	0.10	0.91	0.79	1.48
$B^+ \to \psi(2S) K_1(1400)^+$ Phase	0.29	0.34	0.33	0.13	0.49	0.36	0.10	0.26	0.22	0.27	0.95
$B^+ \to \psi(2S) K(1460)^+$ Amp	0.28	0.37	0.28	0.02	0.38	0.52	0.03	0.23	0.74	2.01	2.31
$B^+ \to \psi(2S) K(1460)^+$ Phase	0.03	0.37	0.21	0.11	0.63	0.21	0.01	0.35	0.22	0.24	0.93
$B^+ \to \psi(2S) K^*(1410)^+$ Amp	0.01	0.38	0.30	0.08	0.69	0.50	0.10	0.19	0.65	1.92	2.27
$B^+ \to \psi(2S) K^*(1410)^+$ Phase	0.29	0.29	0.27	0.05	0.38	0.21	0.04	0.15	0.15	0.25	0.74
$B^+ \to \psi(2S) K^*(1680)^+$ Amp	0.04	0.30	0.14	0.21	1.20	0.35	0.05	0.15	0.50	1.83	2.31
$B^+ \to \psi(2S) K^*(1680)^+$ Phase	0.31	0.22	0.18	0.12	0.54	0.26	0.03	0.28	0.15	0.26	0.85
$T^*_{c\bar{c}0}(4475)^0$ mass	0.31	0.56	0.38	0.28	0.45	0.54	0.22	0.42	0.81	0.94	1.70
$T^*_{c\bar{c}0}(4475)^0$ width	0.37	0.68	0.24	0.53	0.55	0.54	0.04	0.36	0.75	0.74	1.66
$T^*_{c\bar{c}0}(4710)^0$ mass	0.50	0.63	0.20	0.10	0.22	0.18	0.12	0.23	0.24	0.76	1.22
$T^*_{c\bar{c}0}(4710)^0$ width	0.12	0.44	0.20	0.23	0.17	0.10	0.30	0.26	0.33	0.83	1.14
$T_{c\bar{c}1}(4650)^0$ mass	0.45	0.36	0.33	0.10	0.30	0.14	0.03	0.14	0.32	1.71	1.90
$T_{c\bar{c}1}(4650)^0$ width	0.28	0.26	0.29	0.17	0.12	0.20	0.02	0.12	0.25	0.57	0.85
$T^*_{c\bar{c}1}(4800)^0$ mass	0.09	0.44	0.12	0.48	0.26	0.62	0.12	0.81	0.21	2.93	3.19
$T^*_{c\bar{c}1}(4800)^0$ width	0.18	0.32	0.05	0.29	0.25	0.57	0.02	0.66	0.21	1.32	1.68
$T_{c\bar{c}\bar{s}1}(4600)^0$ mass	0.11	0.42	0.14	0.17	0.46	0.12	0.05	0.14	1.60	0.68	1.88
$T_{c\bar{c}\bar{s}1}(4600)^0$ width	0.31	0.48	0.17	0.14	0.39	0.09	0.01	0.13	2.05	1.08	2.43
$T_{c\bar{c}\bar{s}1}(4900)^0$ mass	0.27	0.25	0.21	0.11	0.83	0.47	0.03	0.15	0.36	1.83	2.14
$T_{c\bar{c}\bar{s}1}(4900)^0$ width	0.38	0.27	0.24	0.04	0.71	0.34	0.01	0.14	0.27	2.11	2.33
$T^*_{c\bar{c}\bar{s}1}(5200)^0$ mass	0.04	0.38	0.61	0.71	1.01	1.01	0.20	0.89	0.49	0.60	2.11
$T^*_{c\bar{c}\bar{s}1}(5200)^0$ width	0.38	1.42	1.48	1.46	2.51	1.44	1.27	1.69	1.15	1.97	4.96
$T_{c\bar{c}1}(4200)^+$ mass	0.30	0.51	0.14	0.14	0.32	0.43	0.11	0.15	0.28	1.30	1.57
$T_{c\bar{c}1}(4200)^+$ width	0.20	0.36	0.05	0.26	0.41	0.38	0.08	0.16	0.23	1.33	1.55
$T_{c\bar{c}1}(4430)^+$ mass	0.56	0.80	0.18	0.09	0.22	0.30	0.01	0.20	0.10	3.66	3.82
$T_{c\bar{c}1}(4430)^+$ width	0.16	0.61	0.12	0.05	0.23	0.16	0.21	0.39	0.17	1.78	1.97

Table 11. Systematic uncertainties on the fit parameters in units of statistical standard deviations, part 1. The different contributions are: 1) fit bias, 2) MC integration precision, 3) acceptance, 4) background, 5) masses and widths of resonances, 6) form factors, 7) $\rho - \omega$ mixing, 8) S-wave model, 9) lineshapes, 10) alternative amplitude models.

JHEP01(2025)054

Fit Parameter	1	2	3	4	5	6	7	8	9	10	Total
$K_1(1270)^+[D] \to K^*(892)^0\pi^+$ Amp	0.17	0.38	0.21	0.11	0.24	0.23	0.04	0.14	0.35	1.60	1.75
$K_1(1270)^+[D] \to K^*(892)^0\pi^+$ Phase	0.61	0.39	0.27	0.02	0.27	0.12	0.13	0.14	0.24	0.57	1.05
$K_1(1270)^+ \to K^*(892)^0\pi^+$ Amp	0.09	0.38	0.28	0.07	0.40	0.44	0.02	0.16	0.36	0.94	1.28
$K_1(1270)^+ \to K^*(892)^0\pi^+$ Phase	0.20	0.48	0.20	0.10	0.65	0.23	0.16	0.21	0.30	0.44	1.07
$K_1(1270)^+ \to [K^+\pi^-]_S\,\pi^+$ Amp	0.40	0.34	0.20	0.30	0.41	0.41	0.03	1.68	0.51	0.57	2.04
$K_1(1270)^+ \to [K^+\pi^-]_S\,\pi^+$ Phase	0.35	0.29	0.43	0.35	0.56	0.33	0.14	0.38	0.27	0.47	1.18
$K_1(1400)^+ \to \rho(770)^0K^+$ Amp	0.32	0.46	0.18	0.07	0.28	0.13	0.19	0.11	0.53	1.11	1.42
$K_1(1400)^+ \to \rho(770)^0K^+$ Phase	0.23	0.22	0.25	0.18	0.42	0.09	0.19	0.22	0.18	0.24	0.75
$K(1460)^+ \to [\pi^+\pi^-]_S\,K^+$ Amp	0.00	0.00	0.28	0.05	0.35	0.33	0.24	3.98	0.27	2.93	4.99
$K(1460)^+ \to [\pi^+\pi^-]_S\,K^+$ Phase	0.00	0.00	0.30	0.17	0.50	0.27	0.19	0.27	0.24	0.34	0.85
$K_2^*(1430)^+ \to \rho(770)^0K^+$ Amp	0.21	0.29	0.17	0.03	0.08	0.10	0.02	0.07	0.11	0.65	0.78
$K_2^*(1430)^+ \to \rho(770)^0K^+$ Phase	0.49	0.27	0.24	0.10	0.20	0.23	0.05	0.17	0.11	0.25	0.76
$K^*(1410)^+ \to \rho(770)^0K^+$ Amp	0.16	0.35	0.13	0.17	0.39	0.32	0.06	0.08	0.30	1.65	1.81
$K^*(1410)^+ \to \rho(770)^0K^+$ Phase	0.06	0.20	0.19	0.13	0.33	0.13	0.05	0.14	0.10	0.19	0.53
$K^*(1680)^+ \to \rho(770)^0K^+$ Amp	0.18	0.35	0.25	0.19	0.71	0.31	0.07	0.14	0.29	1.61	1.89
$K^*(1680)^+ \to \rho(770)^0K^+$ Phase	0.10	0.21	0.15	0.05	0.41	0.14	0.04	0.17	0.14	0.19	0.59
$T^*_{c\bar{c}0}(4475)^0 \to T_{c\bar{c}1}(4200)^+\,\pi^-$ Amp	0.05	0.34	0.21	0.32	0.47	0.28	0.08	0.69	0.39	0.80	1.35
$T^*_{c\bar{c}0}(4475)^0 \to T_{c\bar{c}1}(4200)^+\,\pi^-$ Phase	0.25	0.12	0.12	0.26	0.25	0.13	0.05	0.17	0.08	0.16	0.55
$T^*_{c\bar{c}0}(4475)^0 \to \rho(770)^0\psi(2S)$ Amp	0.13	0.34	0.24	0.22	0.14	0.48	0.13	0.18	0.91	1.24	1.70
$T^*_{c\bar{c}0}(4475)^0 \to \rho(770)^0\psi(2S)$ Phase	0.12	0.32	0.39	0.12	0.54	0.14	0.11	0.25	0.19	0.28	0.89
$T_{c\bar{c}1}(4650)^0 \to T_{c\bar{c}1}(4200)^+\,\pi^-$ Amp	0.49	0.47	0.32	0.42	0.26	0.41	0.22	0.13	0.49	0.87	1.43
$T_{c\bar{c}1}(4650)^0 \to T_{c\bar{c}1}(4200)^+\,\pi^-$ Phase	0.01	0.18	0.21	0.15	0.23	0.16	0.10	0.11	0.06	0.17	0.48
$T_{c\bar{c}1}(4650)^0 \to \rho(770)^0\psi(2S)$ Amp	0.11	0.27	0.33	0.17	0.21	0.20	0.10	0.10	0.60	0.85	1.19
$T_{c\bar{c}1}(4650)^0 \to \rho(770)^0\psi(2S)$ Phase	0.16	0.20	0.18	0.07	0.25	0.14	0.11	0.10	0.12	0.15	0.49
$T^*_{c\bar{c}0}(4710)^0 \to T_{c\bar{c}1}(4430)^+\,\pi^-$ Amp	0.21	0.49	0.25	0.03	0.17	0.42	0.20	0.32	0.46	5.34	5.42
$T^*_{c\bar{c}0}(4710)^0 \to T_{c\bar{c}1}(4430)^+\,\pi^-$ Phase	0.11	0.19	0.19	0.15	0.24	0.21	0.07	0.22	0.11	0.16	0.55
$T^*_{c\bar{c}0}(4710)^0 \to \rho(770)^0\psi(2S)$ Amp	0.39	0.41	0.39	0.17	0.14	0.35	0.31	0.25	0.58	0.76	1.31
$T^*_{c\bar{c}0}(4710)^0 \to \rho(770)^0\psi(2S)$ Phase	0.17	0.18	0.22	0.08	0.41	0.18	0.03	0.17	0.16	0.19	0.64
$T^*_{c\bar{c}1}(4800)^0 \to T_{c\bar{c}1}(4200)^+\,\pi^-$ Amp	0.99	0.50	0.17	0.40	0.34	0.41	0.12	0.37	0.37	1.57	2.11
$T^*_{c\bar{c}1}(4800)^0 \to T_{c\bar{c}1}(4200)^+\,\pi^-$ Phase	0.18	0.16	0.12	0.20	0.17	0.13	0.03	0.16	0.14	0.19	0.48
$T^*_{c\bar{c}1}(4800)^0 \to T_{c\bar{c}1}(4430)^+\,\pi^-$ Amp	0.33	0.39	0.13	0.24	0.13	0.43	0.11	0.33	0.19	1.66	1.86
$T^*_{c\bar{c}1}(4800)^0 \to T_{c\bar{c}1}(4430)^+\,\pi^-$ Phase	0.09	0.11	0.08	0.12	0.18	0.10	0.05	0.12	0.06	0.11	0.34
$T^*_{c\bar{c}1}(4800)^0 \to \rho(770)^0\psi(2S)$ Amp	0.20	0.39	0.42	0.10	0.14	0.51	0.04	0.42	0.43	2.87	3.05
$T^*_{c\bar{c}1}(4800)^0 \to \rho(770)^0\psi(2S)$ Phase	0.15	0.20	0.16	0.29	0.32	0.22	0.11	0.12	0.08	0.17	0.62
$T_{c\bar{c}\bar{s}1}(4600)^0 \to T_{c\bar{c}1}(4200)^-\,K^+$ Amp	0.04	0.35	0.19	0.12	0.25	0.48	0.12	0.11	0.60	2.52	2.68
$T_{c\bar{c}\bar{s}1}(4600)^0 \to T_{c\bar{c}1}(4200)^-\,K^+$ Phase	0.23	0.19	0.22	0.05	0.40	0.18	0.09	0.11	0.12	0.16	0.63
$T_{c\bar{c}\bar{s}1}(4600)^0 \to T_{c\bar{c}\bar{s}1}(4000)^+\,\pi^-$ Amp	0.06	0.38	0.26	0.33	0.23	0.37	0.08	0.28	0.40	0.97	1.30
$T_{c\bar{c}\bar{s}1}(4600)^0 \to T_{c\bar{c}\bar{s}1}(4000)^+\,\pi^-$ Phase	0.03	0.18	0.16	0.06	0.37	0.22	0.01	0.08	0.13	0.21	0.57
$T_{c\bar{c}\bar{s}1}(4600)^0 \to \psi(2S)\,K^*(892)^0$ Amp	0.17	0.25	0.20	0.06	0.28	0.28	0.01	0.10	0.76	1.91	2.13
$T_{c\bar{c}\bar{s}1}(4600)^0 \to \psi(2S)\,K^*(892)^0$ Phase	0.10	0.13	0.13	0.19	0.20	0.17	0.04	0.10	0.09	0.12	0.43
$T_{c\bar{c}\bar{s}1}(4900)^0 \to \psi(2S)\,K^*(892)^0$ Amp	0.00	0.26	0.22	0.06	0.88	0.56	0.00	0.11	0.45	2.75	3.00
$T_{c\bar{c}\bar{s}1}(4900)^0 \to \psi(2S)\,K^*(892)^0$ Phase	0.39	0.18	0.14	0.17	0.33	0.16	0.01	0.17	0.11	0.19	0.67
$T^*_{c\bar{c}\bar{s}1}(5200)^0 \to T_{c\bar{c}\bar{s}1}(4000)^+\,\pi^-$ Amp	0.22	0.96	0.66	0.39	0.83	0.95	0.53	1.34	0.57	1.06	2.58
$T^*_{c\bar{c}\bar{s}1}(5200)^0 \to T_{c\bar{c}\bar{s}1}(4000)^+\,\pi^-$ Phase	0.08	0.05	0.06	0.06	0.10	0.07	0.08	0.06	0.03	0.05	0.21
$T^*_{c\bar{c}\bar{s}1}(5200)^0 \to \psi(2S)\,[K^+\pi^-]_S$ Amp	0.28	0.85	0.74	0.50	0.88	1.19	0.50	1.17	0.57	0.96	2.58
$T^*_{c\bar{c}\bar{s}1}(5200)^0 \to \psi(2S)\,[K^+\pi^-]_S$ Phase	0.16	0.12	0.12	0.08	0.28	0.07	0.19	0.13	0.10	0.11	0.47
$\psi(4360) \to \psi(2S)\,[\pi^+\pi^-]_S$ Amp	0.13	0.15	0.19	0.17	0.36	0.29	0.24	1.26	0.50	0.67	1.63
$\psi(4360) \to \psi(2S)\,[\pi^+\pi^-]_S$ Phase	0.19	0.21	0.27	0.24	0.31	0.25	0.05	0.34	0.15	0.24	0.75

Table 12. Systematic uncertainties on the fit parameters in units of statistical standard deviations, part 2. The different contributions are: 1) fit bias, 2) MC integration precision, 3) acceptance, 4) background, 5) masses and widths of resonances, 6) form factors, 7) $\rho-\omega$ mixing, 8) S-wave model, 9) lineshapes, 10) alternative amplitude models.

JHEP01(2025)054

Fit fraction	1	2	3	4	5	6	7	8	9	10	Total
$B^+ \to T^*_{c\bar{c}0}(4475)^0 K^+$	0.21	0.36	0.26	0.29	0.60	0.50	0.08	0.39	0.58	1.88	2.22
$B^+ \to \psi(2S)\, K^*(1680)^+$	0.02	0.34	0.30	0.15	1.42	0.44	0.03	0.15	0.29	2.15	2.68
$B^+ \to \psi(2S)\, K_1(1270)^+$	0.16	0.41	0.30	0.06	0.45	0.42	0.19	0.32	0.75	1.07	1.59
$B^+[P] \to \psi(2S)\, K_1(1270)^+$	0.39	0.27	0.26	0.13	0.42	0.30	0.01	0.25	0.61	1.50	1.81
$B^+[D] \to \psi(2S)\, K_1(1270)^+$	0.26	0.30	0.25	0.11	0.07	0.06	0.14	0.13	0.17	2.59	2.64
$B^+ \to \psi(2S)\, K_1(1400)^+$	0.03	0.36	0.21	0.11	0.72	0.19	0.10	0.17	0.78	0.92	1.49
$B^+ \to \psi(2S)\, K(1460)^+$	0.48	0.30	0.42	0.10	0.46	0.78	0.08	0.48	0.27	1.31	1.83
$B^+[P] \to T_{c\bar{c}1}(4200)^+ K^*(892)^0$	0.00	0.33	0.25	0.05	0.47	0.37	0.07	0.12	0.29	3.94	4.02
$B^+ \to T_{c\bar{c}\bar{s}1}(4600)^0 \pi^+$	0.24	0.26	0.11	0.04	0.42	0.22	0.01	0.05	0.30	2.12	2.22
$B^+ \to K^*_2(1430)^+ \psi(2S)$	0.07	0.31	0.21	0.04	0.25	0.14	0.06	0.08	0.16	0.75	0.91
$B^+ \to T_{c\bar{c}1}(4200)^+ K^*(892)^0$	0.30	0.43	0.16	0.19	0.42	0.11	0.01	0.10	0.26	0.84	1.14
$B^+ \to T_{c\bar{c}1}(4430)^+ \left[K^+\pi^-\right]_S$	0.11	0.25	0.10	0.12	0.08	0.19	0.23	0.53	0.11	1.26	1.44
$B^+ \to T^*_{c\bar{c}1}(4800)^0 K^+$	0.49	0.23	0.13	0.01	0.11	0.28	0.15	0.24	0.09	1.42	1.59
$B^+ \to T_{c\bar{c}1}(4650)^0 K^+$	0.03	0.22	0.23	0.21	0.18	0.09	0.17	0.06	0.26	0.86	1.01
$B^+[D] \to T_{c\bar{c}1}(4200)^+ K^*(892)^0$	0.22	0.26	0.17	0.10	0.19	0.33	0.04	0.25	0.28	1.70	1.82
$B^+ \to T_{c\bar{c}\bar{s}1}(4900)^0 \pi^+$	0.07	0.23	0.10	0.05	0.81	0.36	0.06	0.14	0.19	2.78	2.94
$B^+[D] \to \rho(770)^0 T_{c\bar{c}\bar{s}1}(4000)^+$	0.39	0.38	0.12	0.14	0.09	0.24	0.11	0.26	0.21	3.82	3.89
$B^+ \to \psi(2S)\, K^*(1410)^+$	0.02	0.37	0.33	0.12	0.92	0.30	0.00	0.16	0.54	1.69	2.09
$B^+ \to T^*_{c\bar{c}0}(4710)^0 K^+$	0.55	0.36	0.31	0.08	0.15	0.23	0.32	0.22	0.37	1.08	1.43
$B^+ \to T^*_{c\bar{c}\bar{s}1}(5200)^0 \pi^+$	0.11	0.37	0.31	0.38	0.49	0.55	0.22	0.81	0.28	0.27	1.33
$B^+ \to T_{c\bar{c}\bar{s}1}(4000)^+ \left[\pi^+\pi^-\right]_S$	0.39	0.22	0.38	0.29	0.38	0.65	0.08	0.55	0.25	0.91	1.48
$B^+ \to T_{c\bar{c}1}(4430)^+ K^*(892)^0$	0.19	1.39	0.16	0.08	0.35	0.22	0.11	0.25	0.27	5.05	5.27
$B^+ \to \psi(4360) K^+$	0.07	0.19	0.09	0.16	0.14	0.16	0.18	0.47	0.15	0.55	0.83
$B^+ \to T^*_{c\bar{c}1}(4055)\, K^*(892)^0$	0.24	0.30	0.14	0.06	0.18	0.07	0.04	0.10	0.17	0.97	1.09
$B^+[P] \to \psi(2S)\, K_1(1400)^+$	0.00	0.38	0.25	0.30	0.67	0.21	0.06	0.17	0.41	2.03	2.26
Sum B^+	0.58	0.33	0.15	0.18	0.27	0.09	0.04	0.36	0.13	1.45	1.68

Table 13. Systematic uncertainties on the fit fractions in units of statistical standard deviations, part 1. The different contributions are: 1) fit bias, 2) MC integration precision, 3) acceptance, 4) background, 5) masses and widths of resonances, 6) form factors, 7) $\rho - \omega$ mixing, 8) S-wave model, 9) lineshapes, 10) alternative amplitude models.

JHEP01(2025)054

Fit fraction	1	2	3	4	5	6	7	8	9	10	Total
$K_1(1270)^+ \to \rho(770)^0 K^+$	0.37	0.30	0.29	0.05	0.35	0.50	0.10	0.21	0.22	1.16	1.46
$K_1(1270)^+ \to K^*(892)^0 \pi^+$	0.06	0.37	0.21	0.06	0.43	0.33	0.09	0.14	0.46	1.14	1.42
$K_1(1270)^+ \to [K^+\pi^-]_S \pi^+$	0.35	0.40	0.27	0.36	0.43	0.35	0.00	0.65	0.57	0.76	1.46
$K_1(1270)^+[D] \to K^*(892)^0 \pi^+$	0.07	0.39	0.17	0.12	0.19	0.15	0.01	0.19	0.38	1.69	1.82
Sum $K_1(1270)^+$	0.21	0.32	0.35	0.28	0.56	0.38	0.19	0.39	0.50	1.67	2.01
$K_1(1400)^+ \to K^*(892)^0 \pi^+$	0.25	0.42	0.22	0.09	0.20	0.14	0.22	0.12	0.56	1.13	1.41
$K_1(1400)^+ \to \rho(770)^0 K^+$	0.21	0.45	0.18	0.07	0.29	0.13	0.19	0.11	0.53	1.14	1.42
Sum $K_1(1400)^+$	0.20	0.55	0.11	0.07	0.77	0.38	0.00	0.12	0.59	1.89	2.24
$K(1460)^+ \to [\pi^+\pi^-]_S K^+$	0.00	0.01	0.25	0.05	0.28	0.49	0.22	0.46	0.25	2.44	2.58
$K(1460)^+ \to K^*(892)^0 \pi^+$	0.00	0.01	0.30	0.06	0.34	0.77	0.25	0.26	0.28	2.16	2.38
Sum $K(1460)^+$	0.00	0.14	0.27	0.15	0.34	1.69	0.12	3.01	0.19	4.19	5.45
$K_2^*(1430)^+ \to K^*(892)^0 \pi^+$	0.19	0.29	0.17	0.03	0.07	0.10	0.01	0.07	0.11	0.68	0.80
$K_2^*(1430)^+ \to \rho(770)^0 K^+$	0.20	0.29	0.17	0.03	0.08	0.10	0.02	0.07	0.11	0.65	0.78
Sum $K_2^*(1430)^+$	0.16	0.28	0.17	0.02	0.08	0.19	0.01	0.07	0.11	0.77	0.88
$K^*(1410)^+ \to K^*(892)^0 \pi^+$	0.05	0.36	0.22	0.12	0.44	0.27	0.07	0.12	0.26	1.31	1.51
$K^*(1410)^+ \to \rho(770)^0 K^+$	0.10	0.36	0.09	0.19	0.49	0.33	0.06	0.06	0.32	1.64	1.82
Sum $K^*(1410)^+$	0.16	0.29	0.19	0.20	1.25	0.29	0.02	0.08	0.37	2.39	2.77
$K^*(1680)^+ \to K^*(892)^0 \pi^+$	0.07	0.34	0.25	0.19	0.69	0.29	0.06	0.14	0.31	1.74	1.98
$K^*(1680)^+ \to \rho(770)^0 K^+$	0.07	0.34	0.25	0.19	0.72	0.32	0.07	0.14	0.29	1.56	1.84
Sum $K^*(1680)^+$	0.06	0.36	0.23	0.17	0.55	0.10	0.01	0.15	0.48	6.04	6.10
$T^*_{c\bar{c}0}(4475)^0 \to \rho(770)^0 \psi(2S)$	0.17	0.66	0.28	0.27	0.49	0.27	0.13	0.72	0.17	3.16	3.39
$T^*_{c\bar{c}0}(4475)^0 \to T_{c\bar{c}1}(4200)^- \pi^+$	0.17	0.69	0.28	0.27	0.49	0.27	0.13	0.72	0.18	0.93	1.55
$T^*_{c\bar{c}0}(4475)^0 \to T_{c\bar{c}1}(4200)^+ \pi^-$	0.17	0.69	0.28	0.27	0.49	0.27	0.13	0.72	0.18	0.93	1.55
Sum $T^*_{c\bar{c}0}(4475)^0$	0.09	1.81	0.26	0.28	0.46	0.32	0.14	0.70	0.17	69.58	69.61
$T_{c\bar{c}1}(4650)^0 \to \rho(770)^0 \psi(2S)$	0.60	0.34	0.10	0.10	0.09	0.46	0.14	0.06	0.23	0.62	1.08
$T_{c\bar{c}1}(4650)^0 \to T_{c\bar{c}1}(4200)^- \pi^+$	0.58	0.43	0.20	0.33	0.13	0.35	0.27	0.06	0.11	0.75	1.21
$T_{c\bar{c}1}(4650)^0 \to T_{c\bar{c}1}(4200)^+ \pi^-$	0.58	0.44	0.20	0.32	0.14	0.35	0.27	0.06	0.11	0.75	1.21
Sum $T_{c\bar{c}1}(4650)^0$	0.54	0.33	0.11	0.08	0.10	0.57	0.00	0.05	0.24	0.49	1.03
$T^*_{c\bar{c}0}(4710)^0 \to \rho(770)^0 \psi(2S)$	0.50	0.44	0.21	0.18	0.39	0.39	0.00	0.30	0.20	0.99	1.39
$T^*_{c\bar{c}0}(4710)^0 \to T_{c\bar{c}1}(4430)^+ \pi^-$	0.17	0.46	0.16	0.12	0.06	0.21	0.03	0.15	0.10	0.65	0.88
$T^*_{c\bar{c}0}(4710)^0 \to T_{c\bar{c}1}(4430)^- \pi^+$	0.17	0.46	0.16	0.12	0.06	0.21	0.03	0.15	0.10	0.65	0.88
Sum $T^*_{c\bar{c}0}(4710)^0$	0.58	0.66	0.25	0.14	0.43	0.41	0.02	0.32	0.22	0.71	1.36
$T^*_{c\bar{c}1}(4800)^0 \to \rho(770)^0 \psi(2S)$	0.42	0.35	0.40	0.26	0.17	0.21	0.15	0.29	0.16	1.82	2.01
$T^*_{c\bar{c}1}(4800)^0 \to T_{c\bar{c}1}(4200)^- \pi^+$	0.81	0.46	0.22	0.28	0.26	0.14	0.05	0.31	0.17	0.66	1.28
$T^*_{c\bar{c}1}(4800)^0 \to T_{c\bar{c}1}(4200)^+ \pi^-$	0.81	0.46	0.22	0.28	0.26	0.14	0.05	0.31	0.17	0.66	1.28
$T^*_{c\bar{c}1}(4800)^0 \to T_{c\bar{c}1}(4430)^+ \pi^-$	0.18	0.21	0.16	0.14	0.07	0.18	0.08	0.34	0.13	0.75	0.93
$T^*_{c\bar{c}1}(4800)^0 \to T_{c\bar{c}1}(4430)^- \pi^+$	0.18	0.21	0.16	0.14	0.07	0.18	0.08	0.34	0.13	0.76	0.93
Sum $T^*_{c\bar{c}1}(4800)^0$	0.65	0.40	0.19	0.20	0.19	0.16	0.01	0.28	0.15	0.73	1.16
$T_{c\bar{c}\bar{s}1}(4600)^0 \to \psi(2S)\, K^*(892)^0$	0.06	0.20	0.18	0.03	0.13	0.22	0.09	0.04	0.38	1.38	1.48
$T_{c\bar{c}\bar{s}1}(4600)^0 \to T_{c\bar{c}1}(4200)^- K^+$	0.07	0.38	0.09	0.20	0.42	0.40	0.09	0.08	0.36	3.26	3.36
$T_{c\bar{c}\bar{s}1}(4600)^0 \to T_{c\bar{c}\bar{s}1}(4000)^+ \pi^-$	0.11	0.31	0.20	0.35	0.25	0.25	0.05	0.22	0.22	1.47	1.63
Sum $T_{c\bar{c}\bar{s}1}(4600)^0$	0.05	0.35	0.20	0.11	0.42	0.21	0.03	0.11	0.24	3.34	3.41
$T^*_{c\bar{c}\bar{s}1}(5200)^0 \to \psi(2S)\ [K^+\pi^-]_S$	0.15	0.39	0.10	0.12	0.09	0.03	0.09	0.50	0.60	0.71	1.15
$T^*_{c\bar{c}\bar{s}1}(5200)^0 \to T_{c\bar{c}\bar{s}1}(4000)^+ \pi^-$	0.01	0.32	0.14	0.06	0.25	0.14	0.15	0.71	0.20	0.31	0.94
Sum $T^*_{c\bar{c}\bar{s}1}(5200)^0$	0.14	0.59	0.21	0.30	0.24	0.19	0.09	0.50	0.71	0.87	1.46

Table 14. Systematic uncertainties on the fit fractions in units of statistical standard deviations, part 2. The different contributions are: 1) fit bias, 2) MC integration precision, 3) acceptance, 4) background, 5) masses and widths of resonances, 6) form factors, 7) $\rho - \omega$ mixing, 8) S-wave model, 9) lineshapes, 10) alternative amplitude models.

JHEP01(2025)054

Decay channel i	Decay channel j	IF_{ij}[%]
$B^+ \to T^*_{c\bar{c}0}(4475)^0 K^+$	$B^+ \to \psi(2S)\, K_1(1270)^+$	7.87 ± 0.61
$B^+ \to T_{c\bar{c}1}(4200)^+ K^*(892)^0$	$B^+ \to \psi(2S)\, K_1(1400)^+$	-4.88 ± 0.68
$B^+ \to T^*_{c\bar{c}0}(4475)^0 K^+$	$B^+ \to T^*_{c\bar{c}0}(4710)^0 K^+$	-4.63 ± 0.48
$B^+ \to T^*_{c\bar{c}0}(4475)^0 K^+$	$B^+ \to \psi(2S)\, K_1(1400)^+$	4.62 ± 0.59
$B^+ \to T_{c\bar{c}s\bar{1}}(4600)^0 \pi^+$	$B^+ \to \psi(2S)\, K^*(1680)^+$	-4.62 ± 1.52
$B^+ \to \psi(2S)\, K^*(1410)^+$	$B^+ \to \psi(2S)\, K^*(1680)^+$	3.74 ± 0.68
$B^+ \to T_{c\bar{c}1}(4650)^0 K^+$	$B^+ \to \psi(2S)\, K^*(1680)^+$	3.27 ± 0.56
$B^+ \to \psi(2S)\, K_1(1270)^+$	$B^+ \to \psi(2S)\, K_1(1400)^+$	2.84 ± 0.70
$B^+ \to T^*_{c\bar{c}0}(4475)^0 K^+$	$B^+ \to T^*_{c\bar{c}s\bar{1}}(5200)^0 \pi^+$	-2.57 ± 2.56
$B^+ \to T^*_{c\bar{c}0}(4475)^0 K^+$	$B^+ \to T_{c\bar{c}1}(4430)^+ \left[K^+\pi^-\right]_{\rm S}$	2.32 ± 0.19
$B^+ \to T^*_{c\bar{c}1}(4800)^0 K^+$	$B^+ \to T_{c\bar{c}1}(4430)^+ \left[K^+\pi^-\right]_{\rm S}$	-2.18 ± 0.37
$B^+[D] \to \psi(2S)\, K_1(1270)^+$	$B^+ \to \psi(2S)\, K_1(1270)^+$	2.04 ± 0.14
$B^+ \to T_{c\bar{c}s\bar{1}}(4000)^+ \left[\pi^+\pi^-\right]_{\rm S}$	$B^+ \to \psi(2S)\, K(1460)^+$	-1.96 ± 0.34
$B^+ \to T_{c\bar{c}s\bar{1}}(4900)^0 \pi^+$	$B^+ \to \psi(2S)\, K^*(1680)^+$	-1.94 ± 0.82
$B^+ \to T_{c\bar{c}1}(4430)^+ \left[K^+\pi^-\right]_{\rm S}$	$B^+ \to \psi(2S)\, K_1(1270)^+$	1.50 ± 0.13
$B^+ \to T^*_{c\bar{c}s\bar{1}}(5200)^0 \pi^+$	$B^+ \to \psi(2S)\, K_1(1270)^+$	-1.46 ± 1.17
$B^+[D] \to \rho(770)^0 T_{c\bar{c}s\bar{1}}(4000)^+$	$B^+ \to T^*_{c\bar{c}0}(4475)^0 K^+$	-1.45 ± 0.10
$B^+[P] \to T_{c\bar{c}1}(4200)^+ K^*(892)^0$	$B^+ \to K_2^*(1430)^+ \psi(2S)$	1.34 ± 0.14
$B^+[D] \to T_{c\bar{c}1}(4200)^+ K^*(892)^0$	$B^+ \to \psi(2S)\, K(1460)^+$	-1.28 ± 0.19
$B^+ \to T_{c\bar{c}s\bar{1}}(4900)^0 \pi^+$	$B^+ \to \psi(2S)\, K^*(1410)^+$	-1.17 ± 0.26
$B^+[P] \to T_{c\bar{c}1}(4200)^+ K^*(892)^0$	$B^+ \to \psi(2S)\, K^*(1680)^+$	1.11 ± 0.77
$B^+ \to T^*_{c\bar{c}1}(4800)^0 K^+$	$B^+ \to \psi(2S)\, K_1(1400)^+$	-1.10 ± 0.17
$B^+[D] \to T_{c\bar{c}1}(4200)^+ K^*(892)^0$	$B^+ \to \psi(2S)\, K_1(1270)^+$	1.03 ± 0.08
$B^+ \to T^*_{c\bar{c}0}(4475)^0 K^+$	$B^+ \to T_{c\bar{c}1}(4200)^+ K^*(892)^0$	1.01 ± 0.19
$B^+ \to T_{c\bar{c}1}(4430)^+ K^*(892)^0$	$B^+ \to \psi(2S)\, K_1(1270)^+$	-0.95 ± 0.34
$B^+ \to T^*_{c\bar{c}0}(4710)^0 K^+$	$B^+ \to \psi(2S)\, K_1(1270)^+$	-0.92 ± 0.36
$B^+ \to T^*_{c\bar{c}1}(4800)^0 K^+$	$B^+ \to T_{c\bar{c}1}(4200)^+ K^*(892)^0$	0.92 ± 0.19
$B^+ \to T^*_{c\bar{c}0}(4710)^0 K^+$	$B^+ \to T_{c\bar{c}1}(4430)^+ \left[K^+\pi^-\right]_{\rm S}$	-0.80 ± 0.13
$B^+ \to T^*_{c\bar{c}0}(4710)^0 K^+$	$B^+ \to \psi(2S)\, K_1(1400)^+$	-0.79 ± 0.15
$B^+[P] \to T_{c\bar{c}1}(4200)^+ K^*(892)^0$	$B^+ \to T_{c\bar{c}s\bar{1}}(4600)^0 \pi^+$	-0.77 ± 0.10
$B^+ \to T_{c\bar{c}1}(4200)^+ K^*(892)^0$	$B^+ \to T_{c\bar{c}1}(4430)^+ K^*(892)^0$	0.72 ± 0.89
$B^+[P] \to T_{c\bar{c}1}(4200)^+ K^*(892)^0$	$B^+[P] \to \psi(2S)\, K_1(1400)^+$	-0.67 ± 0.23
$B^+[D] \to T_{c\bar{c}1}(4200)^+ K^*(892)^0$	$B^+[D] \to \psi(2S)\, K_1(1270)^+$	0.62 ± 0.06
$B^+ \to T_{c\bar{c}1}(4430)^+ \left[K^+\pi^-\right]_{\rm S}$	$B^+ \to \psi(2S)\, K_1(1400)^+$	0.61 ± 0.09
$B^+ \to T^*_{c\bar{c}0}(4710)^0 K^+$	$B^+ \to T^*_{c\bar{c}s\bar{1}}(5200)^0 \pi^+$	0.61 ± 0.61
$B^+ \to T_{c\bar{c}s\bar{1}}(4600)^0 \pi^+$	$B^+ \to \psi(2S)\, K^*(1410)^+$	-0.61 ± 0.49
$B^+ \to T_{c\bar{c}s\bar{1}}(4900)^0 \pi^+$	$B^+ \to T^*_{c\bar{c}1}(4055)\, K^*(892)^0$	0.61 ± 0.09
$B^+[P] \to T_{c\bar{c}1}(4200)^+ K^*(892)^0$	$B^+ \to T_{c\bar{c}1}(4650)^0 K^+$	-0.60 ± 0.28
$B^+ \to T_{c\bar{c}1}(4650)^0 K^+$	$B^+ \to T_{c\bar{c}s\bar{1}}(4600)^0 \pi^+$	-0.60 ± 0.23
$B^+[P] \to T_{c\bar{c}1}(4200)^+ K^*(892)^0$	$B^+ \to \psi(2S)\, K^*(1410)^+$	-0.59 ± 0.37
$B^+ \to T_{c\bar{c}s\bar{1}}(4600)^0 \pi^+$	$B^+ \to T^*_{c\bar{c}1}(4055)\, K^*(892)^0$	-0.59 ± 0.16
$B^+[P] \to \psi(2S)\, K_1(1400)^+$	$B^+ \to T_{c\bar{c}s\bar{1}}(4600)^0 \pi^+$	-0.58 ± 0.20
$B^+ \to T_{c\bar{c}1}(4650)^0 K^+$	$B^+ \to \psi(2S)\, K^*(1410)^+$	-0.57 ± 0.26
$B^+ \to T_{c\bar{c}1}(4200)^+ K^*(892)^0$	$B^+ \to \psi(2S)\, K_1(1270)^+$	0.55 ± 0.39
$B^+ \to T_{c\bar{c}s\bar{1}}(4600)^0 \pi^+$	$B^+ \to T_{c\bar{c}s\bar{1}}(4900)^0 \pi^+$	-0.55 ± 1.15
$B^+[D] \to \psi(2S)\, K_1(1270)^+$	$B^+ \to T_{c\bar{c}1}(4430)^+ \left[K^+\pi^-\right]_{\rm S}$	0.55 ± 0.09
$B^+[D] \to T_{c\bar{c}1}(4200)^+ K^*(892)^0$	$B^+ \to T^*_{c\bar{c}1}(4800)^0 K^+$	-0.54 ± 0.11
$B^+ \to K_2^*(1430)^+ \psi(2S)$	$B^+ \to T^*_{c\bar{c}1}(4055)\, K^*(892)^0$	0.52 ± 0.05
$B^+ \to T^*_{c\bar{c}1}(4800)^0 K^+$	$B^+ \to \psi(2S)\, K_1(1270)^+$	-0.48 ± 0.43
$B^+ \to T_{c\bar{c}1}(4200)^+ K^*(892)^0$	$B^+ \to \psi(2S)\, K(1460)^+$	0.46 ± 0.16
$B^+ \to T_{c\bar{c}1}(4200)^+ K^*(892)^0$	$B^+ \to \psi(4360) K^+$	-0.42 ± 0.07
$B^+ \to T^*_{c\bar{c}s\bar{1}}(5200)^0 \pi^+$	$B^+ \to \psi(2S)\, K_1(1400)^+$	-0.42 ± 0.45
$B^+[D] \to \rho(770)^0 T_{c\bar{c}s\bar{1}}(4000)^+$	$B^+ \to \psi(2S)\, K_1(1400)^+$	-0.40 ± 0.05
$B^+[P] \to \psi(2S)\, K_1(1270)^+$	$B^+[P] \to \psi(2S)\, K_1(1400)^+$	0.38 ± 0.39
$B^+[D] \to \rho(770)^0 T_{c\bar{c}s\bar{1}}(4000)^+$	$B^+ \to \psi(2S)\, K(1460)^+$	0.38 ± 0.03
$B^+[D] \to T_{c\bar{c}1}(4200)^+ K^*(892)^0$	$B^+ \to T^*_{c\bar{c}0}(4475)^0 K^+$	0.38 ± 0.10
$B^+ \to K_2^*(1430)^+ \psi(2S)$	$B^+ \to T_{c\bar{c}s\bar{1}}(4600)^0 \pi^+$	0.36 ± 0.19
$B^+[D] \to T_{c\bar{c}1}(4200)^+ K^*(892)^0$	$B^+ \to T_{c\bar{c}1}(4430)^+ K^*(892)^0$	-0.36 ± 0.11
$B^+ \to T^*_{c\bar{c}0}(4475)^0 K^+$	$B^+ \to T_{c\bar{c}1}(4430)^+ K^*(892)^0$	-0.34 ± 0.16
$B^+ \to T^*_{c\bar{c}1}(4800)^0 K^+$	$B^+ \to T^*_{c\bar{c}s\bar{1}}(5200)^0 \pi^+$	0.34 ± 0.34
$B^+ \to \psi(2S)\, K_1(1400)^+$	$B^+ \to \psi(2S)\, K(1460)^+$	-0.33 ± 0.03
$B^+ \to \psi(2S)\, K(1460)^+$	$B^+ \to \psi(4360) K^+$	-0.32 ± 0.08
$B^+[P] \to \psi(2S)\, K_1(1270)^+$	$B^+ \to T_{c\bar{c}1}(4650)^0 K^+$	-0.31 ± 0.48
$B^+[P] \to \psi(2S)\, K_1(1270)^+$	$B^+ \to T^*_{c\bar{c}1}(4055)\, K^*(892)^0$	0.30 ± 0.06
$B^+[D] \to T_{c\bar{c}1}(4200)^+ K^*(892)^0$	$B^+ \to T_{c\bar{c}1}(4200)^+ K^*(892)^0$	-0.30 ± 0.13

Table 15. Interference fractions with $|IF_{ij}| \geq 0.30\%$ for the *baseline model*. The uncertainties are statistical only.

JHEP01(2025)054

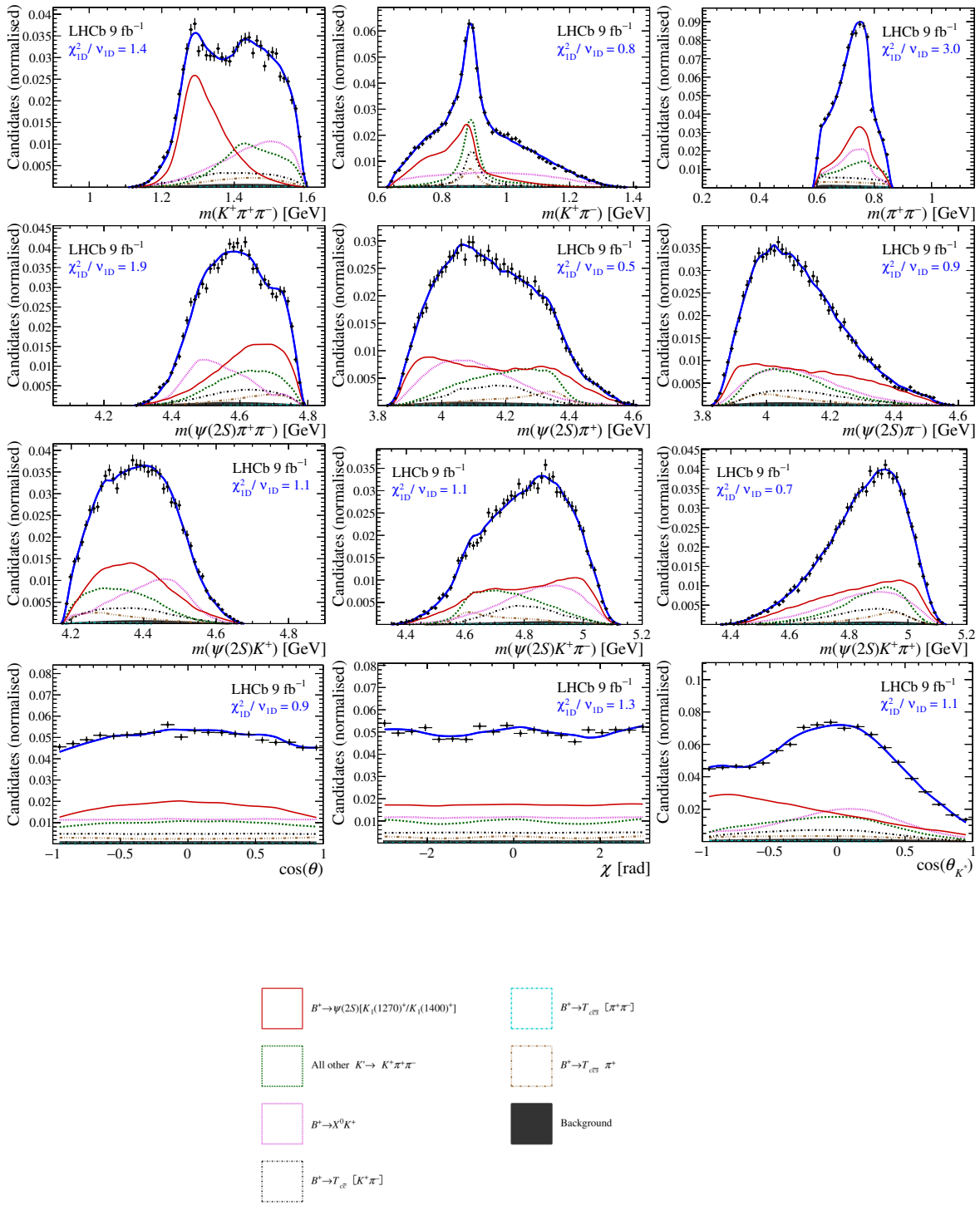

Figure 7. Phase-space projections of $B^+ \to \psi(2S)K^+\pi^+\pi^-$ candidates in the $m(\pi^+\pi^-)$ region around the $\rho(770)$ resonance (points with error bars) and fit projections (solid, blue line) for the *baseline* model. The displayed χ^2_{1D}/ν_{1D} value on each projection gives the sum of squared normalised residuals divided by the number of bins minus one. The multi-dimensional χ^2 value is $\chi^2/\nu = 1.19$ with $\nu = 737$.

JHEP01(2025)054

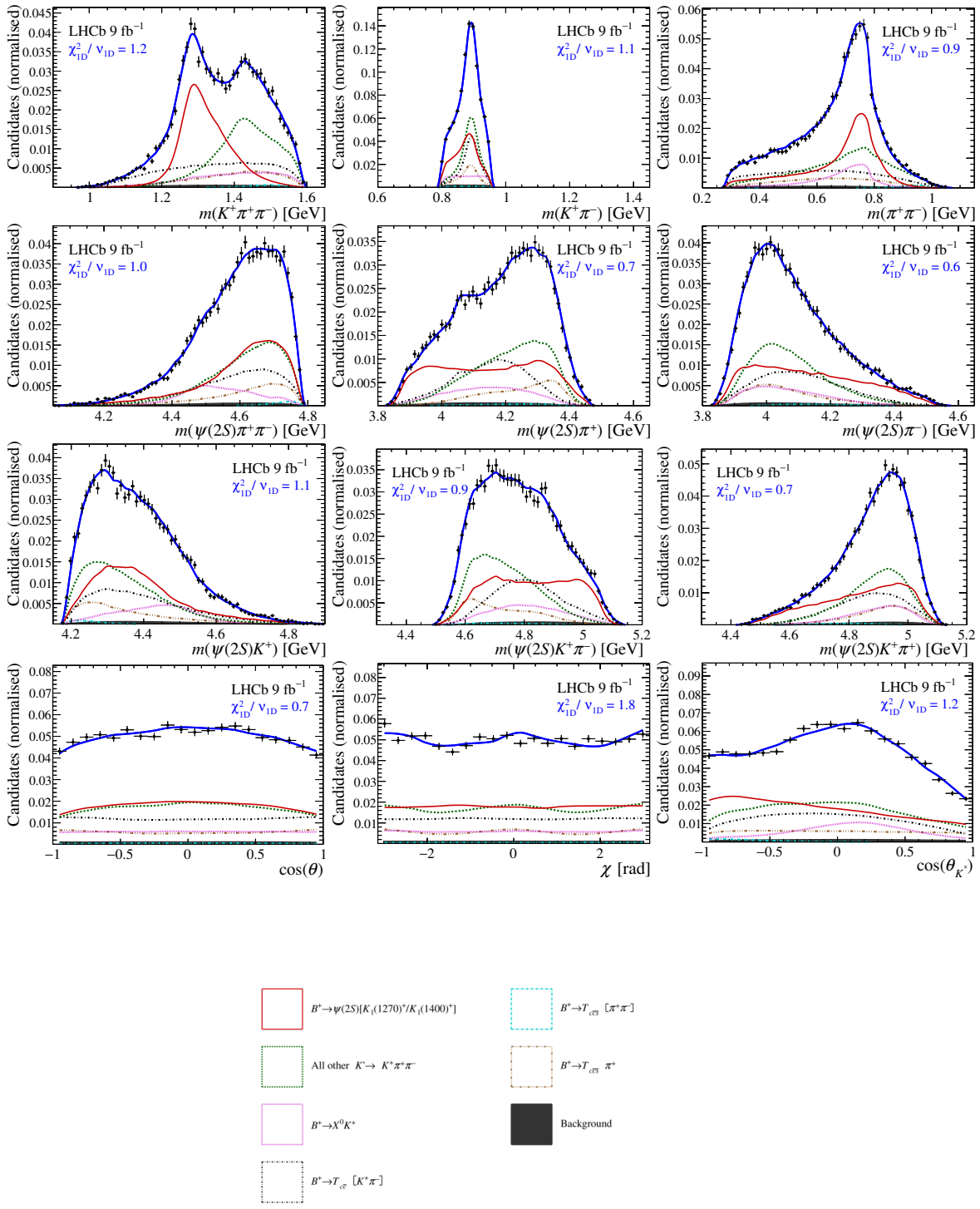

Figure 8. Phase-space projections of $B^+ \to \psi(2S)K^+\pi^+\pi^-$ candidates in the $m(K^+\pi^-)$ region around the $K^*(892)$ resonance (points with error bars) and fit projections (solid, blue line) for the *baseline* model. The displayed χ^2_{1D}/ν_{1D} value on each projection gives the sum of squared normalised residuals divided by the number of bins minus one. The multi-dimensional χ^2 value is $\chi^2/\nu = 1.09$ with $\nu = 577$.

JHEP01(2025)054

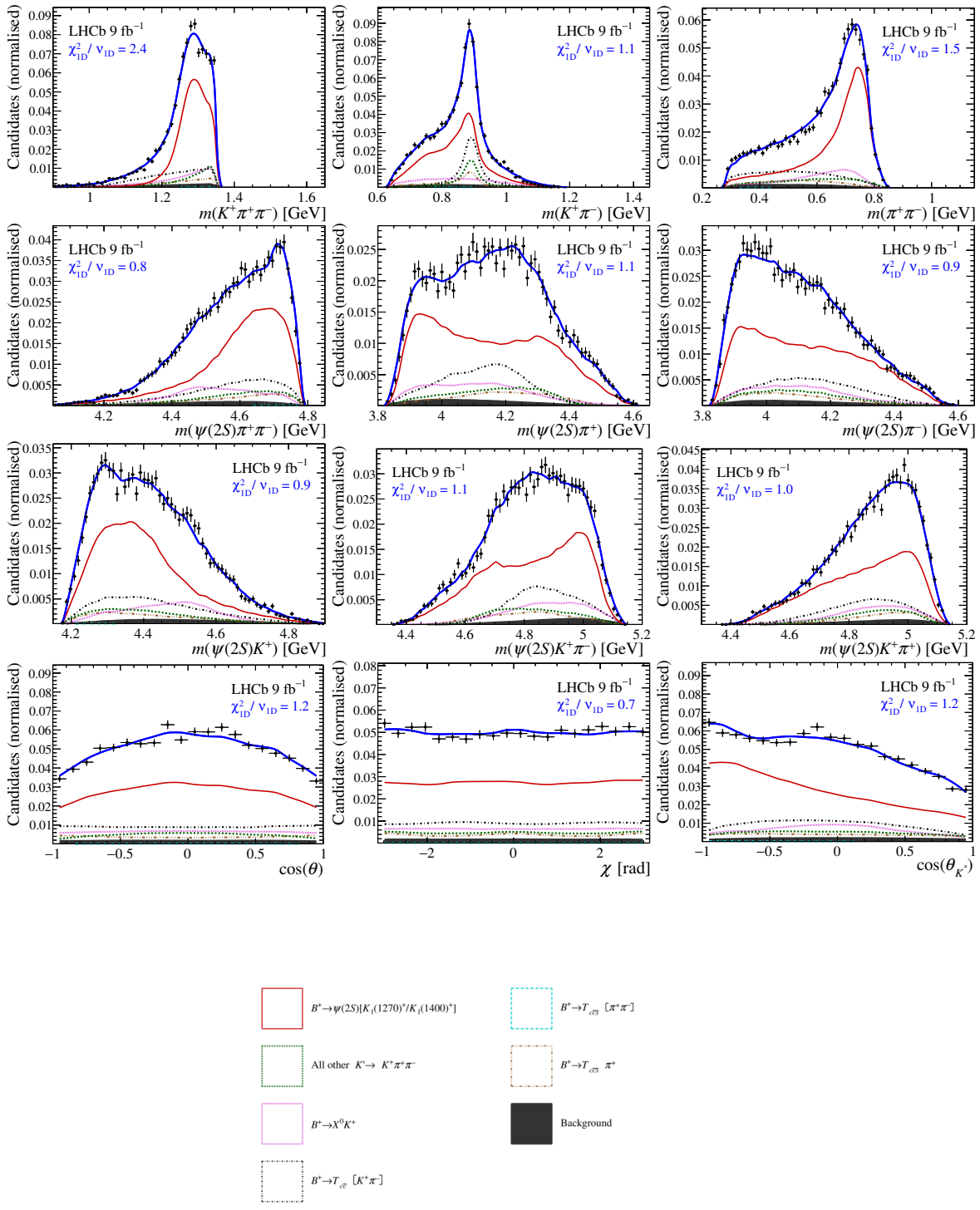

Figure 9. Phase-space projections of $B^+ \to \psi(2S)K^+\pi^+\pi^-$ candidates in the in low $m(K^+\pi^+\pi^-)$ region (points with error bars) and fit projections (solid, blue line) for the *baseline* model. The displayed χ^2_{1D}/ν_{1D} value on each projection gives the sum of squared normalised residuals divided by the number of bins minus one. The multi-dimensional χ^2 value is $\chi^2/\nu = 1.09$ with $\nu = 652$.

JHEP01(2025)054

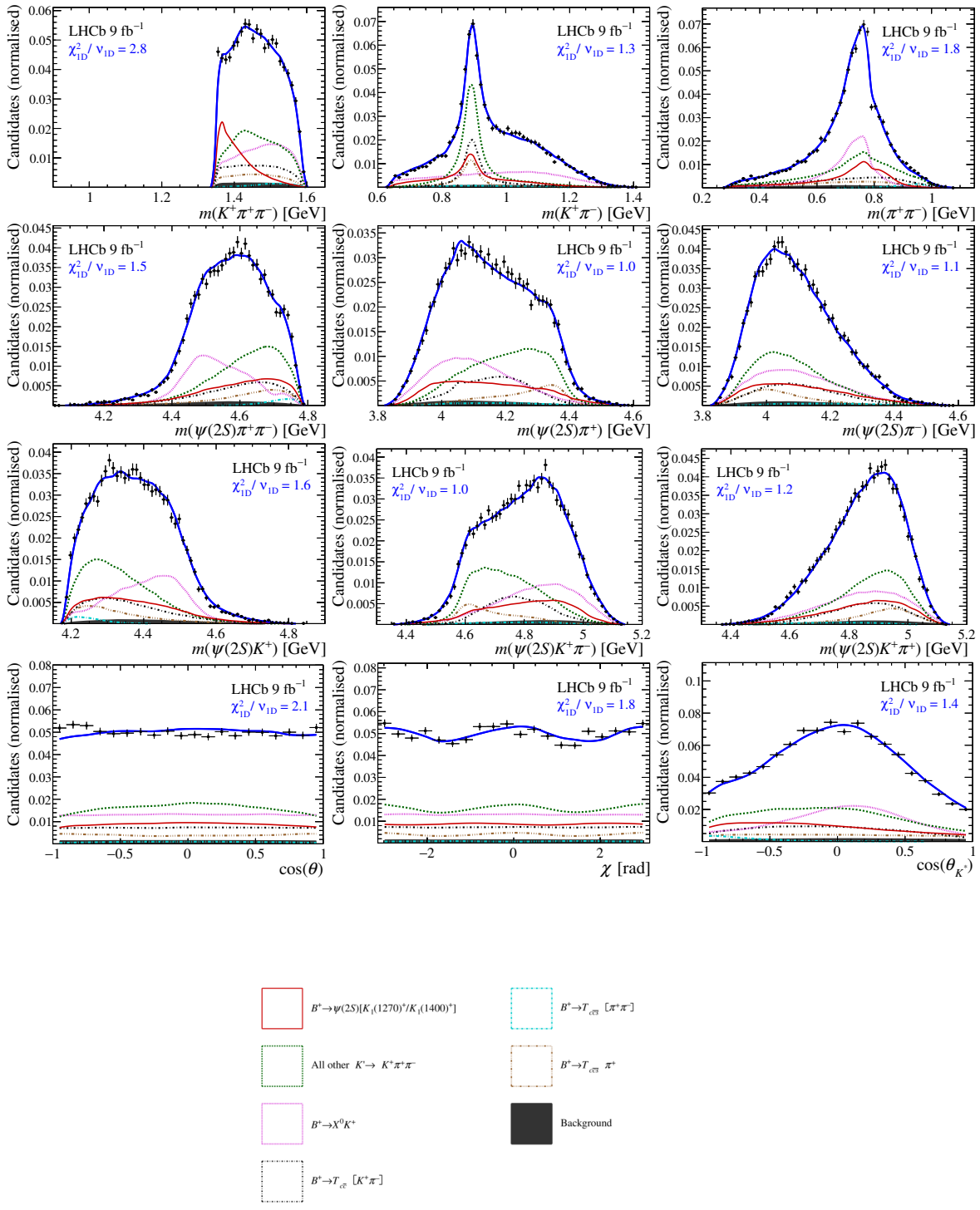

Figure 10. Phase-space projections of $B^+ \to \psi(2S)K^+\pi^+\pi^-$ candidates in the high $m(K^+\pi^+\pi^-)$ region (points with error bars) and fit projections (solid, blue line) for the *baseline* model. The displayed χ^2_{1D}/ν_{1D} value on each projection gives the sum of squared normalised residuals divided by the number of bins minus one. The multi-dimensional χ^2 value is $\chi^2/\nu = 1.00$ with $\nu = 426$.

JHEP01(2025)054

Decay channel F_i[%]	*Baseline*	Model 1	Model 2	Model 3	Model 4	Model 5
$B^+ \to T^*_{c\bar{c}0}(4475)^0 K^+$	18.45 ± 1.31	18.09 ± 1.21	16.42 ± 1.79	17.21 ± 1.20	17.66 ± 1.13	18.52 ± 1.20
$B^+ \to \psi(2S)\, K^*(1680)^+$	8.15 ± 1.31	10.22 ± 1.64	7.04 ± 1.26	12.10 ± 1.79	13.76 ± 1.69	7.97 ± 1.29
$B^+ \to \psi(2S)\, K_1(1270)^+$	7.60 ± 0.85	7.48 ± 0.92	8.18 ± 0.96	7.76 ± 0.76	8.30 ± 0.81	7.58 ± 0.84
$B^+[P] \to \psi(2S)\, K_1(1270)^+$	7.52 ± 0.60	6.75 ± 0.63	7.11 ± 0.61	6.58 ± 0.63	5.40 ± 0.50	7.70 ± 0.61
$B^+[D] \to \psi(2S)\, K_1(1270)^+$	6.81 ± 0.45	6.41 ± 0.44	6.80 ± 0.47	6.58 ± 0.46	6.21 ± 0.42	6.78 ± 0.44
$B^+ \to \psi(2S)\, K_1(1400)^+$	5.78 ± 0.62	5.94 ± 0.64	4.58 ± 0.71	5.68 ± 0.65	4.90 ± 0.57	5.47 ± 0.62
$B^+ \to \psi(2S)\, K(1460)^+$	5.26 ± 0.48	5.31 ± 0.43	4.90 ± 0.43	5.36 ± 0.44	4.86 ± 0.43	5.15 ± 0.42
$B^+[P] \to T_{c\bar{c}1}(4200)^+\, K^*(892)^0$	4.60 ± 0.54	4.85 ± 0.58	4.68 ± 0.56	9.64 ± 1.48	3.76 ± 0.51	4.72 ± 0.55
$B^+ \to T_{c\bar{c}\bar{s}1}(4600)^0 \pi^+$	4.42 ± 0.98	3.95 ± 0.84	3.92 ± 0.90	4.90 ± 1.01	9.02 ± 1.78	4.35 ± 0.98
$B^+ \to K^*_2(1430)^+ \psi(2S)$	4.35 ± 0.29	4.33 ± 0.30	4.26 ± 0.29	4.25 ± 0.31	4.53 ± 0.29	4.34 ± 0.29
$B^+ \to T_{c\bar{c}1}(4200)^+\, K^*(892)^0$	4.02 ± 0.88	5.42 ± 1.18	3.75 ± 1.18	3.76 ± 0.88	4.31 ± 0.96	4.19 ± 1.00
$B^+ \to T_{c\bar{c}1}(4430)^+\, [K^+\pi^-]_S$	3.41 ± 0.54	3.09 ± 0.48	3.08 ± 0.53	2.03 ± 0.63	3.39 ± 0.58	3.58 ± 0.61
$B^+ \to T^*_{c\bar{c}1}(4800)^0 K^+$	3.24 ± 0.50	3.31 ± 0.51	2.29 ± 0.48	2.81 ± 0.45	3.26 ± 0.49	2.09 ± 0.42
$B^+ \to T_{c\bar{c}1}(4650)^0 K^+$	2.89 ± 0.45	2.59 ± 0.49	2.87 ± 0.47	3.94 ± 0.58	3.05 ± 0.60	2.85 ± 0.44
$B^+[D] \to T_{c\bar{c}1}(4200)^+\, K^*(892)^0$	2.78 ± 0.33	2.83 ± 0.39	2.91 ± 0.35	3.18 ± 0.35	3.19 ± 0.36	2.90 ± 0.33
$B^+ \to T_{c\bar{c}\bar{s}1}(4900)^0 \pi^+$	2.60 ± 0.66	2.81 ± 0.68	2.80 ± 0.67	3.40 ± 0.75	1.92 ± 0.49	2.66 ± 0.68
$B^+[D] \to \rho(770)^0 T_{c\bar{c}\bar{s}1}(4000)^+$	2.06 ± 0.22	3.42 ± 0.37	2.06 ± 0.23	1.51 ± 0.22	2.16 ± 0.23	2.34 ± 0.24
$B^+ \to \psi(2S)\, K^*(1410)^+$	1.79 ± 0.35	1.47 ± 0.36	1.64 ± 0.34	2.13 ± 0.38	1.84 ± 0.37	1.71 ± 0.35
$B^+ \to T^*_{c\bar{c}0}(4710)^0 K^+$	1.73 ± 0.28	1.42 ± 0.24	1.67 ± 0.30	2.34 ± 0.46	1.71 ± 0.28	1.62 ± 0.26
$B^+ \to T^*_{c\bar{c}\bar{s}1}(5200)^0 \pi^+$	1.59 ± 0.46	1.60 ± 0.43	1.47 ± 4.30	1.35 ± 1.50	1.51 ± 0.70	1.37 ± 0.58
$B^+ \to T_{c\bar{c}\bar{s}1}(4000)^+\, [\pi^+\pi^-]_S$	1.24 ± 0.23	1.16 ± 0.20	1.10 ± 0.21	1.44 ± 0.24	1.30 ± 0.23	1.13 ± 0.20
$B^+ \to T_{c\bar{c}1}(4430)^+\, K^*(892)^0$	0.75 ± 0.43	0.75 ± 0.44	0.50 ± 0.58	0.56 ± 0.35	0.64 ± 0.41	1.25 ± 1.19
$B^+ \to \psi(4360) K^+$	0.64 ± 0.14	0.67 ± 0.14	0.60 ± 0.13	0.63 ± 0.14	0.51 ± 0.12	0.68 ± 0.14
$B^+ \to T^*_{c\bar{c}1}(4055)\, K^*(892)^0$	0.52 ± 0.10	0.52 ± 0.10	0.51 ± 0.10	0.44 ± 0.10	0.42 ± 0.09	0.55 ± 0.11
$B^+[P] \to \psi(2S)\, K_1(1400)^+$	0.48 ± 0.18	0.69 ± 0.21	0.49 ± 0.19	0.40 ± 0.15	1.55 ± 0.30	0.45 ± 0.17
$B^+[P] \to \psi(2S)\, K^*(1680)^+$	–	0.43 ± 0.18	–	–	–	–
$B^+[P] \to \psi(2S)\, K^*(1410)^+$	–	0.23 ± 0.11	–	–	–	–
$B^+ \to \psi(2S)\, K_1(1650)^+$	–	–	0.84 ± 0.42	–	–	–
$B^+ \to K_2(1770)^+ \psi(2S)$	–	–	0.46 ± 0.22	–	–	–
$B^+ \to K_2(1580)^+ \psi(2S)$	–	–	0.17 ± 0.15	–	–	–
$B^+ \to T_{c\bar{c}1}(4200)^+\, [K^+\pi^-]_S$	–	–	–	1.79 ± 0.20	–	–
$B^+[P] \to T_{c\bar{c}1}(4430)^+\, K^*(892)^0$	–	–	–	1.66 ± 0.19	–	–
$B^+[P] \to \rho(770)^0 T_{c\bar{c}\bar{s}1}(4000)^+$	–	–	–	1.45 ± 0.44	–	–
$B^+ \to T^0_{c\bar{c}\bar{s}}(0^+)\pi^+$	–	–	–	0.17 ± 0.08	–	0.65 ± 0.55
$B^+ \to X^0(1^+) K^+$	–	–	–	–	1.28 ± 0.32	–
$B^+ \to T^+_{c\bar{c}}(2^-)\, K^*(892)^0$	–	–	–	–	0.83 ± 0.15	–
$B^+ \to K^*(892)^0 T^+_{c\bar{c}}(0^-)$	–	–	–	–	0.28 ± 0.08	–
$B^+ \to T^{++}_{c\bar{c}\bar{s}}(0^+)\pi^-$	–	–	–	–	–	0.49 ± 0.20
$B^+ \to [\pi^+\pi^-]_S\, T^+_{c\bar{c}\bar{s}}(0^-)$	–	–	–	–	–	0.10 ± 0.04
Sum B^+	102.69 ± 4.40	105.72 ± 2.79	97.08 ± 6.52	115.06 ± 3.96	111.55 ± 3.52	103.16 ± 3.01

Table 16. Fit results of the *baseline* model and of alternative amplitude models 1-5, part 1. Uncertainties are statistical only.

JHEP01(2025)054

Decay channel F_i[%]	*Baseline*	Model 1	Model 2	Model 3	Model 4	Model 5
$K_1(1270)^+ \to \rho(770)^0 K^+$	50.71±2.18	54.95±3.36	49.38±2.22	47.56±2.16	48.89±2.28	51.64±2.18
$K_1(1270)^+ \to K^*(892)^0 \pi^+$	19.86±1.44	20.13±1.71	20.33±1.51	21.98±1.56	22.07±1.57	20.17±1.45
$K_1(1270)^+ \to [K^+\pi^-]_S \pi^+$	11.35±1.45	13.76±3.25	11.44±1.29	11.01±1.35	10.05±1.30	10.26±1.25
$K_1(1270)^+[D] \to K^*(892)^0 \pi^+$	8.32±0.85	8.13±0.89	8.04±0.88	7.96±0.86	7.10±0.83	8.26±0.84
$K_1(1270)^+ \to \rho(1450)^0 K^+$	–	0.69±1.03	–	–	–	–
$K_1(1270)^+ \to K^*(1410)^0 \pi^+$	–	0.00±0.02	–	–	–	–
Sum $K_1(1270)^+$	90.24±1.83	97.66±6.26	89.18±1.70	88.50±1.69	88.10±1.65	90.34±1.68
$K_1(1400)^+ \to K^*(892)^0 \pi^+$	86.80±3.78	87.20±3.81	86.15±5.02	86.25±3.64	83.15±3.87	89.99±3.59
$K_1(1400)^+ \to \rho(770)^0 K^+$	22.08±4.40	22.23±4.51	23.30±5.86	23.03±4.27	26.46±4.43	18.32±4.34
Sum $K_1(1400)^+$	108.88±0.82	109.44±0.76	109.44±0.98	109.27±0.77	109.61±0.71	108.31±0.91
$K(1460)^+ \to [\pi^+\pi^-]_S K^+$	45.13±4.22	40.89±3.94	42.12±4.28	48.39±3.90	50.70±4.19	44.72±3.86
$K(1460)^+ \to K^*(892)^0 \pi^+$	35.41±4.08	38.66±3.87	38.28±4.19	32.10±3.56	29.52±3.74	35.50±3.63
$K(1460)^+ \to \rho(770)^0 K^+$	–	4.78±1.76	–	–	–	–
Sum $K(1460)^+$	80.54±0.67	84.33±1.03	80.40±0.65	80.48±0.61	80.22±0.59	80.22±0.57
$K_2^*(1430)^+ \to K^*(892)^0 \pi^+$	76.70±3.04	77.74±3.07	76.02±3.14	74.77±3.23	74.32±3.07	76.00±3.08
$K_2^*(1430)^+ \to \rho(770)^0 K^+$	12.71±2.30	11.93±2.28	13.22±2.39	14.20±2.50	14.57±2.39	13.25±2.34
Sum $K_2^*(1430)^+$	89.41±0.75	89.67±0.79	89.24±0.75	88.97±0.73	88.89±0.69	89.25±0.73
$K^*(1410)^+ \to K^*(892)^0 \pi^+$	88.50±8.39	84.79±12.04	88.16±8.90	87.81±7.92	95.50±7.08	91.81±7.99
$K^*(1410)^+ \to \rho(770)^0 K^+$	38.36±10.46	52.39±14.83	36.70±10.90	20.75±8.09	27.72±9.53	33.76±10.44
Sum $K^*(1410)^+$	126.86±4.83	137.18±2.80	124.87±5.45	108.56±6.22	123.22±5.15	125.57±5.14
$K^*(1680)^+ \to K^*(892)^0 \pi^+$	49.69±6.72	45.79±6.54	49.06±7.60	49.31±7.07	50.45±5.25	46.95±6.94
$K^*(1680)^+ \to \rho(770)^0 K^+$	31.16±6.11	33.91±6.76	32.00±7.00	34.82±6.62	30.88±4.76	33.80±6.51
$K^*(1680)^+ \to K^*(1410)^0 \pi^+$	–	1.72±2.26	–	–	–	–
$K^*(1680)^+ \to \rho(1450)^0 K^+$	–	0.96±1.91	–	–	–	–
Sum $K^*(1680)^+$	80.85±0.64	82.39±7.29	81.05±0.84	84.13±1.76	81.33±0.72	80.74±0.57
$K_1(1650)^+ \to K^*(892)^0 \pi^+$	–	–	65.27±22.53	–	–	–
$K_1(1650)^+ \to \rho(770)^0 K^+$	–	–	28.80±21.48	–	–	–
Sum $K_1(1650)^+$	–	–	94.07±2.32	–	–	–
$K_2(1580)^+ \to K^*(892)^0 \pi^+$	–	–	78.59±30.58	–	–	–
$K_2(1580)^+ \to \rho(770)^0 K^+$	–	–	19.46±30.69	–	–	–
Sum $K_2(1580)^+$	–	–	98.05±9.36	–	–	–
$K_2(1770)^+ \to K^*(892)^0 \pi^+$	–	–	43.07±24.48	–	–	–
$K_2(1770)^+ \to \rho(770)^0 K^+$	–	–	11.25±16.00	–	–	–
$K_2(1770)^+ \to K_2^*(1430)^0 \pi^+$	–	–	0.47±0.52	–	–	–
$K_2(1770)^+ \to f_2(1270)^0 K^+$	–	–	0.18±0.29	–	–	–
Sum $K_2(1770)^+$	–	–	108.74±15.75	–	–	–
$T^*_{c\bar{c}0}(4475)^0 \to \rho(770)^0 \psi(2S)$	99.04±0.49	98.51±0.56	98.76±0.57	99.83±0.62	99.46±0.33	99.16±0.39
$T^*_{c\bar{c}0}(4475)^0 \to T_{c\bar{c}1}(4200)^- \pi^+$	0.50±0.25	0.77±0.29	0.64±0.30	0.62±0.29	0.28±0.17	0.43±0.20
$T^*_{c\bar{c}0}(4475)^0 \to T_{c\bar{c}1}(4200)^+ \pi^-$	0.50±0.25	0.77±0.29	0.64±0.30	0.62±0.29	0.28±0.17	0.43±0.20
$T^*_{c\bar{c}0}(4475)^0[D] \to \rho(770)^0 \psi(2S)$	–	–	–	0.49±0.07	–	–
Sum $T^*_{c\bar{c}0}(4475)^0$	100.03±0.02	100.06±0.03	100.04±0.03	101.54±0.23	100.01±0.01	100.02±0.02
$T_{c\bar{c}1}(4650)^0 \to \rho(770)^0 \psi(2S)$	86.66±7.85	83.93±10.64	88.81±8.08	79.98±6.98	91.07±6.96	86.29±7.77
$T_{c\bar{c}1}(4650)^0 \to T_{c\bar{c}1}(4200)^- \pi^+$	6.62±2.03	9.46±3.11	5.79±1.96	6.10±1.76	6.79±1.96	6.59±2.00
$T_{c\bar{c}1}(4650)^0 \to T_{c\bar{c}1}(4200)^+ \pi^-$	6.61±2.03	9.46±3.11	5.79±1.96	6.09±1.76	6.78±1.96	6.59±2.00
$T_{c\bar{c}1}(4650)^0[D] \to \rho(770)^0 \psi(2S)$	–	–	–	1.43±0.98	–	–
Sum $T_{c\bar{c}1}(4650)^0$	99.89±7.37	102.84±10.42	100.38±7.65	93.59±6.16	104.64±7.07	99.47±7.25
$T^*_{c\bar{c}0}(4710)^0 \to \rho(770)^0 \psi(2S)$	92.35±10.83	95.95±10.14	88.23±10.77	60.65±11.58	91.02±9.77	93.52±10.93
$T^*_{c\bar{c}0}(4710)^0 \to T_{c\bar{c}1}(4430)^+ \pi^-$	17.00±3.82	18.39±4.14	15.94±3.94	21.40±5.89	12.77±3.77	17.24±4.05
$T^*_{c\bar{c}0}(4710)^0 \to T_{c\bar{c}1}(4430)^- \pi^+$	17.00±3.82	18.37±4.13	15.95±3.94	21.43±5.90	12.78±3.77	17.25±4.05
$T^*_{c\bar{c}0}(4710)^0 \to \rho(1450)^0 \psi(2S)$	–	–	–	3.46±0.80	–	–
$T^*_{c\bar{c}0}(4710)^0[D] \to \rho(770)^0 \psi(2S)$	–	–	–	2.85±2.32	–	–
Sum $T^*_{c\bar{c}0}(4710)^0$	126.35±10.56	132.71±9.44	120.13±9.79	109.79±10.66	116.57±9.00	128.01±9.78
$T^*_{c\bar{c}1}(4800)^0 \to \rho(770)^0 \psi(2S)$	41.52±5.19	40.07±5.41	40.73±6.85	57.24±6.84	42.38±5.24	52.64±7.37
$T^*_{c\bar{c}1}(4800)^0 \to T_{c\bar{c}1}(4200)^- \pi^+$	18.03±5.14	21.59±5.72	19.85±6.88	14.79±4.79	18.75±5.62	11.16±4.96
$T^*_{c\bar{c}1}(4800)^0 \to T_{c\bar{c}1}(4200)^+ \pi^-$	18.03±5.14	21.60±5.72	19.85±6.88	14.79±4.79	18.75±5.62	11.16±4.96
$T^*_{c\bar{c}1}(4800)^0 \to T_{c\bar{c}1}(4430)^+ \pi^-$	5.44±2.45	4.59±2.32	6.03±3.29	2.20±1.71	5.14±2.45	2.22±1.86
$T^*_{c\bar{c}1}(4800)^0 \to T_{c\bar{c}1}(4430)^- \pi^+$	5.44±2.45	4.58±2.32	6.03±3.29	2.20±1.71	5.14±2.45	2.22±1.86
$T^*_{c\bar{c}1}(4800)^0 \to \rho(1450)^0 \psi(2S)$	–	–	–	2.91±0.56	–	–
Sum $T^*_{c\bar{c}1}(4800)^0$	88.47±11.26	92.43±13.00	92.48±15.23	94.14±9.82	90.16±12.22	79.41±8.39
$T_{c\bar{c}s1}(4600)^0 \to \psi(2S)\, K^*(892)^0$	50.87±7.79	44.74±8.18	48.30±8.20	51.78±7.33	70.29±5.41	50.84±8.05
$T_{c\bar{c}s1}(4600)^0 \to T_{c\bar{c}1}(4200)^- K^+$	16.53±3.79	19.29±4.44	15.83±3.99	53.60±13.86	6.84±1.82	15.77±3.69
$T_{c\bar{c}s1}(4600)^0 \to T_{c\bar{c}s1}(4000)^+ \pi^-$	9.84±3.28	10.24±3.68	11.76±3.77	4.29±2.85	5.81±1.85	11.65±3.59
$T_{c\bar{c}s1}(4600)^0 \to \psi(2S)\ [K^+\pi^-]_S$	–	–	–	24.65±9.72	–	–
Sum $T_{c\bar{c}s1}(4600)^0$	77.23±5.22	74.27±5.47	75.89±5.58	134.32±20.64	82.94±3.87	78.27±5.68
$T_{c\bar{c}s1}(4900)^0 \to \psi(2S)\, K^*(892)^0$	100	100	100	96.88±1.74	100	100
$T_{c\bar{c}s1}(4900)^0 \to \psi(2S)\ [K^+\pi^-]_S$	–	–	–	3.08±1.73	–	–
$T_{c\bar{c}s1}(4900)^0 \to \psi(2S)\, K^*(1410)^0$	–	–	–	0.00±0.00	–	–
Sum $T_{c\bar{c}s1}(4900)^0$	100	100	100	99.97±0.01	100	100
$T^*_{c\bar{c}s1}(5200)^0 \to \psi(2S)\ [K^+\pi^-]_S$	66.28±15.03	71.07±13.65	67.65±55.07	66.33±14.75	58.02±12.27	84.86±14.81
$T^*_{c\bar{c}s1}(5200)^0 \to T_{c\bar{c}s1}(4000)^+ \pi^-$	9.37±14.12	13.15±7.05	8.91±21.77	6.18±5.77	9.65±5.76	1.36±2.43
Sum $T^*_{c\bar{c}s1}(5200)^0$	75.65±9.18	84.22±11.83	76.56±75.85	72.51±9.68	67.67±6.55	86.21±12.39
$T^{++}_{c\bar{c}s}(0^+) \to T_{c\bar{c}1}(4200)^+ K^+$	–	–	–	–	–	85.89±11.39
$T^{++}_{c\bar{c}s}(0^+) \to T_{c\bar{c}s1}(4000)^+ \pi^+$	–	–	–	–	–	9.47±9.49
Sum $T^{++}_{c\bar{c}s}(0^+)$	–	–	–	–	–	95.36±2.21

Table 17. Fit results of the *baseline* model and of alternative amplitude models 1-5, part 2. Uncertainties are statistical only.

JHEP01(2025)054

Fit parameter	*Baseline*	Model 1	Model 2	Model 3	Model 4	Model 5
$T^*_{c\bar{c}0}(4475)^0$ mass [MeV]	4474.5± 6.9	4470.5± 6.0	4473.1± 7.0	4471.0± 5.2	4471.2± 5.8	4474.3± 6.1
$T^*_{c\bar{c}0}(4475)^0$ width [MeV]	230.8 ±19.5	228.7 ± 17.1	210.5 ± 18.2	218.6 ± 15.2	218.4 ± 15.7	233.2 ± 17.7
$T_{c\bar{c}1}(4650)^0$ mass [MeV]	4652.5±14.4	4634.3± 21.1	4644.3± 15.2	4687.9± 12.7	4704.9± 14.9	4655.0± 14.0
$T_{c\bar{c}1}(4650)^0$ width [MeV]	227.0 ±26.3	246.7 ±154.0	234.1 ± 28.0	249.4 ±162.7	238.0 ± 32.5	223.2 ± 26.2
$T^*_{c\bar{c}0}(4710)^0$ mass [MeV]	4710.2± 4.4	4710.2± 4.2	4710.5± 4.4	4707.0± 4.4	4707.4± 5.0	4713.1± 3.8
$T^*_{c\bar{c}0}(4710)^0$ width [MeV]	63.6 ± 8.7	53.9 ± 8.0	61.2 ± 8.7	73.5 ± 9.3	66.6 ± 9.1	56.4 ± 7.4
$T^*_{c\bar{c}1}(4800)^0$ mass [MeV]	4784.6±37.4	4751.3± 29.3	4765.6± 33.2	4781.0± 41.8	4784.0± 36.5	4706.6± 29.9
$T^*_{c\bar{c}1}(4800)^0$ width [MeV]	457.1 ±93.4	386.4 ± 68.7	356.0 ± 76.4	476.7 ±104.1	476.1 ± 95.8	322.4 ± 59.1
$T_{c\bar{c}\bar{s}1}(4600)^0$ mass [MeV]	4577.8± 9.5	4581.8± 10.1	4578.5± 9.5	4568.4± 9.1	4579.6± 9.9	4576.1± 9.3
$T_{c\bar{c}\bar{s}1}(4600)^0$ width [MeV]	133.0 ±28.4	128.8 ± 29.0	127.4 ± 28.7	130.0 ± 28.8	170.0 ± 34.4	127.9 ± 27.1
$T_{c\bar{c}\bar{s}1}(4900)^0$ mass [MeV]	4924.9±22.0	4922.2± 20.7	4929.9± 21.8	4935.6± 20.5	4890.7± 15.0	4930.0± 23.6
$T_{c\bar{c}\bar{s}1}(4900)^0$ width [MeV]	255.0 ±54.6	259.6 ± 57.1	263.5 ± 54.3	275.6 ± 56.0	191.8 ± 41.7	267.8 ± 59.0
$T^*_{c\bar{c}\bar{s}1}(5200)^0$ mass [MeV]	5225.1±85.7	5227.1± 26.7	5281.2± 51.9	5216.1± 81.1	5176.1± 70.8	5141.1± 72.4
$T^*_{c\bar{c}\bar{s}1}(5200)^0$ width [MeV]	226.2 ±75.5	50.0 ± 79.5	127.9 ±292.4	297.1 ±185.0	395.5 ± 85.9	367.0 ± 81.0
$T_{c\bar{c}1}(4200)^+$ mass [MeV]	4257.3±10.8	4276.9± 12.7	4259.6± 11.3	4268.4± 10.7	4254.9± 10.9	4249.3± 10.1
$T_{c\bar{c}1}(4200)^+$ width [MeV]	308.2 ±20.4	340.8 ± 21.9	312.1 ± 21.5	334.7 ± 23.6	307.6 ± 23.0	298.6 ± 20.1
$T_{c\bar{c}1}(4430)^+$ mass [MeV]	4468.2±21.0	4465.0± 16.5	4479.2± 26.7	4619.0± 59.8	4455.2± 26.1	4510.9± 33.5
$T_{c\bar{c}1}(4430)^+$ width [MeV]	250.9 ±41.6	207.6 ± 35.6	283.4 ± 58.0	249.7 ± 64.7	271.8 ± 40.2	301.1 ± 59.6
$T^0_{cc\bar{s}}(0^+)$ mass [MeV]	–	–	–	4410.8± 1.9	–	4403.3± 12.9
$T^0_{cc\bar{s}}(0^+)$ width [MeV]	–	–	–	10.0 ± 8.4	–	29.6 ± 14.6
$X^0(1^+)$ mass [MeV]	–	–	–	–	4324.8± 17.9	–
$X^0(1^+)$ width [MeV]	–	–	–	–	137.3 ± 59.0	–
$T^+_{c\bar{c}}(2^-)$ mass [MeV]	–	–	–	–	4597.1± 85.2	–
$T^+_{c\bar{c}}(2^-)$ width [MeV]	–	–	–	–	573.2 ±438.4	–
$T^+_{c\bar{c}}(0^-)$ mass [MeV]	–	–	–	–	3982.2± 55.0	–
$T^+_{c\bar{c}}(0^-)$ width [MeV]	–	–	–	–	284.0 ±246.6	–
$T^{++}_{cc\bar{s}}(0^+)$ mass [MeV]	–	–	–	–	–	4656.0± 64.7
$T^{++}_{cc\bar{s}}(0^+)$ width [MeV]	–	–	–	–	–	368.1 ±292.2
$T^+_{cc\bar{s}}(0^-)$ mass [MeV]	–	–	–	–	–	4455.9± 5.4
$T^+_{cc\bar{s}}(0^-)$ width [MeV]	–	–	–	–	–	29.1 ± 12.3
$\Delta(-2\ln\mathcal{L})$	0.0	−75.7	−86.9	−195.4	−236.9	−80.1
$N_{\rm par}$	98	112	116	118	110	112
χ^2/ν	1.21	1.21	1.21	1.22	1.20	1.23
$\chi^2/N_{\rm bins}$	1.10	1.08	1.08	1.08	1.08	1.10

Table 18. Fit results of the *baseline* model and of alternative amplitude models 1-5, part 3. Uncertainties are statistical only.

JHEP01(2025)054

Decay channel F_i[%]	Model 6	Model 7	Model 8	Model 9	Model 10	Model 11
$B^+ \to T^*_{c\bar{c}0}(4475)^0 K^+$	13.29 ± 1.61	20.50 ± 1.35	22.65 ± 1.57	18.12 ± 1.19	15.38 ± 1.11	16.86 ± 1.81
$B^+ \to \psi(2S)\, K^*(1680)^+$	9.07 ± 1.46	6.89 ± 1.19	8.09 ± 1.36	7.40 ± 1.32	15.22 ± 2.20	10.53 ± 2.01
$B^+ \to \psi(2S)\, K_1(1270)^+$	10.08 ± 0.97	6.95 ± 0.78	8.06 ± 0.88	9.44 ± 0.84	8.90 ± 1.05	8.64 ± 1.52
$B^+[P] \to \psi(2S)\, K_1(1270)^+$	6.31 ± 0.55	8.67 ± 0.55	7.55 ± 0.55	6.30 ± 0.56	6.67 ± 0.62	7.76 ± 0.69
$B^+[D] \to \psi(2S)\, K_1(1270)^+$	5.68 ± 0.40	6.84 ± 0.44	6.45 ± 0.43	6.49 ± 0.43	8.85 ± 0.47	9.51 ± 0.51
$B^+ \to \psi(2S)\, K_1(1400)^+$	4.52 ± 0.62	5.29 ± 0.70	5.77 ± 0.62	4.77 ± 0.61	5.76 ± 0.66	6.11 ± 0.86
$B^+ \to \psi(2S)\, K(1460)^+$	3.45 ± 0.39	4.80 ± 0.42	3.71 ± 0.29	5.17 ± 0.41	4.94 ± 0.42	4.57 ± 0.43
$B^+[P] \to T_{c\bar{c}1}(4200)^+ K^*(892)^0$	3.72 ± 0.50	4.57 ± 0.53	4.46 ± 0.51	4.66 ± 0.54	8.76 ± 0.80	8.18 ± 0.82
$B^+ \to T_{c\bar{c}s1}(4600)^0 \pi^+$	8.15 ± 1.73	4.68 ± 1.07	4.66 ± 1.15	5.15 ± 1.21	2.38 ± 0.60	2.37 ± 0.90
$B^+ \to K^*_2(1430)^+ \psi(2S)$	4.45 ± 0.31	4.38 ± 0.29	4.34 ± 0.29	4.97 ± 0.31	4.74 ± 0.34	4.38 ± 0.37
$B^+ \to T_{c\bar{c}1}(4200)^+ K^*(892)^0$	5.37 ± 2.06	3.95 ± 0.83	3.20 ± 0.69	3.64 ± 0.59	3.61 ± 0.79	3.31 ± 0.71
$B^+ \to T_{c\bar{c}1}(4430)^+ \left[K^+\pi^-\right]_S$	2.81 ± 0.51	2.90 ± 0.50	2.77 ± 0.44	1.20 ± 0.47	3.29 ± 0.52	3.23 ± 0.55
$B^+ \to T^*_{c\bar{c}1}(4800)^0 K^+$	2.28 ± 0.42	3.12 ± 0.34	3.39 ± 0.49	2.61 ± 0.45	4.03 ± 0.51	4.28 ± 0.73
$B^+ \to T_{c\bar{c}1}(4650)^0 K^+$	3.55 ± 0.49	3.41 ± 0.50	3.03 ± 0.54	2.92 ± 0.52	3.00 ± 0.38	2.87 ± 0.51
$B^+[D] \to T_{c\bar{c}1}(4200)^+ K^*(892)^0$	2.37 ± 0.32	3.00 ± 0.34	2.79 ± 0.33	3.42 ± 0.37	1.88 ± 0.27	1.58 ± 0.51
$B^+ \to T_{c\bar{c}s1}(4900)^0 \pi^+$	0.43 ± 0.11	3.25 ± 0.80	3.14 ± 0.85	2.85 ± 0.76	6.46 ± 1.80	6.80 ± 2.35
$B^+[D] \to \rho(770)^0 T_{c\bar{c}s1}(4000)^+$	2.38 ± 0.25	2.02 ± 0.21	3.20 ± 0.35	1.03 ± 0.23	0.89 ± 0.12	1.18 ± 0.24
$B^+ \to \psi(2S)\, K^*(1410)^+$	1.57 ± 0.33	1.70 ± 0.34	1.88 ± 0.36	2.66 ± 0.43	1.17 ± 0.31	0.25 ± 0.17
$B^+ \to T^*_{c\bar{c}0}(4710)^0 K^+$	2.04 ± 0.34	2.08 ± 0.32	2.32 ± 0.36	1.84 ± 0.33	1.95 ± 0.33	1.60 ± 0.32
$B^+ \to T^*_{c\bar{c}s1}(5200)^0 \pi^+$	1.63 ± 0.51	1.61 ± 0.53	1.73 ± 0.43	1.71 ± 0.86	1.53 ± 0.43	1.58 ± 0.45
$B^+ \to T_{c\bar{c}s1}(4000)^+ \left[\pi^+\pi^-\right]_S$	1.27 ± 0.23	0.77 ± 0.16	–	1.49 ± 0.22	1.10 ± 0.20	1.01 ± 0.19
$B^+ \to T_{c\bar{c}1}(4430)^+ K^*(892)^0$	7.72 ± 3.15	1.02 ± 0.49	0.56 ± 0.30	0.00 ± 0.01	0.70 ± 0.40	0.71 ± 0.37
$B^+ \to \psi(4360) K^+$	0.59 ± 0.13	–	0.44 ± 0.11	–	0.59 ± 0.13	0.60 ± 0.13
$B^+ \to T^*_{c\bar{c}1}(4055)\, K^*(892)^0$	0.29 ± 0.07	0.45 ± 0.10	0.49 ± 0.10	0.46 ± 0.10	0.68 ± 0.13	0.60 ± 0.13
$B^+[P] \to \psi(2S)\, K_1(1400)^+$	0.51 ± 0.17	–	–	0.54 ± 0.17	0.55 ± 0.20	0.45 ± 0.27
$B^+ \to \psi(2S)\, K_1(1650)^+$	–	–	–	2.28 ± 0.24	–	–
$B^+ \to K_2(1770)^+ \psi(2S)$	–	0.31 ± 0.09	0.20 ± 0.08	–	–	–
$B^+ \to T_{c\bar{c}1}(4200)^+ \left[K^+\pi^-\right]_S$	–	–	–	2.25 ± 0.24	–	–
$B^+[P] \to \rho(770)^0 T_{c\bar{c}s1}(4000)^+$	–	–	0.95 ± 0.33	1.05 ± 0.35	–	–
$B^+ \to \psi(2S)\, \pi^+_A K^*(892)^0$	4.98 ± 0.55	–	–	–	–	–
$B^+ \to \psi(2S)\, K^*(892)^0_A \pi^+$	4.98 ± 0.57	–	–	–	–	–
$B^+ \to \psi(2S)\, \rho(770)^0_S K^+$	1.64 ± 0.64	–	–	–	–	–
$B^+ \to \psi(2S)\, K^*(892)^0_S \pi^+$	1.57 ± 1.57	–	–	–	–	–
$B^+[P] \to \psi(2S)\, \pi^+_V K^*(892)^0$	1.24 ± 0.21	–	–	–	–	–
$B^+ \to \psi(2S)\, K^+_V \rho(770)^0$	1.22 ± 0.40	–	–	–	–	–
$B^+ \to \psi(2S)\, K^+_P \rho(770)^0$	0.11 ± 0.01	–	–	–	–	–
$B^+ \to \psi(2S)\, K^+_A \rho(770)^0$	0.00 ± 0.00	–	–	–	–	–
$B^+ \to \psi(2S)\, K^*(892)^0_V \pi^+$	–	0.12 ± 0.06	–	–	–	–
$B^+ \to X(4350)^0_A K^+$	–	0.08 ± 0.05	–	–	–	–
$B^+ \to \psi(4660) K^+$	–	0.03 ± 0.02	–	–	–	–
$B^+[D] \to T_{c\bar{c}1}(4430)^+ K^*(892)^0$	–	–	–	–	–	1.02 ± 0.41
$B^+[D] \to \psi(2S)\, K^*(1410)^+$	–	–	–	–	–	0.52 ± 0.11
$B^+ \to \rho(770)^0 T_{c\bar{c}s1}(4000)^+$	–	–	–	–	–	0.08 ± 0.19
$B^+[D] \to \psi(2S)\, K_1(1400)^+$	–	–	–	–	–	0.00 ± 0.00
Sum B^+	119.28 ± 5.81	103.36 ± 2.69	105.83 ± 2.82	104.44 ± 3.11	113.05 ± 3.63	110.61 ± 4.74

Table 19. Fit results of alternative amplitude models 6-11, part 1. Uncertainties are statistical only.

JHEP01(2025)054

Decay channel F_i[%]	Model 6	Model 7	Model 8	Model 9	Model 10	Model 11
$K_1(1270)^+ \to \rho(770)^0 K^+$	49.34±2.18	49.37±2.11	50.84±2.15	44.94±2.10	48.21±2.34	48.42±2.53
$K_1(1270)^+ \to K^*(892)^0 \pi^+$	18.91±1.56	21.47±1.44	24.09±1.48	19.63±1.47	18.26±1.34	20.06±1.54
$K_1(1270)^+ \to [K^+\pi^-]_S \pi^+$	10.10±1.22	11.22±1.22	10.54±1.18	10.90±1.19	12.37±1.29	10.88±1.22
$K_1(1270)^+[D] \to K^*(892)^0 \pi^+$	9.59±0.92	8.01±0.83	7.68±0.81	12.48±1.01	8.70±0.90	8.81±1.01
Sum $K_1(1270)^+$	87.94±1.56	90.08±1.67	93.15±1.65	87.94±1.59	87.54±1.56	88.17±1.54
$K_1(1400)^+ \to K^*(892)^0 \pi^+$	90.40±3.93	76.80±4.75	88.49±3.97	84.07±4.22	80.86±4.56	80.71±7.56
$K_1(1400)^+ \to \rho(770)^0 K^+$	18.42±4.92	30.89±5.05	20.08±4.70	25.40±4.88	31.86±5.12	31.58±8.05
Sum $K_1(1400)^+$	108.82±1.03	107.70±0.97	108.57±0.91	109.47±0.83	112.72±0.84	112.29±0.98
$K(1460)^+ \to [\pi^+\pi^-]_S K^+$	69.53±5.36	39.74±4.10	27.68±3.47	44.43±3.94	49.74±4.15	53.07±4.56
$K(1460)^+ \to K^*(892)^0 \pi^+$	15.89±3.91	40.74±4.13	50.13±4.13	35.64±3.75	29.49±3.71	26.65±3.91
$K(1460)^+ \to \rho(770)^0 K^+$	–	–	9.95±2.93	–	–	–
Sum $K(1460)^+$	85.42±1.79	80.48±0.66	87.76±1.66	80.07±0.52	79.23±0.47	79.72±0.68
$K_2^*(1430)^+ \to K^*(892)^0 \pi^+$	72.70±3.26	74.84±3.15	72.31±3.23	74.56±2.92	78.91±2.85	77.49±3.08
$K_2^*(1430)^+ \to \rho(770)^0 K^+$	15.80±2.58	14.14±2.44	16.11±2.57	14.35±2.26	11.37±2.12	12.45±2.33
Sum $K_2^*(1430)^+$	88.50±0.68	88.98±0.72	88.42±0.67	88.90±0.66	90.27±0.74	89.94±0.75
$K^*(1410)^+ \to K^*(892)^0 \pi^+$	95.94±7.78	80.06±9.47	84.62±8.67	81.37±7.51	56.18±14.19	77.12±9.68
$K^*(1410)^+ \to \rho(770)^0 K^+$	33.60±11.27	41.86±10.86	30.99±10.05	27.78±8.02	82.44±12.36	25.94±10.76
Sum $K^*(1410)^+$	129.55±4.76	121.92±5.53	115.61±6.29	109.15±5.43	138.62±2.06	103.06±6.23
$K^*(1680)^+ \to K^*(892)^0 \pi^+$	45.01±6.83	49.25±7.49	41.14±8.50	32.12±8.55	69.15±4.69	73.33±5.39
$K^*(1680)^+ \to \rho(770)^0 K^+$	35.49±6.49	31.93±6.88	42.70±8.52	51.86±9.33	15.95±3.52	20.71±4.74
Sum $K^*(1680)^+$	80.50±0.34	81.18±0.91	83.84±1.90	83.98±2.07	85.10±1.54	94.04±3.38
$K_2(1770)^+ \to K^*(892)^0 \pi^+$	–	–	29.83±18.08	–	–	–
$K_2(1770)^+ \to \rho(770)^0 K^+$	–	–	83.05±15.34	–	–	–
Sum $K_2(1770)^+$	–	–	112.88±3.14	–	–	–
$T^*_{c\bar{c}0}(4475)^0 \to \rho(770)^0 \psi(2S)$	98.77±0.60	99.27±0.36	100	102.55±0.89	98.26±0.63	96.33±1.25
$T^*_{c\bar{c}0}(4475)^0 \to T_{c\bar{c}1}(4200)^- \pi^+$	0.64±0.31	0.37±0.18	–	0.21±0.15	0.91±0.33	0.82±0.32
$T^*_{c\bar{c}0}(4475)^0 \to T_{c\bar{c}1}(4200)^+ \pi^-$	0.64±0.31	0.37±0.18	–	0.21±0.15	0.91±0.33	0.82±0.32
$T^*_{c\bar{c}0}(4475)^0[D] \to \rho(770)^0 \psi(2S)$	–	–	–	1.47±0.82	–	2.06±1.00
Sum $T^*_{c\bar{c}0}(4475)^0$	100.04±0.03	100.02±0.01	100	104.43±1.23	100.08±0.03	100.03±0.27
$T_{c\bar{c}1}(4650)^0 \to \rho(770)^0 \psi(2S)$	95.30±6.69	87.44±6.95	93.53±6.94	88.54±7.13	82.07±8.61	92.41±7.93
$T_{c\bar{c}1}(4650)^0 \to T_{c\bar{c}1}(4200)^- \pi^+$	4.40±1.55	5.92±1.73	5.61±1.81	4.97±1.71	6.76±2.20	3.53±1.61
$T_{c\bar{c}1}(4650)^0 \to T_{c\bar{c}1}(4200)^+ \pi^-$	4.40±1.55	5.92±1.72	5.60±1.81	4.96±1.70	6.75±2.20	3.54±1.61
$T_{c\bar{c}1}(4650)^0[D] \to \rho(770)^0 \psi(2S)$	–	–	–	–	–	–
Sum $T_{c\bar{c}1}(4650)^0$	104.10±6.93	99.28±6.52	104.74±7.19	98.47±6.86	95.58±7.65	99.48±7.64
$T^*_{c\bar{c}0}(4710)^0 \to \rho(770)^0 \psi(2S)$	95.82±10.39	95.77±9.28	84.78±8.79	75.58±11.10	84.81±9.33	92.15±12.32
$T^*_{c\bar{c}0}(4710)^0 \to T_{c\bar{c}1}(4430)^+ \pi^-$	15.07±3.98	16.57±3.50	19.33±3.39	19.36±4.86	17.12±3.58	20.03±4.32
$T^*_{c\bar{c}0}(4710)^0 \to T_{c\bar{c}1}(4430)^- \pi^+$	15.09±3.99	16.57±3.50	19.28±3.38	19.40±4.87	17.10±3.58	20.03±4.32
Sum $T^*_{c\bar{c}0}(4710)^0$	125.98±8.97	128.91±8.54	123.39±7.97	114.34±8.75	119.03±8.65	132.21±12.09
$T^*_{c\bar{c}1}(4800)^0 \to \rho(770)^0 \psi(2S)$	27.67±5.88	44.59±5.42	24.86±4.71	35.95±5.00	43.05±4.69	43.95±5.64
$T^*_{c\bar{c}1}(4800)^0 \to T_{c\bar{c}1}(4200)^- \pi^+$	15.16±7.91	15.49±4.02	19.59±4.09	21.62±1.69	17.05±4.16	13.58±3.99
$T^*_{c\bar{c}1}(4800)^0 \to T_{c\bar{c}1}(4200)^+ \pi^-$	15.17±7.91	15.48±4.02	19.59±4.09	21.61±1.69	17.07±4.17	13.62±4.00
$T^*_{c\bar{c}1}(4800)^0 \to T_{c\bar{c}1}(4430)^+ \pi^-$	7.50±4.14	6.98±2.72	4.09±1.75	–	4.66±2.01	2.94±1.47
$T^*_{c\bar{c}1}(4800)^0 \to T_{c\bar{c}1}(4430)^- \pi^+$	7.51±4.14	6.99±2.73	4.07±1.74	–	4.65±2.01	2.94±1.47
Sum $T^*_{c\bar{c}1}(4800)^0$	73.00±15.77	89.52±9.76	72.21±7.64	79.18±1.62	86.47±9.55	77.05±7.14
$T_{c\bar{c}\bar{s}1}(4600)^0 \to \psi(2S) K^*(892)^0$	63.56±5.78	53.92±8.21	54.96±7.97	55.26±7.42	30.09±8.88	41.05±17.91
$T_{c\bar{c}\bar{s}1}(4600)^0 \to T_{c\bar{c}1}(4200)^- K^+$	10.20±2.50	15.26±3.55	14.24±3.43	15.74±3.46	25.12±5.81	20.58±5.79
$T_{c\bar{c}\bar{s}1}(4600)^0 \to T_{c\bar{c}\bar{s}1}(4000)^+ \pi^-$	5.99±2.10	14.21±3.89	10.55±3.47	5.83±2.50	13.74±4.96	20.64±5.87
Sum $T_{c\bar{c}\bar{s}1}(4600)^0$	79.76±3.50	83.39±6.24	79.75±5.44	76.83±4.17	68.95±6.67	82.27±15.59
$T_{c\bar{c}\bar{s}1}(4900)^0 \to \psi(2S) K^*(892)^0$	100	100	100	100	100	100
Sum $T_{c\bar{c}\bar{s}1}(4900)^0$	100	100	100	100	100	100
$T^*_{c\bar{c}\bar{s}1}(5200)^0 \to \psi(2S) [K^+\pi^-]_S$	64.40±11.97	49.32±10.79	53.50±10.38	49.53±11.13	66.75±12.08	71.57±12.68
$T^*_{c\bar{c}\bar{s}1}(5200)^0 \to T_{c\bar{c}\bar{s}1}(4000)^+ \pi^-$	12.76±6.96	15.96±7.14	13.61±6.18	15.04±6.79	15.28±7.33	10.36±6.42
Sum $T^*_{c\bar{c}\bar{s}1}(5200)^0$	77.16±8.69	65.28±5.25	67.11±5.16	64.57±5.08	82.03±9.61	81.92±10.71

Table 20. Fit results of alternative amplitude models 6-11, part 2. Uncertainties are statistical only.

JHEP01(2025)054

Fit parameter	Model 6	Model 7	Model 8	Model 9	Model 10	Model 11
$T^*_{c\bar{c}0}(4475)^0$ mass [MeV]	4461.1± 6.7	4474.2± 5.4	4483.1± 5.9	4478.2± 6.1	4461.4± 5.6	4468.4± 7.5
$T^*_{c\bar{c}0}(4475)^0$ width [MeV]	193.7 ± 17.7	227.8 ±16.3	248.4 ±17.4	226.2 ± 16.3	213.2 ± 15.5	232.3 ± 22.4
$T_{c\bar{c}1}(4650)^0$ mass [MeV]	4691.7± 14.4	4662.0±13.8	4673.1±12.9	4680.2± 12.0	4628.5± 18.4	4651.0± 15.9
$T_{c\bar{c}1}(4650)^0$ width [MeV]	250.0 ±151.6	243.2 ±26.6	219.9 ±26.8	202.8 ± 24.5	250.0 ±176.8	239.3 ± 30.1
$T^*_{c\bar{c}0}(4710)^0$ mass [MeV]	4702.7± 5.9	4710.8± 3.9	4705.6± 4.4	4708.6± 4.1	4702.8± 4.8	4706.1± 6.7
$T^*_{c\bar{c}0}(4710)^0$ width [MeV]	72.0 ± 10.0	68.3 ± 8.9	71.0 ± 9.3	58.0 ± 7.2	75.0 ± 10.3	66.7 ± 11.5
$T^*_{c\bar{c}1}(4800)^0$ mass [MeV]	4727.4± 23.6	5100.0±30.8	4767.1±31.7	4904.1± 38.1	4779.9± 33.9	4798.2± 44.2
$T^*_{c\bar{c}1}(4800)^0$ width [MeV]	301.8 ± 53.5	650.0 ±50.3	426.6 ±81.6	650.0 ±115.2	509.7 ± 95.2	586.1 ±122.4
$T_{c\bar{c}\bar{s}1}(4600)^0$ mass [MeV]	4580.1± 12.6	4569.3± 9.2	4565.8± 9.5	4577.6± 10.6	4585.2± 12.7	4568.2± 14.6
$T_{c\bar{c}\bar{s}1}(4600)^0$ width [MeV]	205.8 ± 54.5	128.0 ±29.1	134.9 ±31.4	164.0 ± 38.4	116.0 ± 28.5	92.3 ± 21.1
$T_{c\bar{c}\bar{s}1}(4900)^0$ mass [MeV]	4872.1± 5.1	4956.1±27.1	4946.4±27.6	4963.8± 30.2	4987.3± 42.0	5014.1± 52.7
$T_{c\bar{c}\bar{s}1}(4900)^0$ width [MeV]	52.1 ± 13.9	332.8 ±79.7	325.3 ±86.6	315.1 ± 74.2	466.8 ±129.9	462.4 ±153.6
$T^*_{c\bar{c}\bar{s}1}(5200)^0$ mass [MeV]	5272.0± 41.6	5305.8±55.7	5262.0±34.3	5165.0± 71.0	5226.1± 26.5	5235.6± 29.3
$T^*_{c\bar{c}\bar{s}1}(5200)^0$ width [MeV]	50.0 ± 61.5	50.1 ±79.3	50.0 ±57.3	336.6 ± 69.9	50.0 ± 86.9	50.1 ± 34.9
$T_{c\bar{c}1}(4200)^+$ mass [MeV]	4267.9± 12.7	4238.1± 9.4	4234.2± 8.7	4245.3± 9.4	4258.1± 9.7	4238.4± 11.0
$T_{c\bar{c}1}(4200)^+$ width [MeV]	276.3 ± 23.3	294.9 ±18.3	278.2 ±17.2	329.9 ± 18.6	350.0 ±214.2	350.0 ± 66.7
$T_{c\bar{c}1}(4430)^+$ mass [MeV]	4460.9± 31.4	4489.2±25.2	4482.6±17.6	4700.0± 20.8	4481.2± 21.6	4485.1± 22.6
$T_{c\bar{c}1}(4430)^+$ width [MeV]	329.0 ± 52.8	266.3 ±50.3	195.1 ±32.3	50.3 ±265.5	255.8 ± 41.4	251.9 ± 44.4
$\Delta(-2\ln\mathcal{L})$	−200.8	+21.2	+88.2	−283.1	+59.5	−68.4
N_{par}	112	102	100	102	98	108
χ^2/ν	1.23	1.21	1.21	1.20	1.21	1.21
χ^2/N_{bins}	1.10	1.09	1.10	1.09	1.10	1.09

Table 21. Fit results of alternative amplitude models 6-11, part 3. Uncertainties are statistical only.

JHEP01(2025)054

Decay mode	PDG (%)	Belle Fit 1 (%)	Belle Fit 2 (%)	*Baseline* (%)
$K\rho(770)$	42±6	57.3±3.5	58.4±4.3	58.8±4.5
$K\omega$	11±2	14.8±4.7	22.5±5.2	6.3±3.1
$K^*(892)\pi$	16±5	26.0±2.1	17.1±2.3	25.0±6.3
$[K\pi]_S\pi$	28±4	1.90±0.66	2.01±0.64	9.9±2.2
$Kf_0(1370)$	3±2	–	–	–

Table 22. Comparison of branching fractions for $K_1(1270)$ decays according to the PDG [32] and to the Belle amplitude analysis [13] with fixed (Fit 1) and free (Fit 2) mass and width of the $K_1(1270)$.

E Resonant substructure of the $K_1(1270)^+$

The $K_1(1270)^+$ resonance is the prominent contribution to $B^+ \to \psi(2S)K^+\pi^+\pi^-$ decays and thus serves as a reference channel for the exotic contributions. Table 22 compares the branching fractions of the $K_1(1270)$ resonances obtained from the baseline model to those from a $B^+ \to J/\psi K^+\pi^+\pi^-$ amplitude analysis by Belle [13] and to those from scattering experiments that constitute the basis for the PDG values [32]. The largest difference between the PDG and Belle branching fractions is observed for the $K\pi$ S-wave, which was considered to be a $K_0^*(1430)^0$ resonance in those measurements. We use a more sophisticated K-matrix approach instead and obtain a reasonable result between the PDG and Belle results.

To translate the fit fractions from table 1 to branching fractions, we include isospin factors [13] and combine the $K_1(1270)^+[S] \to K^*(892)^0\pi^+$ and $K_1(1270)^+[D] \to K^*(892)^0\pi^+$ decay fractions taking their interference into account. We describe $\rho(770)^0 - \omega$ mixing with a combined lineshape 4.8. For the comparison of the branching fractions, it is instructive to separate the $\rho(770)^0$ and ω contributions. We adapt the procedure from the $\chi_{c1}(3872) \to J/\psi\rho(770)^0/\omega$ analysis [15] to quantify the relative rate of the $\rho(770)^0$ and ω contributions by computing the integrals

$$I(s_{123}|a,\delta) = \int_{(2m_\pi)^2}^{(\sqrt{s_{123}}-m_K)^2} |A(s_{123}, s_{23}|a,\delta)|^2 \, ds_{23}, \tag{E.1}$$

where s_{123} and s_{23} refer to the $K^+\pi^+\pi^-$ and $\pi^+\pi^-$ invariant-mass squared. The amplitude is given by $A(s_{123}, s_{23}|a,\delta) = q(s_{123}, s_{23})\, F_1(\tilde{q}(s_{23}))\, \tilde{q}(s_{23})^3\, T_{GS}(s_{23}) \left(a + \delta \frac{s_{23}}{m_\omega^2} T_\omega(s_{23})\right)$, where q and $\tilde{q}$ refer to the break-up momentum of the $K_1(1270)^+$ and $\rho(770)^0/\omega$ decays. In contrast to ref. [15] which evaluates the integral at the resonance mass, i.e. $I(s_{123} = m^2_{K_1(1270)^+}|a,\delta)$, we take the broad lineshape of the $K_1(1270)^+$ into account by weighting with the $K_1(1270)^+$ Breit-Wigner, $T_{K_1(1270)^+}(s_{123})$, as follows:

$$\langle I(a,\delta)\rangle = \int_{(m_K+2m_\pi)^2}^{(m_B-m_{\psi(2S)})^2} I(s_{123}|a,\delta)\, |T_{K_1(1270)^+}(s_{123})|^2 \, ds_{123}. \tag{E.2}$$

A measure of the ω ($\rho(770)^0$) contribution is then obtained as $R_\omega = \frac{\langle I(a=0,\delta)\rangle}{\langle I(a=1,\delta)\rangle}$ ($R_\rho = 1 - R_\omega$). We obtain $R_\omega = (0.49 \pm 0.24)\%$, which is then corrected with $\mathcal{B}(\omega \to \pi\pi) = (1.53 \pm 0.12)\%$ [32] to determine the $K_1(1270) \to K\omega$ branching fraction.

The LHCb collaboration has previously studied the $K_1(1270)^+$ substructure in $D^0 \to K^+K^-\pi^+\pi^-$ [68], $\overline{D}^0 \to K^+\pi^-\pi^+\pi^-$ [70] and $B_s^0 \to D_s^- K^+\pi^+\pi^-$ [85] decays. There

JHEP01(2025)054

are several notable differences in the parameterisations used. The charm amplitude analyses model the $\pi\pi$ P-wave as the sum of $\rho(770)^0$, ω and $\rho(1450)^0$ Breit-Wigner functions. In contrast, a special $\rho(770)^0 - \omega$ mixing lineshape is used for $B_s^0 \to D_s^- K^+\pi^+\pi^-$ and $B^+ \to \psi(2S)K^+\pi^+\pi^-$ decays, without a $\rho(1450)^0$ contribution. The LASS parameterisation [93, 94] is used for the $K\pi$ S-wave in $B_s^0 \to D_s^- K^+\pi^+\pi^-$ decays, while the others use a K-matrix approach.

Table 23 compares the $K_1(1270)^+$ fit fractions from those measurements to the results of the $B^+ \to \psi(2S)K^+\pi^+\pi^-$ *baseline* model. At first glance, the results appear rather inconsistent. There is a large $\rho(1450)^0$ contribution in $\overline{D}^0 \to K^+\pi^-\pi^+\pi^-$ decays, in contrast to the other measurements. The $\rho(1450)^0$ resonance has a huge negative interference with the $\rho(770)^0$ resonance that may hint at overfitting. In $D^0 \to K^+K^-\pi^+\pi^-$ decays, $F_i(K^+\rho(770)^0) \lessapprox F_i(K^*(892)^0\pi^+)$ is observed. The other decays have $F_i(K^+\rho(770)^0) \gg F_i(K^*(892)^0\pi^+)$. As the fit fractions are obtained by integrating over the respective decay phase space, this can be understood as a consequence of different phase-space limits. The kinematically allowed $m(K^+\pi^+\pi^-)$ range extends up to 1367 MeV, 1725 MeV, 3398 MeV and 1593 MeV for $D^0 \to K^+K^-\pi^+\pi^-$, $\overline{D}^0 \to K^+\pi^-\pi^+\pi^-$, $B_s^0 \to D_s^- K^+\pi^+\pi^-$ and $B^+ \to \psi(2S)K^+\pi^+\pi^-$ decays, respectively.[3] The $K^+\rho(770)^0$ threshold is close to the $K_1(1270)^+$ mass, which leads to a highly asymmetric contribution of the $K^+\rho(770)^0$ channel to the $K_1(1270)^+$ lineshape. Therefore a kinematic cut-off in the $m(K^+\pi^+\pi^-)$ range removes more of the $K^+\rho(770)^0$ than of the $K^*(892)^0\pi^+$ contribution. This effect becomes negligible when the cut-off is sufficiently far away from the $K_1(1270)^+$ mass.

For a better comparison of the results, we thus recompute the fit fractions in a consistent phase-space region. First, we take the $K_1(1270)^+$ amplitude models from the $D^0 \to K^+K^-\pi^+\pi^-$, $\overline{D}^0 \to K^+\pi^-\pi^+\pi^-$ and $B_s^0 \to D_s^- K^+\pi^+\pi^-$ measurements and generate pseudoexperiments for $B^+ \to K_1(1270)^+\psi(2S)$ decays. Figure 11 compares the resulting phase-space distributions. Given that these models were obtained from entirely different decays that have a multitude of non-$K_1(1270)^+$ components and use different parameterisations, the distributions agree reasonably well. The corresponding fit fractions, now evaluated in the $B^+ \to \psi(2S)K^+\pi^+\pi^-$ phase space, are given in table 24. Here, we compute a combined $\pi^+\pi^-$ P-wave fit fraction and a combined $[K^*(892)^0\pi]_S + [K^*(892)^0\pi]_D$ fit fraction for a better comparability. The obtained fit fractions are fairly consistent. One outlier is a large $[K\pi]_S\pi$ fit fraction from the $\overline{D}^0 \to K^+\pi^-\pi^+\pi^-$ model.

[3]The considered $B_s^0 \to D_s^- K^+\pi^+\pi^-$ phase-space region is limited to $m(K\pi\pi) < 1950$ MeV in ref. [85].

JHEP01(2025)054

Fit fraction (%)	$D^0 \to K^+K^-\pi^+\pi^-$	$\overline{D}^0 \to K^+\pi^-\pi^+\pi^-$	$B_s^0 \to D_s^- K^+\pi^+\pi^-$	$B^+ \to \psi(2S)K^+\pi^+\pi^-$
$K^+[\rho(770)^0/\omega]$	49.58±1.99±4.35	–	52.5±4.6±5.9±6.9	50.71±2.18±3.19
$K^+\rho(770)^0$	–	96.30±1.64±6.61	–	–
$K^+\omega$	–	1.65±0.11±0.16	–	–
$K^+\rho(1450)^0$	1.50±0.47±1.04	49.09±1.58±11.54	–	–
$[K^*(892)^0\pi^+]_S$	51.22±1.06±3.21	27.08±0.64±2.82	42.7±7.9±8.9±11.2	19.86±1.44±2.05
$[K^*(892)^0\pi^+]_D$	2.03±0.17±0.20	3.47±0.17±0.31	–	8.32±0.85±1.54
$[K\pi]_S\pi^+$	6.27±0.48±1.66	22.90±0.72±1.89	1.2±1.6±3.3±1.3	11.35±1.45±2.11
Sum	110.60±2.20±5.76	200.49	106.4	90.24±1.83±3.67

Table 23. Fit fractions of the $K_1(1270)^+$ substructure in $D^0 \to K^+K^-\pi^+\pi^-$ [68], $\overline{D}^0 \to K^+\pi^-\pi^+\pi^-$ [70] and $B_s^0 \to D_s^- K^+\pi^+\pi^-$ [85] decays compared to the results of the $B^+ \to \psi(2S)K^+\pi^+\pi^-$ *baseline* model.

Fit fraction (%)	$D^0 \to K^+K^-\pi^+\pi^-$	$\overline{D}^0 \to K^+\pi^-\pi^+\pi^-$	$B_s^0 \to D_s^- K^+\pi^+\pi^-$	$B^+ \to \psi(2S)K^+\pi^+\pi^-$
$K^+[\rho(770)^0/\omega/\rho(1450)^0]$	53.6±4.9	58.01±6.7	63.8±10.2	50.7±3.9
$K^*(892)^0\pi^+$	30.3±3.4	22.1±2.9	33.5±16.3	28.4±3.1
$[K\pi]_S\pi^+$	7.0±1.7	24.85±2.0	9.0±3.9	11.4±2.6
Sum	89.2±6.1	103.5	106.3	90.6±4.1

Table 24. Fit fractions of the $K_1(1270)^+$ substructure in $B^+ \to K_1(1270)^+\psi(2S)$ decays using the amplitude models from $D^0 \to K^+K^-\pi^+\pi^-$ [68], $\overline{D}^0 \to K^+\pi^-\pi^+\pi^-$ [70] and $B_s^0 \to D_s^- K^+\pi^+\pi^-$ [85] decays. The results of the $B^+ \to \psi(2S)K^+\pi^+\pi^-$ *baseline* model are shown as comparison.

JHEP01(2025)054

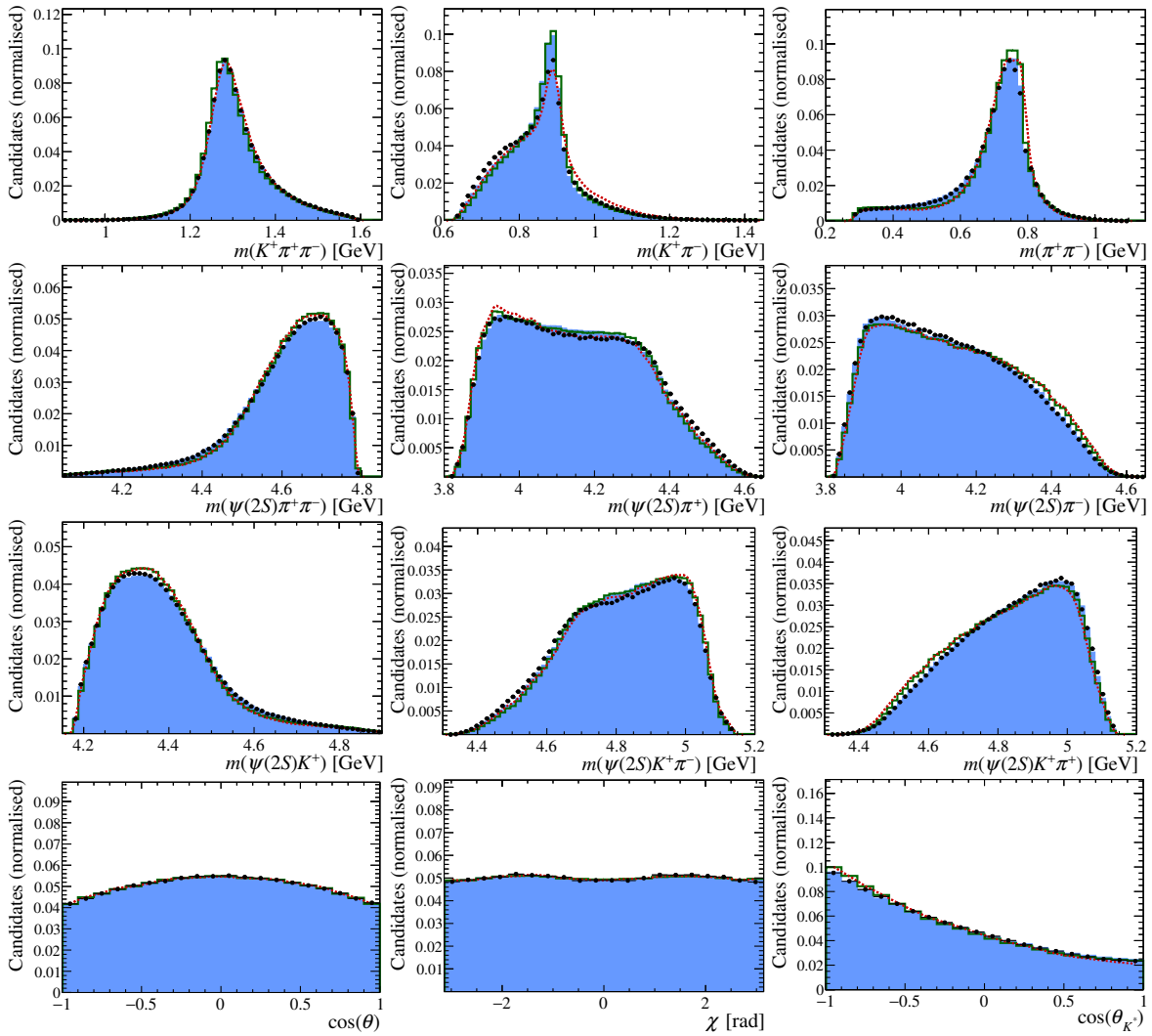

Figure 11. Phase-space distribution of pseudo $B^+ \to K_1(1270)^+\psi(2S)$ events generated using the $B^+ \to \psi(2S)K^+\pi^+\pi^-$ *baseline* model (black data points) or the amplitude models from the $D^0 \to K^+K^-\pi^+\pi^-$ [68] (green histograms), $\overline{D}{}^0 \to K^+\pi^-\pi^+\pi^-$ [70] (dashed, red lines) and $B_s^0 \to D_s^-K^+\pi^+\pi^-$ [85] (filled, blue histograms) analyses.

JHEP01(2025)054

F Quasi-model-independent lineshapes

Figure 12 shows the determined quasi-model-independent lineshapes for the $X^0 \to \psi(2S)\pi^+\pi^-$ resonances, where the expectations from a Breit-Wigner propagator with the mass and width from the nominal fit are superimposed. The $T^*_{c\bar{c}0}(4475)^0$ state has the highest fit fraction of any of the exotic states. Its Argand diagram in figure 12(a) shows a clear circular, counter-clockwise trajectory; which is the expected behaviour of a resonant state. The quasi-model-independent lineshapes of the $T_{c\bar{c}1}(4650)^0$ and $T^*_{c\bar{c}0}(4710)^0$ are qualitatively consistent with the expectations as well. The phase motion of the $T_{c\bar{c}1}(4650)^0$ at low mass hints at a possible second 1^+ resonance that is also part of alternative model 4, see tables 16 to 18. Note that the high-mass tail of the broad $T^*_{c\bar{c}1}(4800)^0$ state is outside of the phase-space boundary such that the full phase motion cannot be investigated.

The quasi-model-independent lineshapes for the $T^0_{c\bar{c}\bar{s}} \to \psi(2S)K^+\pi^-$ resonances are shown in figure 13. The $T_{c\bar{c}\bar{s}1}(4600)^0$ has the highest fit fraction of these states and is shown in figure 13(a). A clear, rapid phase-motion around the resonance pole is observed. The $T_{c\bar{c}\bar{s}1}(4900)^0$ shows an indicative resonant phase-motion as well, see figure 13(b). As the $T^*_{c\bar{c}\bar{s}1}(5200)^0$ state, shown in figure 13(c), has a low fit fraction and is close to the phase-space boundary, no conclusive statements can be made.

The $T_{c\bar{c}1}(4200)^+$ state has the second highest fit fraction among the exotic states. The Argand diagram of the $T_{c\bar{c}1}(4200)^+$, shown in figure 14(a), is consistent with a circular trajectory. The quasi-model-independent lineshape of the $T_{c\bar{c}1}(4430)^+$ state in figure 14(b) is more difficult to interpret, as the mass of the $T_{c\bar{c}1}(4430)^+$ state is close to the phase-space boundary and because of the large correlation with the $T_{c\bar{c}1}(4200)^+$ state. The pole mass of the $T_{c\bar{c}\bar{s}1}(4000)^+$ state is outside of the phase space such that only its tail contributes. The corresponding quasi-model-independent lineshape is consistent with the tail of a Breit-Wigner function, see figure 14(c).

As the investigated resonances have large decay widths and the interpolated spline function requires an extensive amount of free fit parameters (12 more than the Breit-Wigner function), the quasi-model-independent approach is fairly sensitive to statistical fluctuations in the data, especially near the phase-space boundaries. With this in mind, the agreement with the Breit-Wigner expectation can be considered as reasonable in all cases.

JHEP01(2025)054

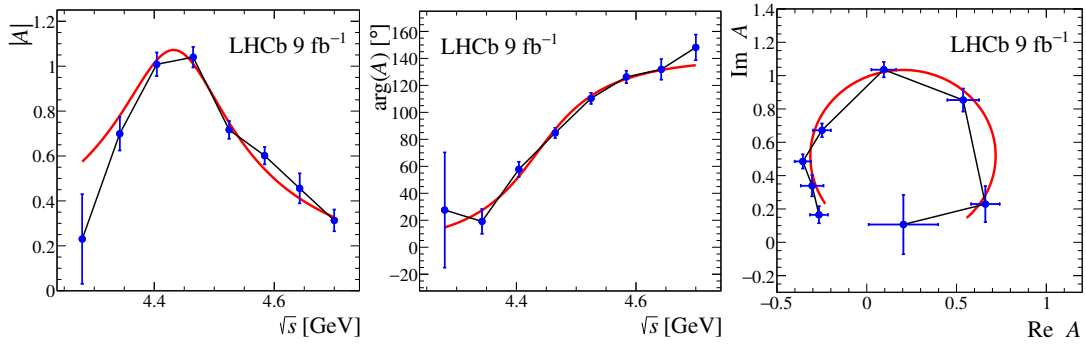

(a) Lineshape of the $T^*_{c\bar{c}0}(4475)^0$ resonance.

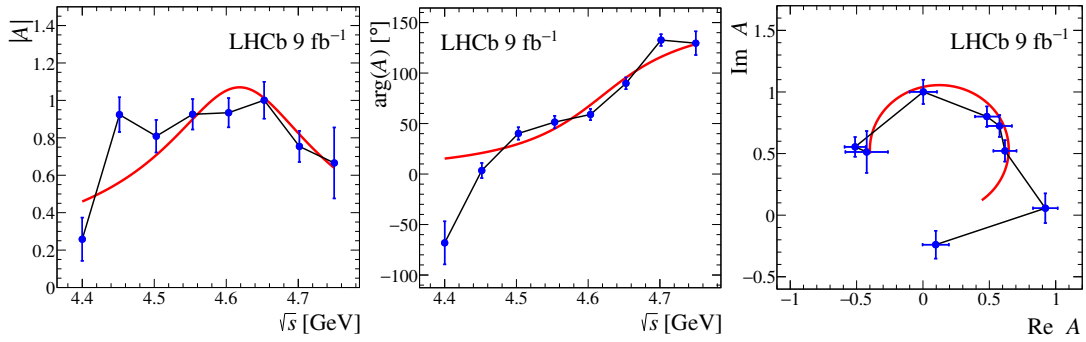

(b) Lineshape of the $T_{c\bar{c}1}(4650)^0$ resonance.

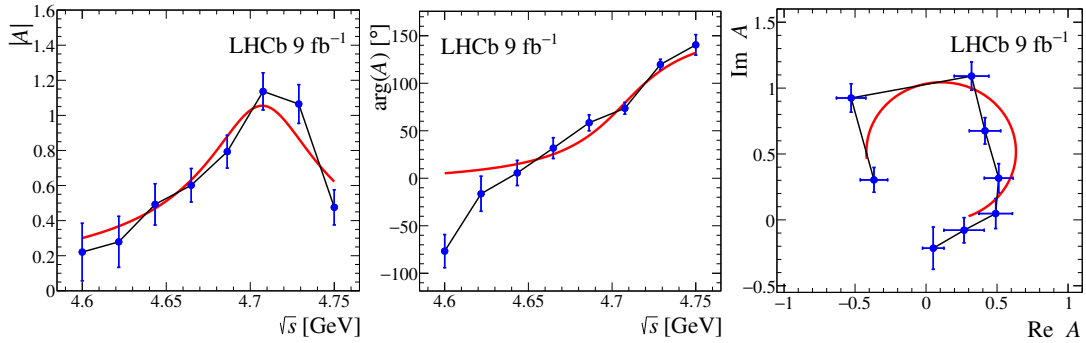

(c) Lineshape of the $T^*_{c\bar{c}0}(4710)^0$ resonance.

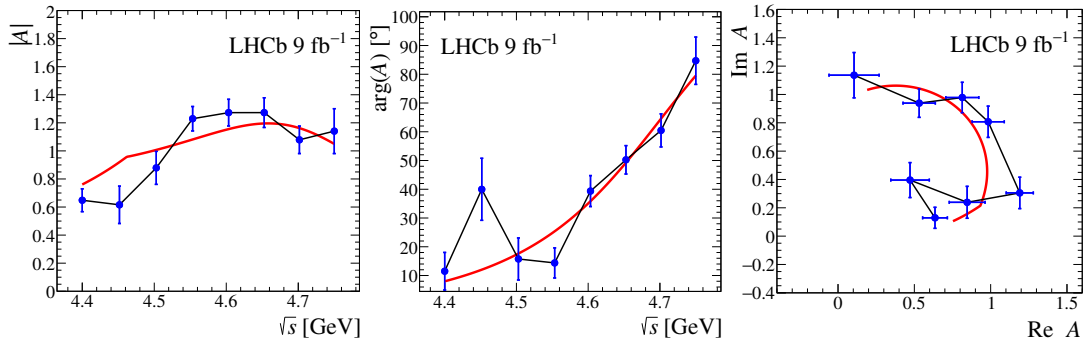

(d) Lineshape of the $T^*_{c\bar{c}1}(4800)^0$ resonance.

Figure 12. (Left) Magnitude, (middle) phase and (right) Argand diagram of the quasi-model-independent lineshape for $X^0 \to \psi(2S)\pi^+\pi^-$ states. The fitted knots are displayed as connected points with error bars. The Breit-Wigner lineshape with the mass and width from the nominal fit is superimposed (red line).

JHEP01(2025)054

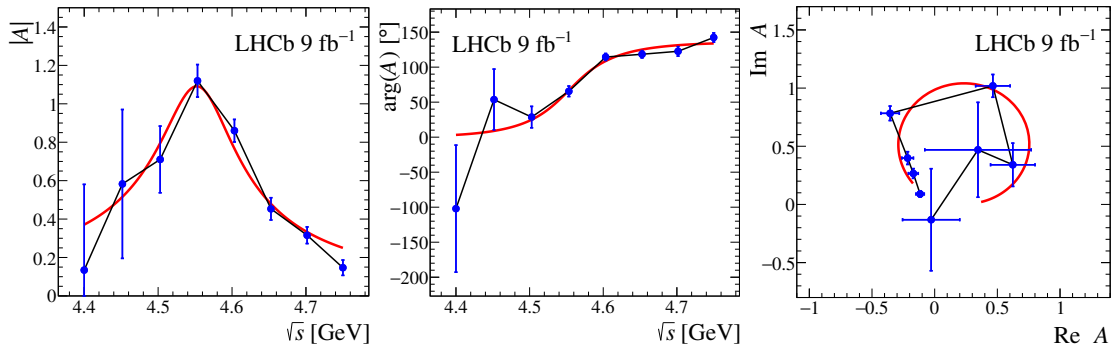

(a) Lineshape of the $T_{c\bar{c}s1}(4600)^0$ resonance.

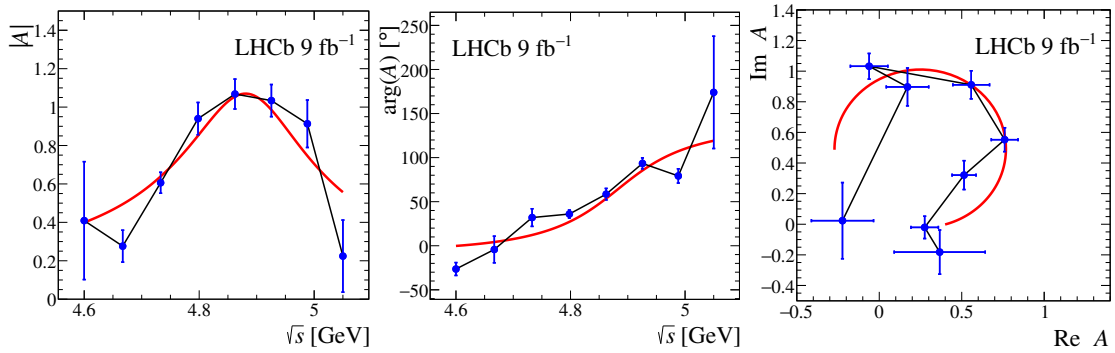

(b) Lineshape of the $T_{c\bar{c}s1}(4900)^0$ resonance.

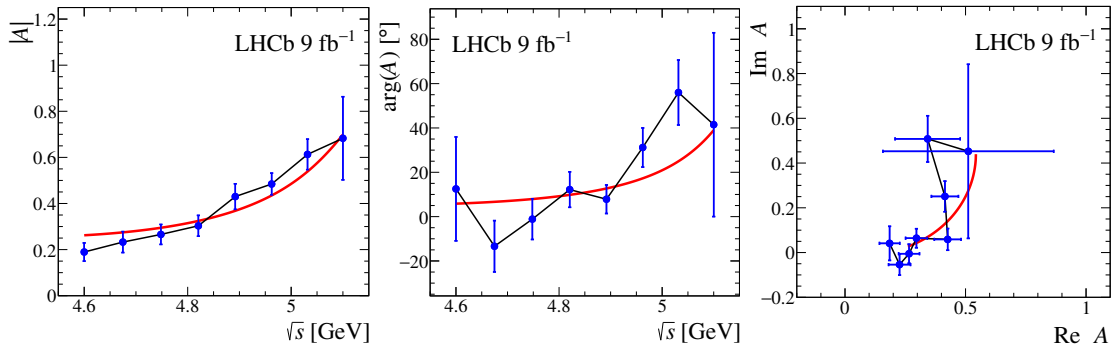

(c) Lineshape of the $T^*_{c\bar{c}s1}(5200)^0$ resonance.

Figure 13. (Left) Magnitude, (middle) phase and (right) Argand diagram of the quasi-model-independent lineshape for $T^0_{c\bar{c}\bar{s}} \to \psi(2S)K^+\pi^-$ states. The fitted knots are displayed as connected points with error bars. The Breit-Wigner lineshape with the mass and width from the nominal fit is superimposed (red line).

JHEP01(2025)054

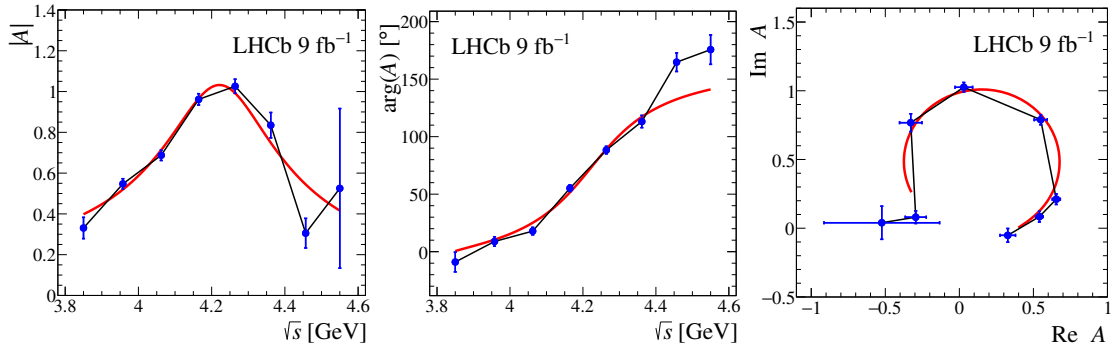

(a) Lineshape of the $T_{c\bar{c}1}(4200)^{\pm}$ resonance.

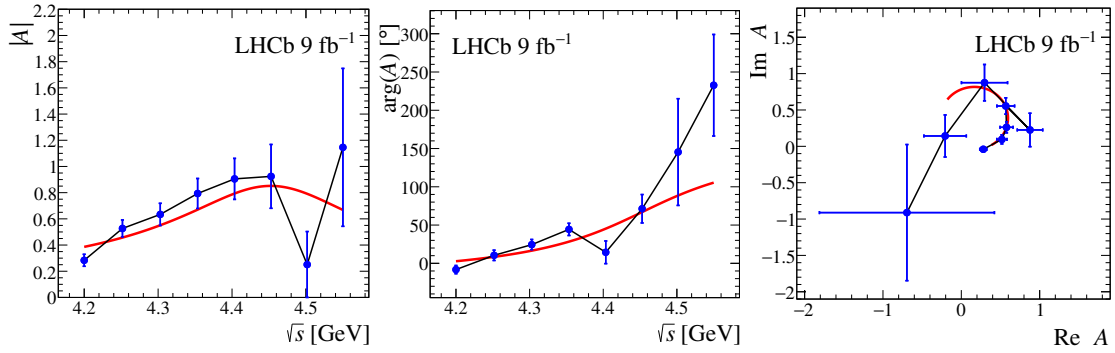

(b) Lineshape of the $T_{c\bar{c}1}(4430)^{\pm}$ resonance.

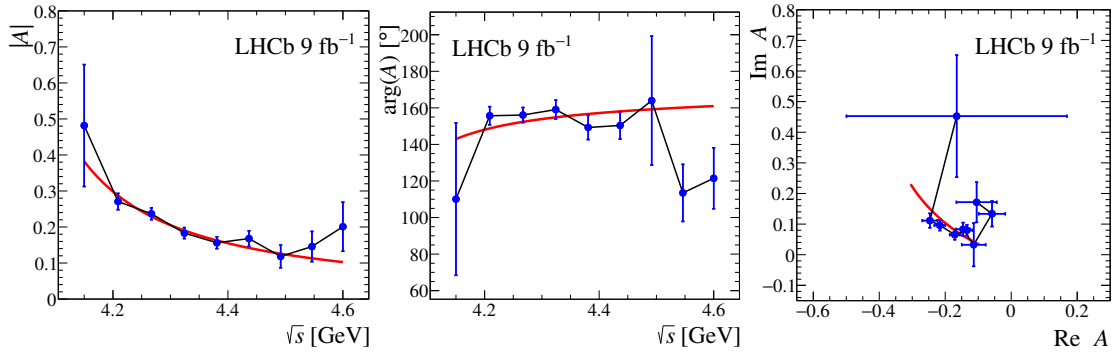

(c) Lineshape of the $T_{c\bar{c}\bar{s}1}(4000)^{+}$ resonance.

Figure 14. (Left) Magnitude, (middle) phase and (right) Argand diagram of the quasi-model-independent lineshape for $T^{\pm}_{c\bar{c}} \to \psi(2S)\pi^{\pm}$ and $T^{+}_{c\bar{c}\bar{s}} \to \psi(2S)K^{+}$ states. The fitted knots are displayed as connected points with error bars. The Breit-Wigner lineshape with the mass and width from the nominal fit is superimposed (red line).

Data Availability Statement. This article has associated data in a data repository. The LHCb experiment has agreed to the CERN open data policy summarised in https://opendata.cern.ch/docs/about. In particular, Level 1 data associated with this publication are made available on the CERN document server at http://cds.cern.ch/record/2904824/files/. These data contain material related to the paper that allows a reinterpretation of the results in the context of new theoretical models.

JHEP01(2025)054

Code Availability Statement. This article has associated code in a code repository. The code implementation of the baseline amplitude model and all alternative models is made available on Zenodo at https://zenodo.org/records/11212410. Other specific analysis software/code used to produce the results shown in the publication is preserved within the LHCb collaboration internally and can be provided on reasonable request, provided it does not contain information that can be associated with unpublished results.

JHEP01(2025)054

References

[1] Belle collaboration, *Observation of a narrow charmonium-like state in exclusive $B^{\pm} \to K^{\pm}\pi^{+}\pi^{-}J/\psi$ decays*, *Phys. Rev. Lett.* **91** (2003) 262001 [hep-ex/0309032] [INSPIRE].

[2] D. Johnson, I. Polyakov, T. Skwarnicki and M. Wang, *Exotic hadrons at LHCb*, *Ann. Rev. Nucl. Part. Sci.* **74** (2024) 583 [arXiv:2403.04051] [INSPIRE].

[3] T. Barnes and S. Godfrey, *Charmonium options for the X(3872)*, *Phys. Rev. D* **69** (2004) 054008 [hep-ph/0311162] [INSPIRE].

[4] N.A. Tornqvist, *Isospin breaking of the narrow charmonium state of Belle at 3872 MeV as a deuson*, *Phys. Lett. B* **590** (2004) 209 [hep-ph/0402237] [INSPIRE].

[5] L. Maiani, F. Piccinini, A.D. Polosa and V. Riquer, *Diquark-antidiquarks with hidden or open charm and the nature of X(3872)*, *Phys. Rev. D* **71** (2005) 014028 [hep-ph/0412098] [INSPIRE].

[6] B.A. Li, *Is X(3872) a possible candidate of hybrid meson*, *Phys. Lett. B* **605** (2005) 306 [hep-ph/0410264] [INSPIRE].

[7] Belle collaboration, *Dalitz analysis of $B \to K\pi^{+}\psi'$ decays and the $Z(4430)^{+}$*, *Phys. Rev. D* **80** (2009) 031104 [arXiv:0905.2869] [INSPIRE].

[8] LHCb collaboration, *Observation of the resonant character of the $Z(4430)^{-}$ state*, *Phys. Rev. Lett.* **112** (2014) 222002 [arXiv:1404.1903] [INSPIRE].

[9] Belle collaboration, *Experimental constraints on the spin and parity of the $Z(4430)^{+}$*, *Phys. Rev. D* **88** (2013) 074026 [arXiv:1306.4894] [INSPIRE].

[10] LHCb collaboration, *Observation of new resonances decaying to $J/\psi K^{+}+$ and $J/\psi\phi$*, *Phys. Rev. Lett.* **127** (2021) 082001 [arXiv:2103.01803] [INSPIRE].

[11] V. Bellée et al., *Using an amplitude analysis to measure the photon polarisation in $B \to K\pi\pi\gamma$ decays*, *Eur. Phys. J. C* **79** (2019) 622 [arXiv:1902.09201] [INSPIRE].

[12] LHCb collaboration, *First observations of the rare decays $B^{+} \to K^{+}\pi^{+}\pi^{-}\mu^{+}\mu^{-}$ and $B^{+} \to \phi K^{+}\mu^{+}\mu^{-}$*, *JHEP* **10** (2014) 064 [arXiv:1408.1137] [INSPIRE].

[13] Belle collaboration, *Study of the $K^{+}\pi^{+}\pi^{-}$ final state in $B^{+} \to J/\psi K^{+}\pi^{+}\pi^{-}$ and $B^{+} \to \psi' K^{+}\pi^{+}\pi^{-}$*, *Phys. Rev. D* **83** (2011) 032005 [arXiv:1009.5256] [INSPIRE].

[14] LHCb collaboration, *Study of the $\psi_2(3823)$ and $\chi_{c1}(3872)$ states in $B^{+} \to (J\psi\pi^{+}\pi^{-})\,K^{+}$ decays*, *JHEP* **08** (2020) 123 [arXiv:2005.13422] [INSPIRE].

[15] LHCb collaboration, *Observation of sizeable ω contribution to $\chi_{c1}(3872) \to \pi^{+}\pi^{-}J/\psi$ decays*, *Phys. Rev. D* **108** (2023) L011103 [arXiv:2204.12597] [INSPIRE].

[16] LHCb collaboration, *The LHCb detector at the LHC*, 2008 *JINST* **3** S08005 [INSPIRE].

[17] LHCb collaboration, *LHCb detector performance*, *Int. J. Mod. Phys. A* **30** (2015) 1530022 [arXiv:1412.6352] [INSPIRE].

[18] R. Aaij et al., *Performance of the LHCb vertex locator*, 2014 *JINST* **9** P09007 [arXiv:1405.7808] [INSPIRE].

[19] LHCb Outer Tracker Group collaboration, *Performance of the LHCb outer tracker*, 2014 *JINST* **9** P01002 [arXiv:1311.3893] [INSPIRE].

[20] LHCb Outer Tracker Group collaboration, *Improved performance of the LHCb outer tracker in LHC run 2*, 2017 *JINST* **12** P11016 [arXiv:1708.00819] [INSPIRE].

[21] LHCb RICH Group collaboration, *Performance of the LHCb RICH detector at the LHC*, *Eur. Phys. J. C* **73** (2013) 2431 [arXiv:1211.6759] [INSPIRE].

[22] R. Aaij et al., *The LHCb trigger and its performance in 2011*, 2013 *JINST* **8** P04022 [arXiv:1211.3055] [INSPIRE].

[23] V.V. Gligorov and M. Williams, *Efficient, reliable and fast high-level triggering using a bonsai boosted decision tree*, 2013 *JINST* **8** P02013 [arXiv:1210.6861] [INSPIRE].

[24] T. Sjostrand, S. Mrenna and P.Z. Skands, *PYTHIA 6.4 physics and manual*, *JHEP* **05** (2006) 026 [hep-ph/0603175] [INSPIRE].

[25] T. Sjostrand, S. Mrenna and P.Z. Skands, *A brief introduction to PYTHIA 8.1*, *Comput. Phys. Commun.* **178** (2008) 852 [arXiv:0710.3820] [INSPIRE].

[26] LHCb collaboration, *Handling of the generation of primary events in Gauss, the LHCb simulation framework*, *J. Phys. Conf. Ser.* **331** (2011) 032047 [INSPIRE].

[27] D.J. Lange, *The EvtGen particle decay simulation package*, *Nucl. Instrum. Meth. A* **462** (2001) 152 [INSPIRE].

[28] P. Golonka and Z. Was, *PHOTOS Monte Carlo: a precision tool for QED corrections in Z and W decays*, *Eur. Phys. J. C* **45** (2006) 97 [hep-ph/0506026] [INSPIRE].

[29] J. Allison et al., *GEANT4 developments and applications*, *IEEE Trans. Nucl. Sci.* **53** (2006) 270 [INSPIRE].

[30] GEANT4 collaboration, *GEANT4 — a simulation toolkit*, *Nucl. Instrum. Meth. A* **506** (2003) 250 [INSPIRE].

[31] LHCb collaboration, *The LHCb simulation application, Gauss: design, evolution and experience*, *J. Phys. Conf. Ser.* **331** (2011) 032023 [INSPIRE].

[32] Particle Data Group collaboration, *Review of particle physics*, *PTEP* **2022** (2022) 083C01 [INSPIRE].

[33] W.D. Hulsbergen, *Decay chain fitting with a Kalman filter*, *Nucl. Instrum. Meth. A* **552** (2005) 566 [physics/0503191] [INSPIRE].

[34] L. Breiman, J. Friedman, R.A. Olshen and C.J. Stone, *Classification and regression trees*, Chapman and Hall/CRC, U.S.A. (2017) [DOI:10.1201/9781315139470] [INSPIRE].

[35] Y. Freund and R.E. Schapire, *A decision-theoretic generalization of on-line learning and an application to boosting*, *J. Comput. Syst. Sci.* **55** (1997) 119 [INSPIRE].

[36] M. Pivk and F.R. Le Diberder, *SPlot: a statistical tool to unfold data distributions*, *Nucl. Instrum. Meth. A* **555** (2005) 356 [physics/0402083] [INSPIRE].

JHEP01(2025)054

[37] N.L. Johnson, *Systems of frequency curves generated by methods of translation*, *Biometrika* **36** (1949) 149 [INSPIRE].

[38] M.E. Peskin and D.V. Schroeder, *An introduction to quantum field theory*, Westview Press, U.S.A. (1995).

[39] M. Beneke, J. Rohrer and D. Yang, *Branching fractions, polarisation and asymmetries of $B \to VV$ decays*, *Nucl. Phys. B* **774** (2007) 64 [hep-ph/0612290] [INSPIRE].

[40] LHCb collaboration, *Measurement of CP asymmetries and polarisation fractions in $B_s^0 \to K^{*0}\bar{K}^{*0}$ decays*, *JHEP* **07** (2015) 166 [arXiv:1503.05362] [INSPIRE].

[41] E. Byckling and K. Kajantie, *Particle kinematics*, John Wiley & Sons, U.S.A. (1973).

[42] S. Mandelstam, J.E. Paton, R.F. Peierls and A.Q. Sarker, *Isobar approximation of production processes*, *Annals Phys.* **18** (1962) 198 [INSPIRE].

[43] D. Herndon, P. Söding and R.J. Cashmore, *A generalized isobar model formalism*, *Phys. Rev. D* **11** (1975) 3165 [INSPIRE].

[44] J.J. Brehm, *Unitarity and the isobar model: two-body discontinuities*, *Annals Phys.* **108** (1977) 454 [INSPIRE].

[45] F. Von Hippel and C. Quigg, *Centrifugal-barrier effects in resonance partial decay widths, shapes, and production amplitudes*, *Phys. Rev. D* **5** (1972) 624 [INSPIRE].

[46] J.D. Jackson, *Remarks on the phenomenological analysis of resonances*, *Nuovo Cim.* **34** (1964) 1644 [INSPIRE].

[47] P. d'Argent et al., *Amplitude analyses of $D^0 \to \pi^+\pi^-\pi^+\pi^-$ and $D^0 \to K^+K^-\pi^+\pi^-$ decays*, *JHEP* **05** (2017) 143 [arXiv:1703.08505] [INSPIRE].

[48] G.J. Gounaris and J.J. Sakurai, *Finite width corrections to the vector meson dominance prediction for $\rho \to e^+e^-$*, *Phys. Rev. Lett.* **21** (1968) 244 [INSPIRE].

[49] CMD-2 collaboration, *Measurement of $e^+e^- \to \pi^+\pi^-$ cross-section with CMD-2 around rho meson*, *Phys. Lett. B* **527** (2002) 161 [hep-ex/0112031] [INSPIRE].

[50] J.T. Daub, C. Hanhart and B. Kubis, *A model-independent analysis of final-state interactions in $\overline{B}^0_{d/s} \to J/\psi\pi\pi$*, *JHEP* **02** (2016) 009 [arXiv:1508.06841] [INSPIRE].

[51] C. Hanhart et al., *The branching ratio $\omega \to \pi^+\pi^-$ revisited*, *Eur. Phys. J. C* **77** (2017) 98 [*Erratum ibid.* **78** (2018) 450] [arXiv:1611.09359] [INSPIRE].

[52] BABAR collaboration, *Precise measurement of the $e^+e^- \to \pi^+\pi^-(\gamma)$ cross section with the initial-state radiation method at BABAR*, *Phys. Rev. D* **86** (2012) 032013 [arXiv:1205.2228] [INSPIRE].

[53] S.U. Chung et al., *Partial wave analysis in K matrix formalism*, *Annalen Phys.* **4** (1995) 404 [INSPIRE].

[54] V.V. Anisovich and A.V. Sarantsev, *K matrix analysis of the ($IJ^{PC} = 00^{++}$)-wave in the mass region below 1900 MeV*, *Eur. Phys. J. A* **16** (2003) 229 [hep-ph/0204328] [INSPIRE].

[55] BABAR collaboration, *Improved measurement of the CKM angle γ in $B^\mp \to D^{(*)}K^{(*\mp)}$ decays with a Dalitz plot analysis of D decays to $K^0_S\pi^+\pi^-$ and $K^0_SK^+K^-$*, *Phys. Rev. D* **78** (2008) 034023 [arXiv:0804.2089] [INSPIRE].

[56] FOCUS collaboration, *Dalitz plot analysis of the $D^+ \to K^-\pi^+\pi^+$ decay in the FOCUS experiment*, *Phys. Lett. B* **653** (2007) 1 [arXiv:0705.2248] [INSPIRE].

JHEP01(2025)054

[57] I.J.R. Aitchison, *K-matrix formalism for overlapping resonances*, *Nucl. Phys. A* **189** (1972) 417 [INSPIRE].

[58] C. Zemach, *Use of angular momentum tensors*, *Phys. Rev.* **140** (1965) B97 [INSPIRE].

[59] W. Rarita and J. Schwinger, *On a theory of particles with half integral spin*, *Phys. Rev.* **60** (1941) 61 [INSPIRE].

[60] S.U. Chung, *A general formulation of covariant helicity coupling amplitudes*, *Phys. Rev. D* **57** (1998) 431 [INSPIRE].

[61] B.S. Zou and D.V. Bugg, *Covariant tensor formalism for partial wave analyses of psi decay to mesons*, *Eur. Phys. J. A* **16** (2003) 537 [hep-ph/0211457] [INSPIRE].

[62] V. Filippini, A. Fontana and A. Rotondi, *Covariant spin tensors in meson spectroscopy*, *Phys. Rev. D* **51** (1995) 2247 [INSPIRE].

[63] J.-J. Zhu, *Explicit expressions of spin wave functions*, hep-ph/9906250 [INSPIRE].

[64] MARK-III collaboration, *Resonant substructure in $\bar{K}\pi\pi\pi$ decays of D mesons*, *Phys. Rev. D* **45** (1992) 2196 [INSPIRE].

[65] FOCUS collaboration, *Study of the $D^0 \to \pi^-\pi^+\pi^-\pi^+$ decay*, *Phys. Rev. D* **75** (2007) 052003 [hep-ex/0701001] [INSPIRE].

[66] CLEO collaboration, *Amplitude analysis of $D^0 \to K^+K^-\pi^+\pi^-$*, *Phys. Rev. D* **85** (2012) 122002 [arXiv:1201.5716] [INSPIRE].

[67] A. Rogozhnikov, *Reweighting with boosted decision trees*, *J. Phys. Conf. Ser.* **762** (2016) 012036 [arXiv:1608.05806] [INSPIRE].

[68] LHCb collaboration, *Search for CP violation through an amplitude analysis of $D^0 \to K^+K^-\pi^+\pi^-$ decays*, *JHEP* **02** (2019) 126 [arXiv:1811.08304] [INSPIRE].

[69] S. Harnew et al., *Model-independent determination of the strong phase difference between D^0 and $\bar{D}^0 \to \pi^+\pi^-\pi^+\pi^-$ amplitudes*, *JHEP* **01** (2018) 144 [arXiv:1709.03467] [INSPIRE].

[70] LHCb collaboration, *Studies of the resonance structure in $D^0 \to K^\mp\pi^\pm\pi^\pm\pi^\mp$ decays*, *Eur. Phys. J. C* **78** (2018) 443 [arXiv:1712.08609] [INSPIRE].

[71] BELLE collaboration, *Observation of a new charged charmoniumlike state in $\bar{B}^0 \to J/\psi K^-\pi^+$ decays*, *Phys. Rev. D* **90** (2014) 112009 [arXiv:1408.6457] [INSPIRE].

[72] BELLE collaboration, *Observation of two resonance-like structures in the $\pi^+\chi_{c1}$ mass distribution in exclusive $\bar{B}^0 \to K^-\pi^+\chi_{c1}$ decays*, *Phys. Rev. D* **78** (2008) 072004 [arXiv:0806.4098] [INSPIRE].

[73] BELLE collaboration, *Measurement of $e^+e^- \to \pi^+\pi^-\psi(2S)$ via initial state radiation at Belle*, *Phys. Rev. D* **91** (2015) 112007 [arXiv:1410.7641] [INSPIRE].

[74] LHCb collaboration, *Evidence for an $\eta_c(1S)\pi^-$ resonance in $B^0 \to \eta_c(1S)K^+\pi^-$ decays*, *Eur. Phys. J. C* **78** (2018) 1019 [arXiv:1809.07416] [INSPIRE].

[75] LHCb collaboration, *Evidence of a $J/\psi K^0_S$ structure in $B^0 \to J/\psi\phi K^0_S$ decays*, *Phys. Rev. Lett.* **131** (2023) 131901 [arXiv:2301.04899] [INSPIRE].

[76] E791 collaboration, *Model independent measurement of S-wave $K^-\pi^+$ systems using $D^+ \to K\pi\pi$ decays from Fermilab E791*, *Phys. Rev. D* **73** (2006) 032004 [*Erratum ibid.* **74** (2006) 059901] [hep-ex/0507099] [INSPIRE].

[77] G. Micula and S. Micula, *Handbook of splines*, Springer, The Netherlands (1999) [DOI:10.1007/978-94-011-5338-6].

JHEP01(2025)054

[78] FORTHEATLASANDALICES collaboration, *The C-RORC PCIe card and its application in the ALICE and ATLAS experiments*, ATL-DAQ-PROC-2014-039, CERN, Geneva, Switzerland (2015) [DOI:10.1088/1748-0221/10/02/C02022].

[79] LHCb collaboration, *Measurement of the track reconstruction efficiency at LHCb*, 2015 *JINST* **10** P02007 [arXiv:1408.1251] [INSPIRE].

[80] ATLAS collaboration, *Prospect for a search for direct stau production in events with at least two hadronic taus and missing transverse momentum at the High Luminosity LHC with the ATLAS detector*, ATL-PHYS-PUB-2016-021, CERN, Geneva, Switzerland (2016).

[81] R. Aaij et al., *Selection and processing of calibration samples to measure the particle identification performance of the LHCb experiment in run 2*, *EPJ Tech. Instrum.* **6** (2019) 1 [arXiv:1803.00824] [INSPIRE].

[82] S. Ropertz, C. Hanhart and B. Kubis, *A new parametrization for the scalar pion form factors*, *Eur. Phys. J. C* **78** (2018) 1000 [arXiv:1809.06867] [INSPIRE].

[83] R. Garcia-Martin et al., *The pion-pion scattering amplitude. IV: improved analysis with once subtracted Roy-like equations up to 1100 MeV*, *Phys. Rev. D* **83** (2011) 074004 [arXiv:1102.2183] [INSPIRE].

[84] B. Guegan, J. Hardin, J. Stevens and M. Williams, *Model selection for amplitude analysis*, 2015 *JINST* **10** P09002 [arXiv:1505.05133] [INSPIRE].

[85] LHCb collaboration, *Measurement of the CKM angle γ and B_s^0-$\bar{B}_s^0$ mixing frequency with $B_s^0 \to D_s^{\mp} h^{\pm}\pi^{\pm}\pi^{\mp}$ decays*, *JHEP* **03** (2021) 137 [arXiv:2011.12041] [INSPIRE].

[86] A. Gelman, A. Jakulin, M.G. Pittau and Y.-S. Su, *A weakly informative default prior distribution for logistic and other regression models*, *Ann. Appl. Statist.* **2** (2008).

[87] R. Tibshirani, *Regression shrinkage and selection via the Lasso*, *J. Roy. Statist. Soc. B* **58** (1996) 267 [INSPIRE].

[88] G. Schwarz, *Estimating the dimension of a model*, *Annals Statist.* **6** (1978) 461 [INSPIRE].

[89] S.-U. Chung and J. Friedrich, *Covariant helicity-coupling amplitudes: a new formulation*, *Phys. Rev. D* **78** (2008) 074027 [arXiv:0711.3143] [INSPIRE].

[90] H. Chen and R.-G. Ping, *Coherent helicity amplitude for sequential decays*, *Phys. Rev. D* **95** (2017) 076010 [arXiv:1704.05184] [INSPIRE].

[91] JPAC collaboration, *What is the right formalism to search for resonances?*, *Eur. Phys. J. C* **78** (2018) 229 [arXiv:1712.02815] [INSPIRE].

[92] P. d'Argent and T. Evans, *phdargen/ampgen-b2vppp: B->psi(2s)kpipi analysis code*, Zenodo, (2024).

[93] D. Aston et al., *A study of $K^-\pi^+$ scattering in the reaction $K^-p \to K^-\pi^+n$ at 11 GeV/c*, *Nucl. Phys. B* **296** (1988) 493 [INSPIRE].

[94] BABAR collaboration, *Dalitz-plot analysis of the decays $B^{\pm} \to K^{\pm}\pi^{\mp}\pi^{\pm}$*, *Phys. Rev. D* **72** (2005) 072003 [*Erratum ibid.* **74** (2006) 099903] [hep-ex/0507004] [INSPIRE].

JHEP01(2025)054

The LHCb collaboration

R. Aaij[36], A.S.W. Abdelmotteleb[55], C. Abellan Beteta[49], F. Abudinén[55], T. Ackernley[59], A. A. Adefisoye[67], B. Adeva[45], M. Adinolfi[53], P. Adlarson[79], C. Agapopoulou[13], C.A. Aidala[80], Z. Ajaltouni[11], S. Akar[64], K. Akiba[36], P. Albicocco[26], J. Albrecht[18], F. Alessio[47], M. Alexander[58], Z. Aliouche[61], P. Alvarez Cartelle[54], R. Amalric[15], S. Amato[3], J.L. Amey[53], Y. Amhis[13,47], L. An[6], L. Anderlini[25], M. Andersson[49], A. Andreianov[42], P. Andreola[49], M. Andreotti[24], D. Andreou[67], A. Anelli[29,p], D. Ao[7], F. Archilli[35,v], M. Argenton[24], S. Arguedas Cuendis[9,47], A. Artamonov[42], M. Artuso[67], E. Aslanides[12], R. Ataíde Da Silva[48], M. Atzeni[63], B. Audurier[14], D. Bacher[62], I. Bachiller Perea[10], S. Bachmann[20], M. Bachmayer[48], J.J. Back[55], P. Baladron Rodriguez[45], V. Balagura[14], W. Baldini[24], L. Balzani[18], H. Bao[7], J. Baptista de Souza Leite[59], C. Barbero Pretel[45], M. Barbetti[25,m], I. R. Barbosa[68], R.J. Barlow[61], M. Barnyakov[23], S. Barsuk[13], W. Barter[57], M. Bartolini[54], J. Bartz[67], J.M. Basels[16], S. Bashir[38], G. Bassi[33,s], B. Batsukh[5], P. B. Battista[13], A. Bay[48], A. Beck[55], M. Becker[18], F. Bedeschi[33], I.B. Bediaga[2], N. B. Behling[18], S. Belin[45], V. Bellee[49], K. Belous[42], I. Belov[27], G. Benane[12], G. Bencivenni[26], E. Ben-Haim[15], A. Berezhnoy[42], R. Bernet[49], S. Bernet Andres[43], A. Bertolin[31], C. Betancourt[49], F. Betti[57], J. Bex[54], Ia. Bezshyiko[49], J. Bhom[39], M.S. Bieker[18], N.V. Biesuz[24], P. Billoir[15], A. Biolchini[36], M. Birch[60], F.C.R. Bishop[10], A. Bitadze[61], A. Bizzeti[], T. Blake[55], F. Blanc[48], J.E. Blank[18], S. Blusk[67], V. Bocharnikov[42], J.A. Boelhauve[18], O. Boente Garcia[14], T. Boettcher[64], A. Bohare[57], A. Boldyrev[42], C.S. Bolognani[76], R. Bolzonella[24,l], N. Bondar[42], F. Borgato[31,q], S. Borghi[61], M. Borsato[29,p], J.T. Borsuk[39], S.A. Bouchiba[48], M. Bovill[62], T.J.V. Bowcock[59], A. Boyer[47], C. Bozzi[24], A. Brea Rodriguez[48], N. Breer[18], J. Brodzicka[39], A. Brossa Gonzalo[45,55,44,†], J. Brown[59], D. Brundu[30], E. Buchanan[57], A. Buonaura[49], L. Buonincontri[31,q], A.T. Burke[61], C. Burr[47], A. Butkevich[42], J.S. Butter[54], J. Buytaert[47], W. Byczynski[47], S. Cadeddu[30], H. Cai[72], A. C. Caillet[15], R. Calabrese[24,l], S. Calderon Ramirez[9], L. Calefice[44], S. Cali[26], M. Calvi[29,p], M. Calvo Gomez[43], P. Camargo Magalhaes[2,z], J. I. Cambon Bouzas[45], P. Campana[26], D.H. Campora Perez[76], A.F. Campoverde Quezada[7], S. Capelli[29], L. Capriotti[24], R. Caravaca-Mora[9], A. Carbone[23,j], L. Carcedo Salgado[45], R. Cardinale[27,n], A. Cardini[30], P. Carniti[29,p], L. Carus[20], A. Casais Vidal[63], R. Caspary[20], G. Casse[59], J. Castro Godinez[9], M. Cattaneo[47], G. Cavallero[24,47], V. Cavallini[24,l], S. Celani[20], D. Cervenkov[62], S. Cesare[28,o], A.J. Chadwick[59], I. Chahrour[80], M. Charles[15], Ph. Charpentier[47], E. Chatzianagnostou[36], C.A. Chavez Barajas[59], M. Chefdeville[10], C. Chen[12], S. Chen[5], Z. Chen[7], A. Chernov[39], S. Chernyshenko[51], X. Chiotopoulos[76], V. Chobanova[78], S. Cholak[48], M. Chrzaszcz[39], A. Chubykin[42], V. Chulikov[42], P. Ciambrone[26], X. Cid Vidal[45], G. Ciezarek[47], P. Cifra[47], P.E.L. Clarke[57], M. Clemencic[47], H.V. Cliff[54], J. Closier[47], C. Cocha Toapaxi[20], V. Coco[47], J. Cogan[12], E. Cogneras[11], L. Cojocariu[41], P. Collins[47], T. Colombo[47], M. C. Colonna[18], A. Comerma-Montells[44], L. Congedo[22], A. Contu[30], N. Cooke[58], I. Corredoira[45], A. Correia[15], G. Corti[47], J.J. Cottee Meldrum[53], B. Couturier[47], D.C. Craik[49], M. Cruz Torres[2,g], E. Curras Rivera[48], R. Currie[57], C.L. Da Silva[66], S. Dadabaev[42], L. Dai[69], X. Dai[6], E. Dall'Occo[18], J. Dalseno[45], C. D'Ambrosio[47],

JHEP01(2025)054

J. Daniel[11], A. Danilina[42], P. d'Argent[22], A. Davidson[55], J.E. Davies[61], A. Davis[61], O. De Aguiar Francisco[61], C. De Angelis[30,k], F. De Benedetti[47], J. de Boer[36], K. De Bruyn[75], S. De Capua[61], M. De Cian[20,47], U. De Freitas Carneiro Da Graca[2,b], E. De Lucia[26], J.M. De Miranda[2], L. De Paula[3], M. De Serio[22,h], P. De Simone[26], F. De Vellis[18], J.A. de Vries[76], F. Debernardis[22], D. Decamp[10], V. Dedu[12], L. Del Buono[15], B. Delaney[63], H.-P. Dembinski[18], J. Deng[8], V. Denysenko[49], O. Deschamps[11], F. Dettori[30,k], B. Dey[74], P. Di Nezza[26], I. Diachkov[42], S. Didenko[42], S. Ding[67], L. Dittmann[20], V. Dobishuk[51], A. D. Docheva[58], C. Dong[4], A.M. Donohoe[21], F. Dordei[30], A.C. dos Reis[2], A. D. Dowling[67], W. Duan[70], P. Duda[77], M.W. Dudek[39], L. Dufour[47], V. Duk[32], P. Durante[47], M. M. Duras[77], J.M. Durham[66], O. D. Durmus[74], A. Dziurda[39], A. Dzyuba[42], S. Easo[56], E. Eckstein[17], U. Egede[1], A. Egorychev[42], V. Egorychev[42], S. Eisenhardt[57], E. Ejopu[61], L. Eklund[79], M. Elashri[64], J. Ellbracht[18], S. Ely[60], A. Ene[41], E. Epple[64], J. Eschle[67], S. Esen[20], T. Evans[61], F. Fabiano[30,k], L.N. Falcao[2], Y. Fan[7], B. Fang[72], L. Fantini[32,r,47], M. Faria[48], K. Farmer[57], D. Fazzini[29,p], L. Felkowski[77], M. Feng[5,7], M. Feo[18,47], A. Fernandez Casani[46], M. Fernandez Gomez[45], A.D. Fernez[65], F. Ferrari[23], F. Ferreira Rodrigues[3], M. Ferrillo[49], M. Ferro-Luzzi[47], S. Filippov[42], R.A. Fini[22], M. Fiorini[24,l], K.L. Fischer[62], D.S. Fitzgerald[80], C. Fitzpatrick[61], F. Fleuret[14], M. Fontana[23], L. F. Foreman[61], R. Forty[47], D. Foulds-Holt[54], M. Franco Sevilla[65], M. Frank[47], E. Franzoso[24,l], G. Frau[61], C. Frei[47], D.A. Friday[61], J. Fu[7], Q. Fuehring[18,54], Y. Fujii[1], T. Fulghesu[15], E. Gabriel[36], G. Galati[22], M.D. Galati[36], A. Gallas Torreira[45], D. Galli[23,j], S. Gambetta[57], M. Gandelman[3], P. Gandini[28], B. Ganie[61], H. Gao[7], R. Gao[62], Y. Gao[8], Y. Gao[6], Y. Gao[8], M. Garau[30,k], L.M. Garcia Martin[48], P. Garcia Moreno[44], J. García Pardiñas[47], K. G. Garg[8], L. Garrido[44], C. Gaspar[47], R.E. Geertsema[36], L.L. Gerken[18], E. Gersabeck[61], M. Gersabeck[61], T. Gershon[55], Z. Ghorbanimoghaddam[53], L. Giambastiani[31,q], F. I. Giasemis[15,e], V. Gibson[54], H.K. Giemza[40], A.L. Gilman[62], M. Giovannetti[26], A. Gioventù[44], L. Girardey[61], P. Gironella Gironell[44], C. Giugliano[24,l], M.A. Giza[39], E.L. Gkougkousis[60], F.C. Glaser[13,20], V.V. Gligorov[15,47], C. Göbel[68], E. Golobardes[43], D. Golubkov[42], A. Golutvin[60,42,47], A. Gomes[2,a,†], S. Gomez Fernandez[44], F. Goncalves Abrantes[62], M. Goncerz[39], G. Gong[4], J. A. Gooding[18], I.V. Gorelov[42], C. Gotti[29], J.P. Grabowski[17], L.A. Granado Cardoso[47], E. Graugés[44], E. Graverini[48,t], L. Grazette[55], G. Graziani[], A. T. Grecu[41], L.M. Greeven[36], N.A. Grieser[64], L. Grillo[58], S. Gromov[42], C. Gu[14], M. Guarise[24], M. Guittiere[13], V. Guliaeva[42], P. A. Günther[20], A.-K. Guseinov[48], E. Gushchin[42], Y. Guz[6,42,47], T. Gys[47], K. Habermann[17], T. Hadavizadeh[1], C. Hadjivasiliou[65], G. Haefeli[48], C. Haen[47], J. Haimberger[47], M. Hajheidari[47], G. H. Hallett[55], M.M. Halvorsen[47], P.M. Hamilton[65], J. Hammerich[59], Q. Han[8], X. Han[20], S. Hansmann-Menzemer[20], L. Hao[7], N. Harnew[62], M. Hartmann[13], S. Hashmi[38], J. He[7,c], F. Hemmer[47], C. Henderson[64], R.D.L. Henderson[1,55], A.M. Hennequin[47], K. Hennessy[59], L. Henry[48], J. Herd[60], P. Herrero Gascon[20], J. Heuel[16], A. Hicheur[3], G. Hijano Mendizabal[49], D. Hill[48], S.E. Hollitt[18], J. Horswill[61], R. Hou[8], Y. Hou[11], N. Howarth[59], J. Hu[20], J. Hu[70], W. Hu[6], X. Hu[4], W. Huang[7], W. Hulsbergen[36], R.J. Hunter[55], M. Hushchyn[42], D. Hutchcroft[59], D. Ilin[42], P. Ilten[64], A. Inglessi[42], A. Iniukhin[42], A. Ishteev[42], K. Ivshin[42], R. Jacobsson[47], H. Jage[16],

JHEP01(2025)054

S.J. Jaimes Elles[46,73], S. Jakobsen[47], E. Jans[36], B.K. Jashal[46], A. Jawahery[65,47], V. Jevtic[18], E. Jiang[65], X. Jiang[5,7], Y. Jiang[7], Y. J. Jiang[6], M. John[62], A. John Rubesh Rajan[21], D. Johnson[52], C.R. Jones[54], T.P. Jones[55], S. Joshi[40], B. Jost[47], J. Juan Castella[54], N. Jurik[47], I. Juszczak[39], D. Kaminaris[48], S. Kandybei[50], M. Kane[57], Y. Kang[4], C. Kar[11], M. Karacson[47], D. Karpenkov[42], A. Kauniskangas[48], J.W. Kautz[64], F. Keizer[47], M. Kenzie[54], T. Ketel[36], B. Khanji[67], A. Kharisova[42], S. Kholodenko[33,47], G. Khreich[13], T. Kirn[16], V.S. Kirsebom[29,p], O. Kitouni[63], S. Klaver[37], N. Kleijne[33,s], K. Klimaszewski[40], M.R. Kmiec[40], S. Koliiev[51], L. Kolk[18], A. Konoplyannikov[42], P. Kopciewicz[38,47], P. Koppenburg[36], M. Korolev[42], I. Kostiuk[36], O. Kot[51], S. Kotriakhova, A. Kozachuk[42], P. Kravchenko[42], L. Kravchuk[42], M. Kreps[55], P. Krokovny[42], W. Krupa[67], W. Krzemien[40], O.K. Kshyvanskyi[51], J. Kubat[20], S. Kubis[77], M. Kucharczyk[39], V. Kudryavtsev[42], E. Kulikova[42], A. Kupsc[79], B. K. Kutsenko[12], D. Lacarrere[47], A. Lai[30], A. Lampis[30], D. Lancierini[54], C. Landesa Gomez[45], J.J. Lane[1], R. Lane[53], C. Langenbruch[20], J. Langer[18], O. Lantwin[42], T. Latham[55], F. Lazzari[33,t], C. Lazzeroni[52], R. Le Gac[12], H. Lee[59], R. Lefèvre[11], A. Leflat[42], S. Legotin[42], M. Lehuraux[55], E. Lemos Cid[47], O. Leroy[12], T. Lesiak[39], B. Leverington[20], A. Li[4], C. Li[12], H. Li[70], K. Li[8], L. Li[61], P. Li[47], P.-R. Li[71], Q. Li[5,7], S. Li[8], T. Li[5,d], T. Li[70], Y. Li[8], Y. Li[5], Z. Lian[4], X. Liang[67], S. Libralon[46], C. Lin[7], T. Lin[56], R. Lindner[47], V. Lisovskyi[48], R. Litvinov[30,47], F. L. Liu[1], G. Liu[70], K. Liu[71], S. Liu[5,7], W. Liu[8], Y. Liu[57], Y. Liu[71], Y. L. Liu[60], A. Lobo Salvia[44], A. Loi[30], J. Lomba Castro[45], T. Long[54], J.H. Lopes[3], A. Lopez Huertas[44], S. López Soliño[45], C. Lucarelli[25,m], D. Lucchesi[31,q], M. Lucio Martinez[76], V. Lukashenko[36,51], Y. Luo[6], A. Lupato[31,i], E. Luppi[24,l], K. Lynch[21], X.-R. Lyu[7], G. M. Ma[4], R. Ma[7], S. Maccolini[18], F. Machefert[13], F. Maciuc[41], B. Mack[67], I. Mackay[62], L. M. Mackey[67], L.R. Madhan Mohan[54], M. J. Madurai[52], A. Maevskiy[42], D. Magdalinski[36], D. Maisuzenko[42], M.W. Majewski[38], J.J. Malczewski[39], S. Malde[62], L. Malentacca[47], A. Malinin[42], T. Maltsev[42], G. Manca[30,k], G. Mancinelli[12], C. Mancuso[28,13,o], R. Manera Escalero[44], D. Manuzzi[23], D. Marangotto[28,o], J.F. Marchand[10], R. Marchevski[48], U. Marconi[23], S. Mariani[47], C. Marin Benito[44], J. Marks[20], A.M. Marshall[53], L. Martel[62], G. Martelli[32,r], G. Martellotti[34], L. Martinazzoli[47], M. Martinelli[29,p], D. Martinez Santos[45], F. Martinez Vidal[46], A. Massafferri[2], R. Matev[47], A. Mathad[47], V. Matiunin[42], C. Matteuzzi[67], K.R. Mattioli[14], A. Mauri[60], E. Maurice[14], J. Mauricio[44], P. Mayencourt[48], J. Mazorra de Cos[46], M. Mazurek[40], M. McCann[60], L. Mcconnell[21], T.H. McGrath[61], N.T. McHugh[58], A. McNab[61], R. McNulty[21], B. Meadows[64], G. Meier[18], D. Melnychuk[40], F. M. Meng[4], M. Merk[36,76], A. Merli[48], L. Meyer Garcia[65], D. Miao[5,7], H. Miao[7], M. Mikhasenko[17,f], D.A. Milanes[73], A. Minotti[29,p], E. Minucci[67], T. Miralles[11], B. Mitreska[18], D.S. Mitzel[18], A. Modak[56], R.A. Mohammed[62], R.D. Moise[16], S. Mokhnenko[42], T. Mombächer[47], M. Monk[55,1], S. Monteil[11], A. Morcillo Gomez[45], G. Morello[26], M.J. Morello[33,s], M.P. Morgenthaler[20], A.B. Morris[47], A.G. Morris[12], R. Mountain[67], H. Mu[4], Z. M. Mu[6], E. Muhammad[55], F. Muheim[57], M. Mulder[75], K. Müller[49], F. Muñoz-Rojas[9], R. Murta[60], P. Naik[59], T. Nakada[48], R. Nandakumar[56], T. Nanut[47], I. Nasteva[3], M. Needham[57], N. Neri[28,o], S. Neubert[17], N. Neufeld[47], P. Neustroev[42], J. Nicolini[18,13], D. Nicotra[76], E.M. Niel[48],

JHEP01(2025)054

N. Nikitin[42], P. Nogarolli[3], P. Nogga[17], N.S. Nolte[63], C. Normand[53], J. Novoa Fernandez[45], G. Nowak[64], C. Nunez[80], H. N. Nur[58], A. Oblakowska-Mucha[38], V. Obraztsov[42], T. Oeser[16], S. Okamura[24,l], A. Okhotnikov[42], O. Okhrimenko[51], R. Oldeman[30,k], F. Oliva[57], M. Olocco[18], C.J.G. Onderwater[76], R.H. O'Neil[57], D. Osthues[18], J.M. Otalora Goicochea[3], P. Owen[49], A. Oyanguren[46], O. Ozcelik[57], A. Padee[40], K.O. Padeken[17], B. Pagare[55], P.R. Pais[20], T. Pajero[47], A. Palano[22], M. Palutan[26], G. Panshin[42], L. Paolucci[55], A. Papanestis[56], M. Pappagallo[22,h], L.L. Pappalardo[24,l], C. Pappenheimer[64], C. Parkes[61], B. Passalacqua[24], G. Passaleva[25], D. Passaro[33,s], A. Pastore[22], M. Patel[60], J. Patoc[62], C. Patrignani[23,j], A. Paul[67], C.J. Pawley[76], A. Pellegrino[36], J. Peng[5,7], M. Pepe Altarelli[26], S. Perazzini[23], D. Pereima[42], H. Pereira Da Costa[66], A. Pereiro Castro[45], P. Perret[11], A. Perro[47], K. Petridis[53], A. Petrolini[27,n], J. P. Pfaller[64], H. Pham[67], L. Pica[33,s], M. Piccini[32], B. Pietrzyk[10], G. Pietrzyk[13], D. Pinci[34], F. Pisani[47], M. Pizzichemi[29,p], V. Placinta[41], M. Plo Casasus[45], T. Poeschl[47], F. Polci[15,47], M. Poli Lener[26], A. Poluektov[12], N. Polukhina[42], I. Polyakov[47], E. Polycarpo[3], S. Ponce[47], D. Popov[7], S. Poslavskii[42], K. Prasanth[57], C. Prouve[45], V. Pugatch[51], G. Punzi[33,t], S. Qasim[49], Q. Q. Qian[6], W. Qian[7], N. Qin[4], S. Qu[4], R. Quagliani[47], R.I. Rabadan Trejo[55], J.H. Rademacker[53], M. Rama[33], M. Ramírez García[80], V. Ramos De Oliveira[68], M. Ramos Pernas[55], M.S. Rangel[3], F. Ratnikov[42], G. Raven[37], M. Rebollo De Miguel[46], F. Redi[28,i], J. Reich[53], F. Reiss[61], Z. Ren[7], P.K. Resmi[62], R. Ribatti[48], G. R. Ricart[14,81], D. Riccardi[33,s], S. Ricciardi[56], K. Richardson[63], M. Richardson-Slipper[57], K. Rinnert[59], P. Robbe[13], G. Robertson[58], E. Rodrigues[59], E. Rodriguez Fernandez[45], J.A. Rodriguez Lopez[73], E. Rodriguez Rodriguez[45], J. Roensch[18], A. Rogovskiy[56], D.L. Rolf[47], P. Roloff[47], V. Romanovskiy[42], M. Romero Lamas[45], A. Romero Vidal[45], G. Romolini[24], F. Ronchetti[48], T. Rong[6], M. Rotondo[26], S. R. Roy[20], M.S. Rudolph[67], M. Ruiz Diaz[20], R.A. Ruiz Fernandez[45], J. Ruiz Vidal[79,aa], A. Ryzhikov[42], J. Ryzka[38], J. J. Saavedra-Arias[9], J.J. Saborido Silva[45], R. Sadek[14], N. Sagidova[42], D. Sahoo[74], N. Sahoo[52], B. Saitta[30,k], M. Salomoni[29,p,47], C. Sanchez Gras[36], I. Sanderswood[46], R. Santacesaria[34], C. Santamarina Rios[45], M. Santimaria[26,47], L. Santoro[2], E. Santovetti[35], A. Saputi[24,47], D. Saranin[42], A. Sarnatskiy[75], G. Sarpis[57], M. Sarpis[61], C. Satriano[34,u], A. Satta[35], M. Saur[6], D. Savrina[42], H. Sazak[16], L.G. Scantlebury Smead[62], A. Scarabotto[18], S. Schael[16], S. Scherl[59], M. Schiller[58], H. Schindler[47], M. Schmelling[19], B. Schmidt[47], S. Schmitt[16], H. Schmitz[17], O. Schneider[48], A. Schopper[47], N. Schulte[18], S. Schulte[48], M.H. Schune[13], R. Schwemmer[47], G. Schwering[16], B. Sciascia[26], A. Sciuccati[47], S. Sellam[45], A. Semennikov[42], T. Senger[49], M. Senghi Soares[37], A. Sergi[27,47], N. Serra[49], L. Sestini[31], A. Seuthe[18], Y. Shang[6], D.M. Shangase[80], M. Shapkin[42], R. S. Sharma[67], I. Shchemerov[42], L. Shchutska[48], T. Shears[59], L. Shekhtman[42], Z. Shen[6], S. Sheng[5,7], V. Shevchenko[42], B. Shi[7], Q. Shi[7], Y. Shimizu[13], E. Shmanin[42], R. Shorkin[42], J.D. Shupperd[67], R. Silva Coutinho[67], G. Simi[31,q], S. Simone[22,h], N. Skidmore[55], T. Skwarnicki[67], M.W. Slater[52], J.C. Smallwood[62], E. Smith[63], K. Smith[66], M. Smith[60], A. Snoch[36], L. Soares Lavra[57], M.D. Sokoloff[64], F.J.P. Soler[58], A. Solomin[42,53], A. Solovev[42], I. Solovyev[42], R. Song[1], Y. Song[48], Y. Song[4], Y. S. Song[6], F.L. Souza De Almeida[67],

JHEP01(2025)054

B. Souza De Paula[3], E. Spadaro Norella[27], E. Spedicato[23], J.G. Speer[18], E. Spiridenkov[42], P. Spradlin[58], V. Sriskaran[47], F. Stagni[47], M. Stahl[47], S. Stahl[47], S. Stanislaus[62], E.N. Stein[47], O. Steinkamp[49], O. Stenyakin[42], H. Stevens[18], D. Strekalina[42], Y. Su[7], F. Suljik[62], J. Sun[30], L. Sun[72], Y. Sun[65], D. Sundfeld[2], W. Sutcliffe[49], P.N. Swallow[52], F. Swystun[54], A. Szabelski[40], T. Szumlak[38], Y. Tan[4], M.D. Tat[62], A. Terentev[42], F. Terzuoli[33,w,47], F. Teubert[47], E. Thomas[47], D.J.D. Thompson[52], H. Tilquin[60], V. Tisserand[11], S. T'Jampens[10], M. Tobin[5,47], L. Tomassetti[24,l], G. Tonani[28,o,47], X. Tong[6], D. Torres Machado[2], L. Toscano[18], D.Y. Tou[4], C. Trippl[43], G. Tuci[20], N. Tuning[36], L.H. Uecker[20], A. Ukleja[38], D.J. Unverzagt[20], E. Ursov[42], A. Usachov[37], A. Ustyuzhanin[42], U. Uwer[20], V. Vagnoni[23], G. Valenti[23], N. Valls Canudas[47], H. Van Hecke[66], E. van Herwijnen[60], C.B. Van Hulse[45,y], R. Van Laak[48], M. van Veghel[36], G. Vasquez[49], R. Vazquez Gomez[44], P. Vazquez Regueiro[45], C. Vázquez Sierra[45], S. Vecchi[24], J.J. Velthuis[53], M. Veltri[25,x], A. Venkateswaran[48], M. Vesterinen[55], D. Vico Benet[62], M. Vieites Diaz[47], X. Vilasis-Cardona[43], E. Vilella Figueras[59], A. Villa[23], P. Vincent[15], F.C. Volle[52], D. vom Bruch[12], N. Voropaev[42], K. Vos[76], G. Vouters[10,47], C. Vrahas[57], J. Wagner[18], J. Walsh[33], E.J. Walton[1,55], G. Wan[6], C. Wang[20], G. Wang[8], J. Wang[6], J. Wang[5], J. Wang[4], J. Wang[72], M. Wang[28], N. W. Wang[7], R. Wang[53], X. Wang[8], X. Wang[70], X. W. Wang[60], Y. Wang[6], Z. Wang[13], Z. Wang[4], Z. Wang[28], J.A. Ward[55,1], M. Waterlaat[47], N.K. Watson[52], D. Websdale[60], Y. Wei[6], J. Wendel[78], B.D.C. Westhenry[53], C. White[54], M. Whitehead[58], E. Whiter[52], A.R. Wiederhold[55], D. Wiedner[18], G. Wilkinson[62], M.K. Wilkinson[64], M. Williams[63], M.R.J. Williams[57], R. Williams[54], Z. Williams[53], F.F. Wilson[56], W. Wislicki[40], M. Witek[39], L. Witola[20], C.P. Wong[66], G. Wormser[13], S.A. Wotton[54], H. Wu[67], J. Wu[8], Y. Wu[6], Z. Wu[7], K. Wyllie[47], S. Xian[70], Z. Xiang[5], Y. Xie[8], A. Xu[33], J. Xu[7], L. Xu[4], L. Xu[4], M. Xu[55], Z. Xu[11], Z. Xu[7], Z. Xu[5], D. Yang[], K. Yang[60], S. Yang[7], X. Yang[6], Y. Yang[27,n], Z. Yang[6], Z. Yang[65], V. Yeroshenko[13], H. Yeung[61], H. Yin[8], C. Y. Yu[6], J. Yu[69], X. Yuan[5], Y Yuan[5,7], E. Zaffaroni[48], M. Zavertyaev[19], M. Zdybal[39], C. Zeng[5,7], M. Zeng[4], C. Zhang[6], D. Zhang[8], J. Zhang[7], L. Zhang[4], S. Zhang[69], S. Zhang[62], Y. Zhang[6], Y. Z. Zhang[4], Y. Zhao[20], A. Zharkova[42], A. Zhelezov[20], S. Z. Zheng[6], X. Z. Zheng[4], Y. Zheng[7], T. Zhou[6], X. Zhou[8], Y. Zhou[7], V. Zhovkovska[55], L. Z. Zhu[7], X. Zhu[4], X. Zhu[8], V. Zhukov[16], J. Zhuo[46], Q. Zou[5,7], D. Zuliani[31,q], G. Zunica[48]

[1] *School of Physics and Astronomy, Monash University, Melbourne, Australia*
[2] *Centro Brasileiro de Pesquisas Físicas (CBPF), Rio de Janeiro, Brazil*
[3] *Universidade Federal do Rio de Janeiro (UFRJ), Rio de Janeiro, Brazil*
[4] *Center for High Energy Physics, Tsinghua University, Beijing, China*
[5] *Institute Of High Energy Physics (IHEP), Beijing, China*
[6] *School of Physics State Key Laboratory of Nuclear Physics and Technology, Peking University, Beijing, China*
[7] *University of Chinese Academy of Sciences, Beijing, China*
[8] *Institute of Particle Physics, Central China Normal University, Wuhan, Hubei, China*
[9] *Consejo Nacional de Rectores (CONARE), San Jose, Costa Rica*
[10] *Université Savoie Mont Blanc, CNRS, IN2P3-LAPP, Annecy, France*
[11] *Université Clermont Auvergne, CNRS/IN2P3, LPC, Clermont-Ferrand, France*
[12] *Aix Marseille Univ, CNRS/IN2P3, CPPM, Marseille, France*

JHEP01(2025)054

[13] Université Paris-Saclay, CNRS/IN2P3, IJCLab, Orsay, France
[14] Laboratoire Leprince-Ringuet, CNRS/IN2P3, Ecole Polytechnique, Institut Polytechnique de Paris, Palaiseau, France
[15] LPNHE, Sorbonne Université, Paris Diderot Sorbonne Paris Cité, CNRS/IN2P3, Paris, France
[16] I. Physikalisches Institut, RWTH Aachen University, Aachen, Germany
[17] Universität Bonn — Helmholtz-Institut für Strahlen und Kernphysik, Bonn, Germany
[18] Fakultät Physik, Technische Universität Dortmund, Dortmund, Germany
[19] Max-Planck-Institut für Kernphysik (MPIK), Heidelberg, Germany
[20] Physikalisches Institut, Ruprecht-Karls-Universität Heidelberg, Heidelberg, Germany
[21] School of Physics, University College Dublin, Dublin, Ireland
[22] INFN Sezione di Bari, Bari, Italy
[23] INFN Sezione di Bologna, Bologna, Italy
[24] INFN Sezione di Ferrara, Ferrara, Italy
[25] INFN Sezione di Firenze, Firenze, Italy
[26] INFN Laboratori Nazionali di Frascati, Frascati, Italy
[27] INFN Sezione di Genova, Genova, Italy
[28] INFN Sezione di Milano, Milano, Italy
[29] INFN Sezione di Milano-Bicocca, Milano, Italy
[30] INFN Sezione di Cagliari, Monserrato, Italy
[31] INFN Sezione di Padova, Padova, Italy
[32] INFN Sezione di Perugia, Perugia, Italy
[33] INFN Sezione di Pisa, Pisa, Italy
[34] INFN Sezione di Roma La Sapienza, Roma, Italy
[35] INFN Sezione di Roma Tor Vergata, Roma, Italy
[36] Nikhef National Institute for Subatomic Physics, Amsterdam, Netherlands
[37] Nikhef National Institute for Subatomic Physics and VU University Amsterdam, Amsterdam, Netherlands
[38] AGH — University of Krakow, Faculty of Physics and Applied Computer Science, Kraków, Poland
[39] Henryk Niewodniczanski Institute of Nuclear Physics Polish Academy of Sciences, Kraków, Poland
[40] National Center for Nuclear Research (NCBJ), Warsaw, Poland
[41] Horia Hulubei National Institute of Physics and Nuclear Engineering, Bucharest-Magurele, Romania
[42] Affiliated with an institute covered by a cooperation agreement with CERN
[43] DS4DS, La Salle, Universitat Ramon Llull, Barcelona, Spain
[44] ICCUB, Universitat de Barcelona, Barcelona, Spain
[45] Instituto Galego de Física de Altas Enerxías (IGFAE), Universidade de Santiago de Compostela, Santiago de Compostela, Spain
[46] Instituto de Fisica Corpuscular, Centro Mixto Universidad de Valencia — CSIC, Valencia, Spain
[47] European Organization for Nuclear Research (CERN), Geneva, Switzerland
[48] Institute of Physics, Ecole Polytechnique Fédérale de Lausanne (EPFL), Lausanne, Switzerland
[49] Physik-Institut, Universität Zürich, Zürich, Switzerland
[50] NSC Kharkiv Institute of Physics and Technology (NSC KIPT), Kharkiv, Ukraine
[51] Institute for Nuclear Research of the National Academy of Sciences (KINR), Kyiv, Ukraine
[52] School of Physics and Astronomy, University of Birmingham, Birmingham, United Kingdom
[53] H.H. Wills Physics Laboratory, University of Bristol, Bristol, United Kingdom
[54] Cavendish Laboratory, University of Cambridge, Cambridge, United Kingdom
[55] Department of Physics, University of Warwick, Coventry, United Kingdom
[56] STFC Rutherford Appleton Laboratory, Didcot, United Kingdom
[57] School of Physics and Astronomy, University of Edinburgh, Edinburgh, United Kingdom
[58] School of Physics and Astronomy, University of Glasgow, Glasgow, United Kingdom
[59] Oliver Lodge Laboratory, University of Liverpool, Liverpool, United Kingdom
[60] Imperial College London, London, United Kingdom
[61] Department of Physics and Astronomy, University of Manchester, Manchester, United Kingdom
[62] Department of Physics, University of Oxford, Oxford, United Kingdom
[63] Massachusetts Institute of Technology, Cambridge, MA, United States

JHEP01(2025)054

[64] University of Cincinnati, Cincinnati, OH, United States
[65] University of Maryland, College Park, MD, United States
[66] Los Alamos National Laboratory (LANL), Los Alamos, NM, United States
[67] Syracuse University, Syracuse, NY, United States
[68] Pontifícia Universidade Católica do Rio de Janeiro (PUC-Rio), Rio de Janeiro, Brazil, associated to [3]
[69] School of Physics and Electronics, Hunan University, Changsha City, China, associated to [8]
[70] Guangdong Provincial Key Laboratory of Nuclear Science, Guangdong-Hong Kong Joint Laboratory of Quantum Matter, Institute of Quantum Matter, South China Normal University, Guangzhou, China, associated to [4]
[71] Lanzhou University, Lanzhou, China, associated to [5]
[72] School of Physics and Technology, Wuhan University, Wuhan, China, associated to [4]
[73] Departamento de Fisica, Universidad Nacional de Colombia, Bogota, Colombia, associated to [15]
[74] Eotvos Lorand University, Budapest, Hungary, associated to [47]
[75] Van Swinderen Institute, University of Groningen, Groningen, Netherlands, associated to [36]
[76] Universiteit Maastricht, Maastricht, Netherlands, associated to [36]
[77] Tadeusz Kosciuszko Cracow University of Technology, Cracow, Poland, associated to [39]
[78] Universidade da Coruña, A Coruna, Spain, associated to [43]
[79] Department of Physics and Astronomy, Uppsala University, Uppsala, Sweden, associated to [58]
[80] University of Michigan, Ann Arbor, MI, United States, associated to [67]
[81] Departement de Physique Nucleaire (SPhN), Gif-Sur-Yvette, France

[a] Universidade de Brasília, Brasília, Brazil
[b] Centro Federal de Educacão Tecnológica Celso Suckow da Fonseca, Rio De Janeiro, Brazil
[c] Hangzhou Institute for Advanced Study, UCAS, Hangzhou, China
[d] School of Physics and Electronics, Henan University, Kaifeng, China
[e] LIP6, Sorbonne Université, Paris, France
[f] Excellence Cluster ORIGINS, Munich, Germany
[g] Universidad Nacional Autónoma de Honduras, Tegucigalpa, Honduras
[h] Università di Bari, Bari, Italy
[i] Università di Bergamo, Bergamo, Italy
[j] Università di Bologna, Bologna, Italy
[k] Università di Cagliari, Cagliari, Italy
[l] Università di Ferrara, Ferrara, Italy
[m] Università di Firenze, Firenze, Italy
[n] Università di Genova, Genova, Italy
[o] Università degli Studi di Milano, Milano, Italy
[p] Università degli Studi di Milano-Bicocca, Milano, Italy
[q] Università di Padova, Padova, Italy
[r] Università di Perugia, Perugia, Italy
[s] Scuola Normale Superiore, Pisa, Italy
[t] Università di Pisa, Pisa, Italy
[u] Università della Basilicata, Potenza, Italy
[v] Università di Roma Tor Vergata, Roma, Italy
[w] Università di Siena, Siena, Italy
[x] Università di Urbino, Urbino, Italy
[y] Universidad de Alcalá, Alcalá de Henares, Spain
[z] Facultad de Ciencias Fisicas, Madrid, Spain
[aa] Department of Physics/Division of Particle Physics, Lund, Sweden
[†] Deceased

JHEP01(2025)054